UNIVERSITAT DE BARCELONA

Investigating early functional alteration in a human iPSC-based model of Parkinson's Disease

Giulia Carola

UNIVERSITAT DE BARCELONA

Investigating early functional alteration in a human iPSC-based model of Parkinson's Disease

Giulia Carola, B.Sc., M.Sc.

FACULTAT DE FARMÀCIA I CIÈNCIES DE L'ALIMENTACIÓ

PROGRAMA DE DOCTORAT EN BIOMEDICINA

INVESTIGATING EARLY FUNCTIONAL ALTERATION IN A HUMAN IPSC-BASED MODEL OF PARKINSON'S DISEASE

Memòria presentada per Giulia Carola per optar al títol de doctor per la Universitat de Barcelona

_____

Antonella Consiglio, Ph.D
(Directora de la Tesis)

_____

Giulia Carola, MS.c
(Doctoranda)

_____

José Antonio Del Río Fernández, Ph.D
(Tutor Academico)

Barcelona, …….

Al mio papà

"It is IMPERFECTION - not perfection - that is the end result of the program written into that formidably complex engine that is the human brain, and of the influences exerted upon us by the environment and whoever takes care of us during the long years of our physical, psychological and intellectual development."

Rita Levi-Montalcini

DECLARATION

This dissertation is the result of my own work and includes nothing, which is the outcome of work done in collaboration except where specifically indicated in the text. It has not been previously submitted, in part or whole, to any university or institution for any degree, diploma, or other qualification, unless indicated in the text.

This thesis is in accordance with the Department of Biomedicine of the University of Barcelona (Barcelona, Spain) guidelines.

_____

Giulia Carola, MSc. BSc. (Doctoral Student)

_____

Dated, Barcelona

ABSTRACT

Parkinson’s disease (PD) is an incurable, chronically progressive disease leading to premature invalidity and death. Early diagnosis of PD is expected to dramatically improve the outcome of therapies under current development, therefore we interrogated a human neuronal cell-based model of PD for the earliest detectable functional alterations. Neurons derived from induced pluripotent stem cells (iPSC) representing healthy individuals and LRRK2 associated PD patients formed complex networks that showed evident signs of functional maturation over time. However, PD neuronal networks developed abnormal hypersynchrony, in contrast with healthy or gene-edited isogenic PD networks.

By combining functional calcium imaging, biophysical modeling, dopaminergic neuron (DAn)-lineage tracing and gene expression profile analysis, we found that a decrease in DAn neurite length triggered overall functional alterations in the PD networks. Thus, our results identify early alterations in PD neuronal function that predate the onset of neuron degeneration and highlight the extraordinary window of opportunity that iPSC-based experimental models provide in pre-symptomatic assessment of chronic degenerative diseases.

ACKNOWLEDGEMENTS

This is the best moment for me. The moment in which I can say “THANK YOU” to all the people that stayed with me during this long and challenging moment of my life.
Thank you, prof. Antonella Consiglio, for being my PhD supervisor and guide and allowing me to start this new chapter of my professional career.
Thank you prof. Angel Raya and prof. Jordi Soriano for your invaluable and critical support.
Thank you, prof. Alysson Muotri for the *awesome* American adventure.
Thank you, amazing lab friends and colleagues, present and past:
Armida (and Umbi and Luca), for being a lot more than a friend and colleague;
Carles for the all the awesome experiments, CRISPR *in fide* and bike adventures;
Irene for our chats and glances that always say a lot;
Roger for the confocal training and the funky concerts;
Neus for teaching me rigorous cell culture rules with a smile;
Alba and our Prism challenge;
Meritxell for helping me reorganize my thoughts;
Lucas and our floorplates and co-cultures;
Isabel for your “ciao belli” and car songs;
Silvia and our fights with MatLab and Python;
Dani Malagarriga for helping me find a common language between biology and physics and for explaining to me a thousand times all our analysis;
Yvonne, iPSC master.
Thank you: Isabel Fernandez, Chrysanthi, Monika, Marco, Alessia, Alessandra, Julian, Eva, Anna, Ruben, Raquel, Meritxell, Laura, Marc, Yvan, Cristina and Valentina, for being great fellow travellers in this amazing journey.
Thank you Muotri lab, especially Simoni, Fabio, Angela, Xiwei, Pinar, Gabi, Lila and Elsa, for all your help, support, suggestions and conversations. You gave me a home far away from home.
Thank you, my Barcelona’s friends in particular Charlotte, Ina, Irene, Nikki, Laurent, Verena, Frank, Alex, Léa, you all make Barcelona even more beautiful. You gave me new eyes and showed me a different prospective. It’s a pleasure to grow up with you all!
Thank you Danyla and Paola, best flatmates ever!
Thank you Elisa because you NEVER give up on me, Silvia for your smile and enthusiasm and Giulia sweet, strong and always present.
Between us there is no distance, and it never will be.
Thank you Mattia, Matteo, Daniele and Andrea, for your kind, fun and long-lasting friendship.
Thank you to my family. To my sister Chiara for being my REASON; to my mum Wilma that keeps guiding me, even from far away; to my dad Enzo for many reasons but mostly because he believed in me much more than anyone else did, myself included.
Last, but not least, thank you Mike. You met me in one of the craziest moments of my life but, despite everything, you never stop making me smile.

Grazie!

TABLE OF CONTENTS

INTRODUCTION

1. PARKINSON DISEASE (200 years from the discovery of the disease)

1.1 Introduction and clinical features

Two centuries ago, James Parkinson described Parkinson's Disease (PD) as a neurological disorder for the first time in his monograph entitled *An Essay on the Shaking Palsy*[1]*.* In the last 200 years this disease has been extensively studied and today we define PD as a progressive neurodegenerative movement disorder, clinically characterized by distinctive motor symptoms including bradikinesia, resting tremor, rigidity and impaired postural reflex[2]. The disease's progression is characterized by asymmetric onset of the signs and symptoms and a good response to levodopa treatment. However, PD affects many areas of the brain, also causing non-motor symptoms including anosmia, autonomic disturbance, sleep disorders, gastrointestinal dysfunctions, speech/swallowing problems and cognitive decline that may progress to dementia (80% of cases over 20 years of the disease)[3–7].

1.2 Neuropathological features of PD

PD's known hallmarks are the preferential loss of striatal projecting dopaminergic neurons (A9) of the sustantia nigra pars compacta (SNpc) and the presence of ubiquitin-positive inclusions in surviving neurons, mainly composed of the neuronal protein alpha-synuclein (α-syn); known as Lewy Bodies (LB)[8,9].

A9 ventral midbrain dopaminergic neurons display strong neuromelanin pigmentation[10]. They project through the striatum first in the putamen and then in the caudatum, and their main role is to regulate the release of dopamine in the striatum to initiate the execution of movement. During PD pathogenesis the loss of dopaminergic neurons is observable by a SNpc neuromelanin depigmentation and results in a progressive dysfunctionality in the motor circuitry of the basal ganglia that leads to motor impairments[11]. Importantly, when the symptoms display, almost 50% of the dopaminergic neurons (DAn) have already been lost. Reduced levels of dopamine correlates with the severity of the symptoms[12]. Lewy bodies are typical not only in the SNpc but also in other areas of the central nervous system (CNS). They have been characterized as an abnormal, post-translationally modified and aggregated form of the presynaptic protein α-syn with other proteins such ubiquitin, parkin and neurofilaments[13].

1.3 Prevalence and etiology

PD is the second most prevalent movement disorder and chronic neurodegenerative disease, after Alzheimer's disease (AD), affecting between seven to ten million people worldwide [14]. The causes of the neurodegeneration triggering PD are still unknown, however, 15% of patients with PD have a familial history, suggesting a genetic factor. Several mutations in different genes lead to familial PD such as LRRK2, PARK7, PINK1, SNCA, or PARKIN genes[15,16,25–27,17–24]. Other genetic variants, such as mutations in the GBA and UCHL1 genes are known to increase the risk of PD[28], and still others are being investigated.

PD's etiology typically involves an interaction between genetic predispositions and other environmental factors: infectious (influenza, whooping cough), toxic (pesticides, solvents) and other exposure (rural residence, drinking well water) have been identified as possible risk factors.

The most influential risk factor in PD is ageing. It's well known and described that physiological ageing causes changes in gene expression, immune function, mitochondrial integrity, and metabolic efficiency[29,30]. Interestingly, DA neurons seems to be more vulnerable to this age associated degeneration process compared to other types of neuron[11].

Gender is another PD risk factor. The female to male ratio for PD has been demonstrated to be 1:1.5/2 with women developing the disease a mean of 2.2 years later compared to men[31]. Different epidemiologic studies suggest that the differences in the onset of the disease between women and men are due to the fact that women have a higher initial striatal dopamine level compared to men, this could delay the onset of the motor symptoms; and that estrogen seems to have a mild neuroprotective role[32]. Cigarette smoking[33–35], coffee and tea drinking and a high level of physical activity in midlife[34,36] are also associated with lower risk of developing PD.

1.3.1 Environmental causes

Environmental toxins play a role in PD neurodegeneration, however the current consensus is that they do not induce the disease: they are always associated with genetic predispositions. Their influence is nonetheless interesting mainly because the role of environmental toxins in the pathogenesis of PD is still not fully clarified[37].

Several viruses have also been proposed as playing a role in the onset of the disease, with evidence showing that patients contracting influenza in the 1918 epidemic display cases of

lethargic encephalitis, which exhibited Parkinsonism. These patients reacted well to anti-PD medication for a period of time[38], but did not exhibit characteristic Lewy pathology (LP) during autopsy. A hypothesis offers the theory that the influenza virus infection was not a direct cause of PD, but was the "first hit" that opened the way for a second stressor in a "dual-hit" theory [39,40].

Another potential environmental trigger of PD can be exposure to pesticides like rotenone. Infusion of rotenone into the substantia nigra of mice or rats has been found to create PD-like characteristics. The dosage and method of administration of the rotenone change the outcome: a systemic administration causes a multisystemic degeneration unlike the degeneration seen in PD[41], and high doses are selectively damaging to the striatum and globus pallidus, but spare the substantia nigra[42], a chronic, per oral exposure to rotenone (more likely to mimic the natural exposure to this pesticide) was shown to give rise to a PD-like pathology. This pathology originates in the enteric nervous system before spreading to the substantia nigra, causing a loss of dopaminergic neurons and PD-like characteristics[43]. Interestingly, when the vagal nerve was resected in a later study, the disease's progression to the brain was interrupted[44] suggesting a prion-like behavior of this disease.

The case for rotenone as an environmental factor is supported by data showing that living in rural areas (with higher exposure to pesticides) correlates with increased risk of developing PD compared to living in urban areas[45]. This has been disputed by other studies that found no significant difference in the prevalence between urban and rural areas[46].

1.3.2 Autosomal dominant monogenic forms of PD

Several autosomal dominant monogenic mutations are known to be the cause of PD. The first gene discovered to be associated with PD was the SNCA gene (α-syn). The 1997 paper Polymeropoulos et al. used a traditional linkage approach on a large Italian family to track the underlying genetic lesion to an area located in the long arm of human chromosome 4[47]. This discovery corroborated the study by Spillantini et al (1997)[8] that describes how α-synuclein protein is the major component of the LB, the pathological hallmark of PD[48,49], proving a familial form of PD.

A duplication or triplication of the SNCA locus is a frequent cause of PD providing a pathogenic overexpression of wild type α-synuclein; duplication in the gene is often indistinguishable from idiopathic PD while the triplications display an early onset fulminant disease[26,50–52]. A single copy of the SNCA gene with any of five different missense mutations is also linked to PD: A53T, A30P, E46K, H50Q and G51D[53–55].

Another known monogenic cause of PD is mutation in the VPS35 gene. The mutation D620N was described by two groups in 2011 and accounts for ≈1% of all familial cases of PD, though the symptoms are similar to idiopathic PD. Furthermore, several non-synonymous base exchanges have been identified, but their pathogenicity remains unknown[56,57].

R1205H and A502V mutations in the gene eukaryotic translation initiation factor 4 gamma (EIF4G1)[58,59], and Thr6Ile and Arg145Gln in the gene CHCHD2 and its twin gene CHCHD10 are also associated with autosomal dominant PD. Interestingly, mutations in CHCHD2/CHCHD10 seem to be connected with a specific PD phenotype such as mitochondrial dysfunction[60–62].

The most important autosomal dominant mutation in this study is the LRRK2 G2019S, discovered on chromosome 12, by Funayma at al. in 2002 and directly correlated with familial PD in 2004[24,25,63]. The LRRK2's mutations are estimated to be present in approximately 4% of all PD cases and the most frequent of these mutations is the one that we are currently analyzing, G2019S[64–67], this presents in 1% of sporadic cases and 3%-6% of familial PD cases. Clinically PD caused by LRRK2 mutations is indistinguishable from the pathology seen in sporadic cases of PD; the first symptoms appear in the sixth decade and dystonia is typical of the disease progression. Nevertheless, most LRRK2 cases described until now demonstrate common features like LB in the brainstem and loss of neurons in the SNpc, although a minority of cases exhibit neurofibrillary tangle pathology, glial cytoplasmic inclusions reminiscent of multiple system atrophy, or neuronal nigral loss without LB[68].

1.3.3 Autosomal recessive monogenic forms of PD

Autosomal recessive PD is often correlated with early onset and slow progression of the symptoms. Mutations in the *parkin* gene are known to be the most common cause of autosomal recessive early onset parkinsonism and also to be the cause of autosomal – recessive juvenile parkinsonism[22,69]. The connections between this gene and PD are complex; 79 mutations in *parkin* have been reported in familial and sporadic PD patients, but interestingly, PD is associated with heterozygous *parkin* mutations with an apparently dominant pattern of transmission, implying that carriers of a single *parkin* mutation might be at risk of developing PD[70–72]. The heterogeneity of the symptoms makes it difficult to draw clinical connections between a given phenotype and a specific mutation.

Mutations in DJ-1 and PINK1 are also connected with autosomal recessive PD with clinical features similar to the ones observed in patients with *parkin* mutations[20,73–75]. Mutations in RAB39B gene were more recently discovered to cause X-linked and early onset PD[76–78]. Further, in 2012 a connection was described between mutations in the *DNAJC6* gene and childhood Parkinsonism with early onset slow progression PD and good response to dopaminergic therapy[79–81].

1.3.4 Genetic risk factors and susceptibility

The gene most commonly associated with higher susceptibility to develop PD is GBA, the lysosomal enzyme glucocerebrosidase (GCase), which causes the lysosomal storage disorder, Gaucher disease (GD). There are 3 known types of GBA related diseases with a wide range of symptoms. Type 2 and 3 are generally associated with neurological phenotypes but type 1 has often been connected with PD. Heterozygous mutations in GBA are now known to be one of the most common genetic risk factors for Parkinson's disease and dementia with Lewy bodies (DLB) [82–84].

Other PD susceptibility factors involve mutations in MAPT[85], MC1R[86], ADH1C[87] and other genes (view Table 2). In sporadic PD forms, the involvement of environmental factors in initiation and progression of the disease suggests that epigenetics plays an important role[88].

An example of an epigenetic mechanism in PD is the modification of the α-syn gene (SNCA). Matsumoto et al.[89] found that CpGs in SNCA were hyper-methylated in controls, but not methylated in PD patients, suggesting that lack of methylation was an epigenetic risk factor for PD that is related to the pathogenesis of α-syn[90].

Table 1: PD related genetic risk factors

Inheritance pattern	Locus	Mutation site	Involved protein
Autosomal dominant	PARK1	SNCA	α-syn
	PARK3	SPR	Sepiapterin reductase in BH4 pathway
	PARK4	Triplication of SNCA	α-syn
	PARK5	UCHL1	Ubiquitin C-terminal hydrolase
	PARK8	LRRK2	Leucine-reach repeat kinase 2
	PARK11	GIGYF2	GRB10-interacting GYF protein 2
	PARK13	HTRA2	HTRA serine peptidase
	PARK16	Multiple independent sites?	Unknown
	PARK17	VPS35	Vacuolar protein sorting 35
	PARK18	EIF4G1	Eukaryotic translation initiation factor 4 gamma 1
	PARK21	DNAJC13	DNAJ-domain-bearing protein
Autosomal recessive	PARK2/PARKN	Parkin	Ubiquitin-protein ligase
	PARK6	PINK1	PTEN-induced putative kinase 1
	PARK7	DJ1	Oncogene DJ1
	PARK9	ATP13A2	Lysosomal type 5 P-type atpase
	PARK14	PLA2G6	Phospholipase A2
	PARK15	FBXO7	F-BOX only protein
	PARK19	DNAJC6	Putative tyrosine-protein phosphatase auxilin
	PARK20	SYNJ1	Synaptojanin-1
X-linked	PARK12	TAF1	TFIID subunit 1

Table 2: PD related susceptibility factors

	Involved gene	Putative function	Phenotype
Susceptibility factors	GBA	Acid β - glucocerebrosidase	Gaucher disease
	MAPT	Microtubule-associated protein tau	Supranuclear palsy, Dementia
	MC1R	Melanocyte-stimulating hormone receptor	Albinism
	ADH1C	Alcohol dehydrogenase 1C	Alcohol dependence
	ADH4	Alcohol dehydrogenase 4	Alcohol dependence
	HLA	Major histocompatibility complex	Imamura et al., 2003
	ATXN2	Ataxin-2	Spinocerebellar ataxia 2
	ATXN3	Ataxin-3	Machado-Joseph disease
	TBP	TATA box-binding protein	Spinocerebellar ataxia 17
	ATXN8OS	Ataxin-8 opposite strand	Spinocerebellar ataxia 8
	NR4A2	Nuclear receptor subfamily 4 group A member 2 (transcription factor)	Le et al., 2003

1.4 Molecular mechanisms involved in PD

PD is described as a systemic pathology. Neurons, especially DA, are the most involved and present signs typical of the disease but other brain cells are also affected, such as astrocytes and microglial cells, and alterations are observed in other organs including the gut, the immune system and the peripheral nerves.

All these different types of cells have specific PD related cellular features in common, shown in the Figure 1, that together explain the molecular bases of the disease.

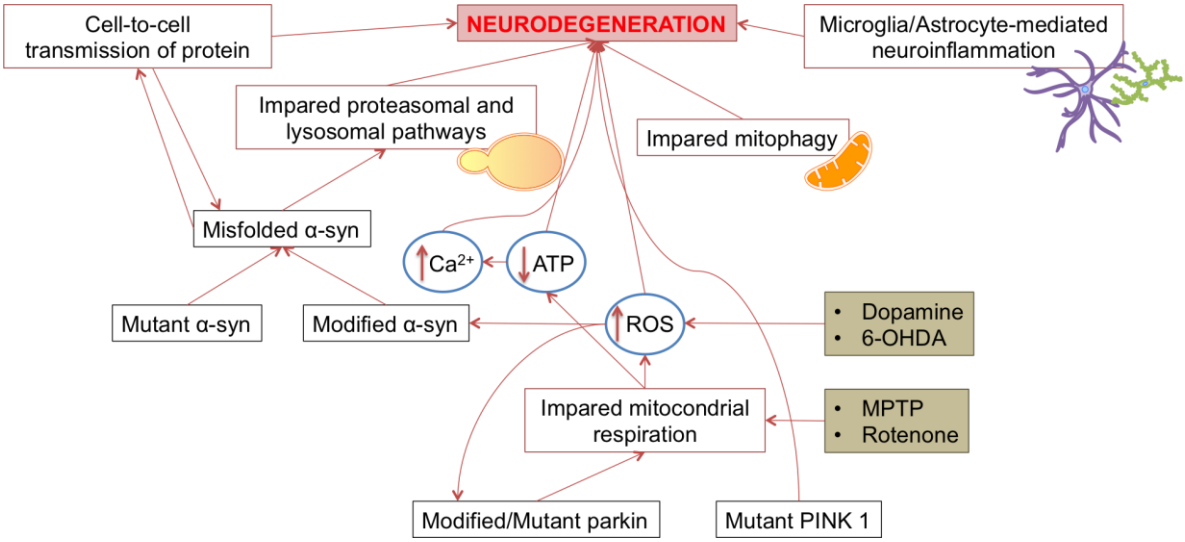

Fig. 1. Different molecular mechanisms contribute to the onset of PD. Adapted from S. Przedborki (2017). DOI: 10.1038/nrn.2017.25[91], this diagram shows the main known mechanisms and their interactions. Critical to PD pathology are the quality-control mechanism regulating production, folding and degradation of proteins and organelles such as α-syn and mitochondria. Misfolded proteins result from gene mutation or post-translational modification induced by ROS. These misfolded proteins can alter the ubiquitine-proteasome and lysosomal degradation pathways. They may also to be able to travel from cell to cell propagating the disease. ROS itself can cause broad cellular damage and directly contribute to neurodegeneration. ROS can be generated by the oxidation of dopamine (the major neurotransmitter used by dopaminergic neurons), by environmental toxins like 6-OHDA and by mitochondrial repair defects. Mutations in PINK1 and Parkin are also connected with mitochondrial impairment and PD. Similar effects are caused by the environmental toxins Rotenone and MPTP. Defective mitochondrial respiration is also responsible for a decrease in the ATP production that causes oxidative stress and accumulation of Ca^{2+} which is toxic for the cells and leads to an energy crisis. All these mechanisms are prevalent in DA neurons but also affect glial cells which are activated by the degeneration process and adopt a pro-inflammatory phenotype. This phenotype enhances the production of cytotoxic molecules, increases stress levels and further promotes degeneration.

1.4.1 α-synuclein

A key component of PD pathogenesis is the intracellular accumulation of misfolded proteins, in particular α-syn[8]. The misfolded proteins are collected in Lewy bodies, hyaline inclusions in cell bodies and neurites across the brain[9]. It has been demonstrated both genetically and pathologically that the autophagic clearance system that maintains proteostasis is impaired in PD; misfolded α-synuclein proteins block their own degradation by autophagic impairment and consequently prevent the degradation of other proteins causing the formation of Lewy bodies[92–94]. Mutated, misfolded or overexpressed α-synuclein is involved in a number of pathways associated with degeneration of SNpc DA neurons including impairment in the synaptic function[95,96], mitochondria respiration and turnover[97,98], microtubule assembly and axonal transportation[99] and endoplasmic reticulum (ER) stress[100]. Recent studies[101,102] propose a *prion-like* hypothesis: it has been demonstrated that α-synuclein aggregates spread between cells and that this contributes to the PD disease process. Interestingly these proteins spread not just in the dopaminergic neurons but also in other neurons and organs like peripheral nerves and the enteric nervous system[103]. The spread of a *prion-like* conformed α-synuclein might play an important role in the progressive worsening of symptoms and the gradual involvement of additional brain and autonomic functions as the disease advances[101].

1.4.2 Mitochondrial dysfunction

Both familial and sporadic PD often display impairments in mitochondrial homeostasis[104,105]. PINK1 and Parkin play an important role in the control of mitochondrial turnover and protection against oxidative stress. The mutations in these genes are implicated in reducing mitochondrial calcium capacity and reactive oxygen species (ROS) induction. These processes increase the vulnerability of the cells[106]. Recent findings also show that mitochondrial transport, necessary for energy supply especially in long axon DA neurons, may be affected in PD. Studies correlate this impairment with mutations in Parkin, α-syn, or LRRK2 because they modulate microtubule stability[107], or by formation of α-syn aggregates[108].

1.4.3 Dopamine impairment

It is long established that in PD patients there is a substantial dopamine deficit both in the striatum and in the SNpc. 2 studies described this characteristic in the 1960s: Sano, I. Biochemistry of the extrapyramidal system. *Shinkei Kennkyu No Shinpo* **5**, 42–48 (in Japanese) (1960)[109]; Ehringer, H. & Hornykiewicz, O. Verteilung von noradrenalin und

dopamin (3-hydroxytyramin) im gehirn des menschen und ihr verhalten bei erkrankungen des extrapyramidalen systems. *Klin. Wochenschr.* **38**, 1236–1239 (in German) (1960)[110].

Dopamine deficit causes motor symptoms in PD due to the disruption of the nigrostriatal pathway in the striatum, which is a crucial part of the basal ganglia circuitry controlling movement[111,112]. The administration of L-DOPA (dopamine precursor) is currently the most used symptomatic treatment to efficiently reduce the motor symptoms[113].

1.4.4 Axonal damage

Neurodegeneration and the loss of dopaminergic neurons are well established causes of PD motor symptoms. New studies focus on the preclinical stage of the disease to understand the early stages of the neurodegeneration, looking for new therapeutic targets and early diagnosis techniques.

A key player in the early stage of the disease seems to be dopaminergic axonal degeneration associated with α-syn accumulation[114]. Over the last decade, different groups have monitored PD patients using imaging techniques including DAT scan and PET[115,116], with tracers applied to measure the activity of vesicular monoamine transporter type 2 (VMAT2), aromatic l-amino-acid decarboxylase (AADC) or the dopamine transporter (DAT), all of which are expressed in or on DA axonal terminals (as well as in DA neuronal soma) and can be used as proxy measures of DA axonal length and integrity of the soma. These studies are in accord that there is a more profound loss of DA striatal axonal terminals at the early stages of PD. In particular, they highlight how dopaminergic fibers in the dorsal striatum, which are known to be part of the nigrostriatal pathway and connected with motor function in PD, are only moderately affected at 1 year post the PD diagnosis, more severely affected at 3 years and virtually absent by years 4–5 and thereafter. Though the data was variable, the decrease in the number of tyrosine hydroxylase dopaminergic neurons (TH) positive neurons in the SNpc was robust even at the earlier time points with a relatively minor loss over time and with a residual population of TH positive neurons even decades after diagnosis[117].

Induced pluripotent stem cell (iPSC) models of PD connect the axonal degeneration phenotype with α-syn accumulation allowing new insights on the timing of the α-syn accumulation and on its correlation with the other pathological phenotypes.

Oliveira and colleagues have demonstrated that iPSC derived neurons from PD patients with SNCA triplication have lower neuronal connectivity and a deficit in spine formation compared to controls[118]. These phenotypes have been confirmed with other iPSC neurons derived from PD patients with SNCA triplication and LRRK2 (G2019S) mutation[18,119,120]. Another study with iPSC-derived DA neurons carrying SNCA triplication or the LRRK2 (G2019S) mutation describes how these neurons display abnormalities in neurite length,

axonal degeneration, blebbing and fragmentation[121]. In an important study, Kouroupi et al. reported significantly increased α-syn load in iPSC-derived DA neurons from two patients with early-onset PD with the p.A53T SNCA mutation, compared to controls. These neurons contain the pathological form of α-syn and exhibit protein aggregation, developed α-syn-positive varicosities, neurite swelling and fragmentation. Interestingly, dopaminergic neurons derived from the p.A53T SNCA PD iPSC show impaired ability to form synapses. All of this evidence connects to α-syn pathology, synaptic and axonal degeneration using iPSC derived DA neurons from PD patients[122].

1.5 Treatments

To date, there is no cure for Parkinson's disease. The treatments on the market are symptomatic, helping patients to control the motor/non-motor symptoms. These treatments improve the quality of life, and, ameliorate some functional capability, but they do not cure the disease and are only have temporary effects on the non-motor symptoms. The DA replacement drug, Levodopa (L-DOPA), remains the most effective treatment for PD motor symptoms and its efficacy and tolerability is firmly established after more than 30 years of use in clinical practice[123,124]. This drug only alleviates the symptoms of PD for a period of approximately 5 years.

L-DOPA is a precursor of dopamine that can cross the cross blood-brain barrier, which dopamine itself cannot[125]. Once in the brain, L-DOPA is processed and converted into dopamine by the enzyme L-amino acid decarboxylase restoring the normal level of this neurotransmitter (which is typically low or absent). L-DOPA is normally administered in combination with Monoamine Oxidase B enzyme (MAO-B) inhibitors, Catechol-O-Methyltransferase (COMT) inhibitors and dopamine agonists (Benserazide, Carbidopa) in order to prevent formation of dopamine in the peripheral tissues, which can result in adverse effects such as nausea and vomiting. L-DOPA treatment improves motor symptoms and patients' quality of life but, after five years of treatment, it causes side effects which can be worse than the actual symptoms of PD[113].

New experimental therapies are in pre-clinical and clinical trial, using non-dopaminergic systems treatments for the symptoms of PD such as adenosine, glutamatergic, adrenergic, serotoninergic, histaminic, and iron chelator pathways. These treatments, administered in conjunction with L-DOPA, represent potential therapeutic targets for motor symptoms but their efficacy is still to be proven[126].

2. Ventral midbrain dopaminergic neurons physiology and pathology during PD

Ventral midbrain dopaminergic (DA) neurons selectively degenerate during the progression of PD, making them the main target of this research.

2.1 Anatomy and neurodevelopment

DA neurons are located in the SNpc (A9 group), ventral tegmental area (VTA, A10 group) and the retrorubral field (RRF, A8 group). These neurons are anatomically very close and share developmental profiles and origin. There are several neural circuits established by DA neurons: the nigrostriatal pathway that connects SNpc with the striatum, the mesolimbic pathway that connects DA neurons in VTA with the nucleus accumbens (NAc) and the limbic systems, and the mesocortical pathway that connect VTA neurons with the prefrontal cortex (Figure 2). Taken together we can confirm that dopaminergic neurons play a key role in motor control, reward behaviors and learning.

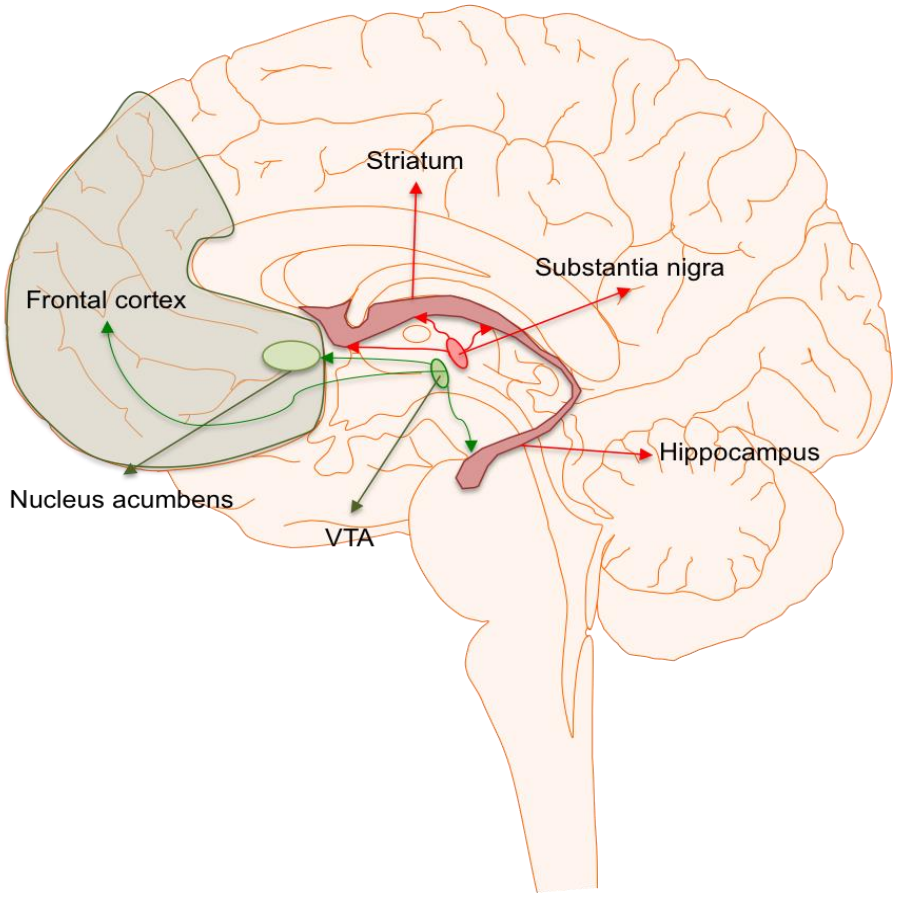

Fig. 2. A schematic diagram illustrating DA neuron clusters in the Substantia nigra (A9) and VTA (A10) in the adult human brain. Indicated with red arrows are the dopaminergic pathways that start from the SNpc and end in the Striatum. Indicated with green arrows are the pathways that start in the VTA and end in the nucleus acumbens, frontal cortex and hippocampus. The dopamine pathways are physiologically involved in many functions such as reward and motivation, pleasure and euphoria, fine tuning in motor functions, compulsion and preservation. Adapted from E. Scarr et al. (2013). DOI: 10.3389/fncel.2013.00055[127].

The development of the midbrain starts during the definition of the neural tube structure when two signaling centers are forming: the isthmic organizer (IsO) that defines the midbrain-hindbrain boundary (MHB)[128–130], and the floor plate (FP), which controls ventral identities[131]. These two areas release transcription factors and morphogens that induce the regional identity of the ventral midbrain (vm) and the specification and proliferation of midbrain dopaminergic progenitors.

The temporal and spatial inhibition/induction of Wingless/Integrated signaling pathway (*Wnt1)* and Sonic Hedgehog signaling pathway (SHH) are crucial for the regulation of ventral midbrain patterning and ventral midbrain dopaminergic neurons have been mapped from progenitors expressing Shh or Wnt1[132–134]. These inputs are integrated in the vm precursors by Forkhead Box Protein A1 and A2 (FOXA1/2) and Orthodentical Homeobox 2 (OTX2)[135] expression that regulates two lim homeobox transcription factors, Lmx1a and Lmx1b. Lmx1b is necessary for the differentiation of mDA progenitors[136]. Lmx1a is required for the specification of mDA neurons in the brain[137,138] and, via muscle segment homeobox homolog 1 (Msx1), to suppress the emergence of basal plate fate[139]. We can conclude that the concerted action of the SHH-FOXA2 and the OTX2-Wnt1-Lmx1a/Msx1 networks is essential not only for the specification of the ventral midbrain floor plate but also for the suppression of alternative neural fates.

After neurogenesis, post mitotic midbrain dopaminergic neurons migrate to reach their final location in the SNpc, VTA and RrF[140,141]. This process is regulated by some early factors described above such as Otx2, Lmx1a/b, Foxa1/2 and the homeobox genes En1/2 (engrailed 1/2), which remain expressed in post mitotic DA cells; these factors also regulate the activity of late transcription factors such as nuclear receptor related 1 protein (Nurr1) that control the progressive acquisition of appropriate neurotrophic factor and DA neurotransmitter phenotype.

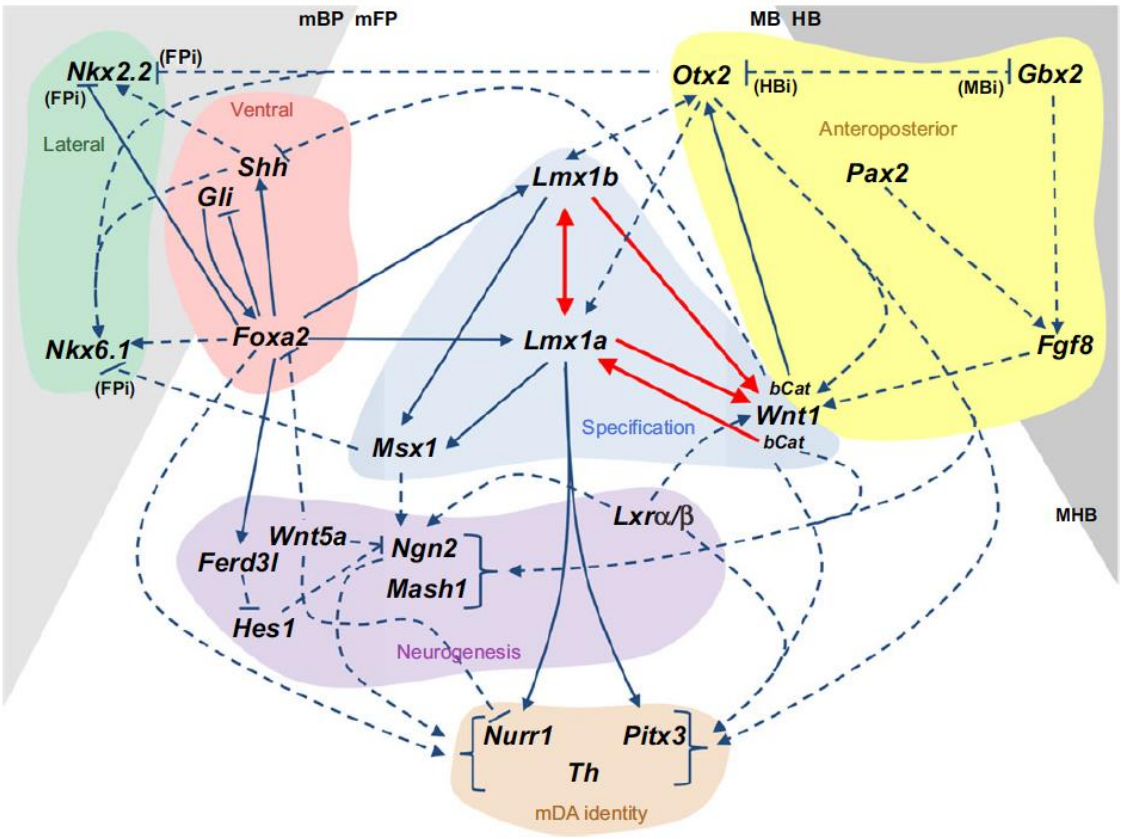

Fig 3. Genetic networks controlling the development of the midbrain-hindbrain and mDA neurons in the mouse brain from E Arenas et al. (2015) DOI: 10.1242/dev.097394[142]

2.2 Main roles and connections

In physiological conditions the dopaminergic neurons present in the SNpc activate the neurons that express D1 dopamine receptor in the striatum through a direct pathway and inhibit the D2-expressing striatal projecting neurons of the indirect pathway[91]. The direct pathway is activated by the cortex and the SNpc, this direct pathway inhibits the globus pallidus internal segment (GPi)–substantia nigra pars reticulata (SNpr). When the indirect pathway is activated by the cortex, and in a minor way inhibited by the SNpc, it inhibits the globus pallidus external segment (GPe), this in turn inhibits the subthalamic nucleus (STN) and the GPi–SNpr. Put together, the direct and indirect pathways on the GPi–SNpr result in a net decrease in inhibition in the thalamus. The thalamus is responsible for activating the motor cortex itself, so an increase in activity in the SNpc promotes motor activity. In pathological conditions like PD, there is a clear degeneration of the SNpc that

causes a pathological dysregulation of the fine balance between the activation of the direct pathway and the inhibition of the indirect pathway. Due to this mechanism there is an increase in the activation caused by STN and a decrease in the GPe-mediated inhibition of the GPi–SNpr, which, in turn, will exert a much stronger inhibition of the thalamus, causing lower activation of the motor cortex. In conclusion, the loss of the inputs of the SNpc direct to the striatum leads to a decrease and impairment in motor activity[143].

2.3 Hypothesis of neurodegeneration

The first steps of neurodegeneration and how the pathogenic mechanisms previously described lead to PD are still not fully understood. The literature attributes neurodegeneration in PD to different hypotheses that collect all the cellular mechanisms described above which lead to the selective loss of dopaminergic neurons. The 2 leading hypotheses are:

a. Aggregation of proteins

b. Mitochondrial dysfunction correlated with oxidative stress.

2.3.1 Aggregation of proteins hypothesis

This hypothesis is supported by the evidence of Lewy pathology (LP) - proteceous inclusions that are rich in fibrillary forms of α-syn, in the SNpc of PD patients[9]. It has been demonstrated that Lewy bodies, the main cause of LP, are present in different stages of the disease in other areas of the brain like the olfactory bulb and the dorsal motor nucleus of vagus (DMV) in the caudal medulla before propagating to the SNpc through synaptically coupled networks[103,144].

Recent studies suggest a *prion-like* behavior of the oligomeric misfolded α-syn. This event may start outside the CNS, in the gut, with the misfolded proteins traveling along the vagus nerve to reach the CNS. Once in the brain, they spread to different areas and are responsible for the proteceous inclusions formation and the neurodegeneration of the SNpc DA

neurons[101]. Even though the connection between α-syn and PD is clear, the molecular mechanisms that connect α-syn pathology with cell death and PD symptoms remains uncertain[145,146].

It is still debated why SNpc DA neurons should be particularly vulnerable to propagated α-syn aggregates and Lewy bodies accumulation given the fact that in low chronic doses these misfolded proteins do not appear to be particularly toxic. In many parts of the brain (particularly the brainstem), Lewy bodies can be present for decades without causing any obvious degeneration or neuronal death[147–149]. Lewy bodies do not spread in the closest neighbor of the SNpc, only in specific areas like DMV, intermediate reticular zone and raphe magnus. There are sporadic PD patients with very little Lewy bodies accumulation and cases in which SNpc DA neurons appear to be lost before Lewy bodies are present in the SNpc. Lewy bodies accumulation is not present in some familial cases despite loss of SNpc DA neurons[11,150–152].

Misfolded proteins are toxic for all neurons as a result of many different mechanisms such as: interference with intracellular neurological traffic pathways, sequestration of key proteins for cell survival, inducing cell cycle arrest and indirectly affecting the process responsible for recognizing and destroying misfolded proteins. It's possible that oligomeric misfolded α-syn is the main player in the SNpc DA neurons degeneration and the Lewy body formation is just a consequence of this process[100,153–157]. To better investigate this hypothesis, techniques for tracking oligomeric α-syn need to be improved.

2.3.2 Mitochondrial dysfunction correlated with oxidative stress hypothesis

An alternative and not mutually exclusive hypothesis for PD neurodegeneration is based on mitochondrial dysfunction correlated with oxidative stress[158].

Studies of different forms of PD including familial early-onset PD (characterized by mutations in DJ-1, PINK1, and parkin genes), dominant forms of PD (characterized by mutations in LRRK2, SNCA and CHCHD2 genes) and non-familial PD (characterized by toxin exposure) all show direct involvement in mitochondrial biology, influencing a range of functions from oxidant defenses, to quality control and oxidative phosphorylation (OXPHOS)[159–162].

DA neurons have three features that make them preferentially vulnerable to these insults:

- **Long and highly branched, unmyelinated axons with an extraordinary number of transmitter release sites.** Mitochondrial oxidative stress is higher in long axons and this causes the axons to decrease in length[163]. The large axonal arbor and high number of transmitter release sites in DA neurons results in a higher expression of the α-syn synaptic protein, giving the potential for a synuclein pathology[164].

- **A specific physiology with slow and broad action potentials that promotes rhythmic activity**[165]. This physiology fulfills two functions, it maintains slow tonic spiking by creating membrane potential oscillations[166] and it promotes calcium entry into mitochondria to stimulates oxidative phosphorylation (OXPHOS) and the production of ATP[167]. These functions can lead to mitochondrial damage, ROS formation, alteration of the autophagy mechanisms and accumulation of misfolded proteins like α-syn[168,169].

- **Usage of dopamine as the preferential neurotransmitter.** Dopamine is known to be potentially toxic because it oxidizes to reactive DA quinones. DA quinones are demonstrated to disrupt the function of glucocerebrosidase (GC) and lysosomes; mechanisms related to neurodegeneration[170–172]. Dopamine also causes mitochondrial alterations through the mitochondrial anchored monoamine oxidase (MAO). The MAO degrades cytosolic dopamine, generating hydrogen peroxide and increasing ROS[173].

The impaired mitochondria become unable to produce energy and this leads to an imbalance in dopamine (DA) vesicular storages, further increasing ROS[174,175].

Given their extraordinary number of transmitter releasers, DA neurons are *per se* more vulnerable to stress and dysfunction that can contribute to neurodegeneration.

Many mechanisms are involved in the preferential neurodegeneration of the dopaminergic neurons during PD but still no research has been able to highlight which one is the most prevalent or the causal order. New models that mimic the slow progression of the disease are needed to test hypotheses about the mechanisms underlying pathogenesis and to connect patient's motor symptoms of PD to the stages of degeneration of SNpc DA neurons.

3. Modelling PD

Our understanding of the relationship of genetic targets with the cellular mechanisms that drive neuronal death in PD is still very fragmentary, making it challenging to create and test therapies which work in models and in clinical trial. The models used often have poor predictive power to determine the human clinical success of a given drug because of the model's relative simplicity compared to the systemic complexity of the disease[176].

3.1 Animal and cellular PD models

Investigating systemic diseases like PD requires different techniques to address the pathogenic role of newly identified mutations including overexpression or knockdown of the gene of interest *in vitro* and *in vivo*. Traditionally engineered animal and cellular models have several limitations:

a. cellular models mainly use standard human tumor cell lines and therefore only partially reflect the characteristics of non-dividing human DA neurons[177,178];

b. genetic animal models based on overexpression (driven by non-native or physiological human promoters) or knockout of the gene of interest, only partially replicate key features of neurodegeneration in PD.

These limitations (and others) mean that traditional animal and cellular models are not ideal for a comprehensive and systemic picture of this complex neurodegenerative disorder.

Patient-derived fibroblasts have also been used to investigate cellular and molecular mechanisms of PD, but they too have some disadvantages:

a. fibroblasts change their clonal composition during passaging in culture;

b. α-syn, which encodes the hallmark protein of PD pathology in neurons, is only marginally expressed in fibroblasts.

A systemic approach can be achieved with animal models of PD. Animal models based on the systemic or local administration of neurotoxins easily and rapidly replicate DA neurodegeneration, but they fail to capture the slow and progressive degenerative changes that occur in human PD pathology. Genetic animal models of PD often do not show all signs and symptoms of the disease.

Although cellular and animal models of PD provide insights into alterations in specific subcellular components (such as proteasome, lysosome and mitochondria), the relevance of these findings for PD pathogenesis is not always immediate, as they do not address the increased susceptibility of DA neurons to undergo PD-related neurodegeneration[179].

Table 3. PD related animal models

Animal model	Motor behavior	SNpc neuron loss	α-syn pathology

Pharmacologic based models of PD		MPTP [180–182]	Reduced locomotion, bradykinesia	High	NO
		6-OHDA[180,183]	Reduced locomotion, altered behavior	High	NO
		Rotenone[42,43,45,184–186]	Reduced locomotion	High	YES
		Paraquat/Maneb[45,187–189]	Reduced locomotion	High	YES
		MET/MDMA[181,190,191]	Reduced locomotion	High	NO
Genetic mutation	α-syn	Familial-PD-associated mutant forms of α-syn A53T, A30P and E46K (under different endogenous promoters)[192,193]	Reduced locomotion anxiety, gastrointestinal dysfunctions.	NO	YES
		Viral overexpression of mutant or wt forms of α-syn[194]	Reduced locomotion	YES	YES
		Transgenic overexpression of the truncated C-terminal form of α-syn[195]	Reduced locomotion	YES	YES
	LRRK2	Overexpression of the G2019S or R1441C/G mutations in LRRK2[196,197]	Reduced locomotion	Not age dependent	NO
		Knock-in mutations of G2019S or R1441C of LRRK2[198]	Reduced locomotion	NO	NO
		Knockout of both LRRK2 and LRRK1[199]	Reduced locomotion	YES	NO
	PINK1[200]		No obvious motor defects	NO	NO
	PARKIN[201]		No obvious motor defects	Partial	NO
	DJ-1[202]		Reduced locomotion	YES	NO
	ATP13A2[203,204]		No obvious motor defects	NO	NO
Others	SHH[205]		Reduced locomotion	YES	NO

Nurr1[206]	Reduced locomotion	YES	NO
Engrailed 1[207]	Reduced locomotion	Partial	NO
Pitx3[208]	Reduced locomotion	YES	NO
C-Rel-NFKB[209]	Bradykinesia, rigidity	YES	YES
MitoPark[210]	Reduced locomotion, tremor and rigidity	YES	YES
Atg7[211]	Late onset locomotor deficit	YES	YES
VMAT2[212]	Reduced locomotion and altered behavior	YES	YES

3.2 Induced pluripotent stem cells (iPSC)

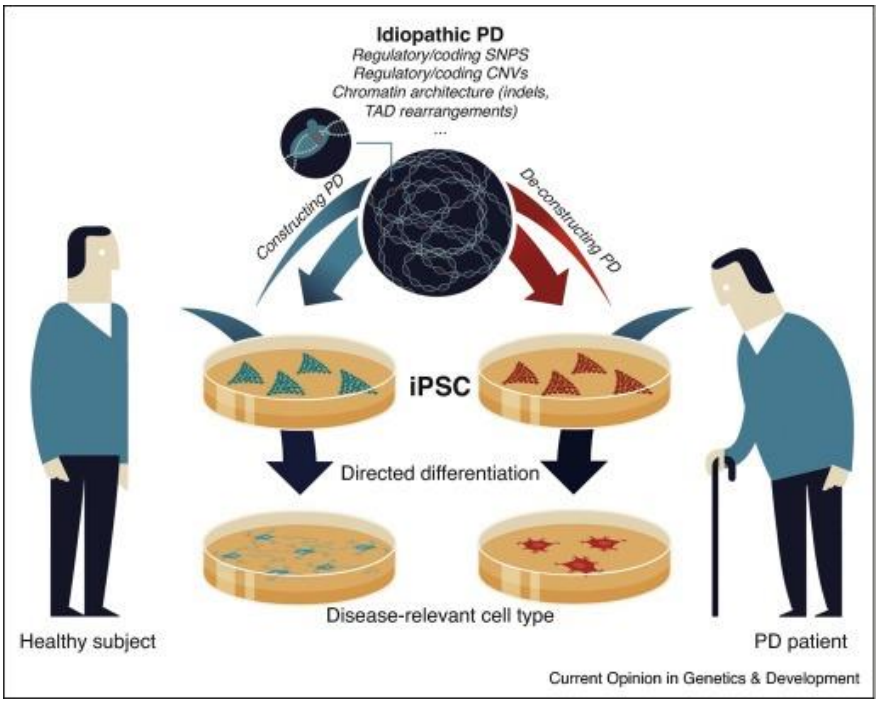

Fig. 4 This diagram represents the potential therapeutic applications of iPSCs in PD studies. iPSCs can be reprogrammed using different techniques suited to different applications such as transplants or *in vitro* study. The most commonly used reprogramming techniques are: viral delivery (retroviruses and adenoviruses), integrative free vectors (piggyBac transposon, plasmid/episomal plasmid vectors, mini-circle vectors) and non-integrating methods (direct protein/microRNA delivery, small molecules). iPSCs from PD patients and healthy age-matched controls can be corrected/edited to receive patient-specific mutations suitable for clinical application. This figure uses PD as an example of the potential therapeutic uses of iPSC but the mechanisms of this are common to many other pathologies. iPSC disease modeling is particularly important for neural diseases because of the difficulties in reaching the affected neural tissue in patients.

From: C.Calatayud et al. (2017). DOI: 10.1016/j.gde.2017.06.002[213]

Induced pluripotent stem cells (iPSC), generated from patients with genetic conditions, can be exploited to create genuinely human experimental models of diseases [214]. Modeling human disease using iPSC technology involves two steps: the generation of iPSC from representative patients, and the differentiation of patient- specific iPSC towards disease-relevant cell type(s). The major advantage of the iPSC approach is the potential to develop human cell-based disease models of sporadic and genetically complex diseases such as PD.

PD is very interesting model for application of iPSC technology, because protocols for generating DA neurons are relatively robust and reproducible[215–217]. Studies from our group and others using iPSC derived from patients with monogenic forms of PD have proven that key features of PD pathophysiology as a late-onset neurodegenerative disorder can be

modeled after differentiation into dopaminergic neurons. Specifically, it was demonstrated not only that iPSC technology can be used to observe phenotypes relevant to neurodegeneration in PD, but also that iPSC-derived neurons with the genome of sporadic PD patients exhibited similar phenotypes to those seen in iPSC derived from patients with monogenic PD[213,217–220]. iPSC technology may also facilitate identification of therapeutic compounds by elucidating authentic signaling pathways in diseased human neurons rather than artificial models. For example, Cooper et al.[221] focused on mitochondrial functions in PD associated with mutation in PINK1 and LRRK2 genes. They found that iPSC-derived neurons are more sensitive to the chemical toxins valinomycin and concanamycin A. Subsequently, the iPSC-derived neurons treated with the antioxidant coenzyme Q10, rapamycin or the LRRK2 inhibitor GW5074 resulted in partial protection against neural degeneration.

Clinical application of iPSC-derived neurons for treatment of PD is still a distant option. The challenge for a more comprehensive study of epigenetic and genetic characteristics of iPSC-derived neurons mainly lies in the necessity to generate a cell population that allows purification based on highly specific midbrain DA markers. An outstanding concern is whether it is prudent to use a patient's own cells to derive DA neurons for therapy, in view of their presumed susceptibility to developing PD pathology. To date, iPSC has been an excellent tool to investigate neurodegenerative diseases like PD but its application in clinical and therapeutic usage requires further analysis for completeness and stability[222].

4. Studying neurodegenerative diseases with calcium imaging

Neurodegenerative diseases like PD, Alzheimer's disease and other types of dementia are in the top five causes of death worldwide, in the top 3 if we consider only high-income countries[223]. Tremendous efforts are being taken to cure these diseases, but clinical researchers have made very limited progress due to the difficulties in studying the etiology and pathophysiology of these disorders. As already mentioned, the lack of robust animal models and the difficulties in obtaining early human samples make the investigation of neurodegenerative causes even harder.

Calcium imaging techniques have been widely applied to study neuronal behavior and have given the scientific community important insights to understand the physiology and pathophysiology that relates to these cells[224–226].

The possibility to capture images and record the live motion of calcium ions in neurons allows the investigation of different mechanisms connected with this type of cell. In the synaptic terminals, calcium influx regulates exocytosis[227] and the synaptic plasticity that happens in response to a stimulus[228]. In cell nuclei, calcium is able to regulate gene transcription[229] and overall in the neurons it is the sign of an event of action potential[230]

because the Ca^{2+} channels connect the “electrical” and the “signaling” worlds in the neurons[231].

4.1 Calcium imaging techniques

Calcium imaging requires the use of two techniques working together to allow robust and repeatable results:

a. the development and continuous improvement of calcium sensors;

b. the development and the implementation of the appropriate instrumentation to detect and record the calcium fluctuations.

Bioluminescent calcium-binding photoproteins, such as aequorin[232,233], were the first proteins to be discovered and applied to achieve this goal. The implementation of these indicators was slow due to problems of dye delivery. Tsien and colleagues succeeded in developing the first generation of fluorescent calcium indicators consisting of quin-2, fura-2, indo-1, and fluo-3[234]. Among these, fura-2 was considered particularly useful because more quantitative calcium measurements were able to be detected[235] with this marker. An important next breakthrough, again from the laboratory of Roger Tsien[236], was the introduction of protein-based genetically encoded calcium indicators (GECIs). These were optimized and made more user friendly by Looger and Griesbeck and Rochefort et al[237,238]. The development of new imaging techniques evolved in parallel with the discovery of calcium binding photo proteins and dyes. This included the implementation of video imaging[239,240], charge-coupled device (CCD) cameras[241] and high-speed confocal microscopy[242] for calcium imaging. The introduction of two-photon microscopy in the early 1990s, by Winfried Denk and colleagues, represented a major advance in calcium imaging of the nervous system[243,244].

4.2 DA neurons, calcium homeostasis and electrophysiological characteristics

Ventral midbrain dopaminergic neurons located in the SNpc have a distinctive physiological phenotype. They are autonomously active and generate action potentials in a clock-like manner even without synaptic inputs. This capability is called pacemaker activity[245]. They also display an elevated intracellular Ca^{2+} concentration due to the fact that they use ion channels to allow the Ca^{2+} to enter the cell[246,247]. Cav1.3 pore-forming subunits are the channels used by DA neurons to evoke pacemaker action potentials. They are relatively rare, constituting only 10% of all the L-type Ca^{2+} channels found in the brain[248]. They have the capability of opening at relatively hyperpolarized potentials, enabling them to push the

cells to spike thresholds[249]. The sustained engagement of Cav1.3 Ca^{2+} channels during pacemaker activity comes at a great metabolic cost to the SNpc DA neurons. To avoid cellular stress and damage, Ca^{2+} entering the neurons is rapidly sequestered or pumped back across the steep plasma membrane concentration gradient. To do so it's necessary to use energy stored in ATP or in ion gradients that are maintained with ATP-dependent pumps. The two organelles most responsible for handling the Ca^{2+} crossing the plasma membrane are the same two organelles most closely linked to PD: the ER and the mitochondrion[246,250].

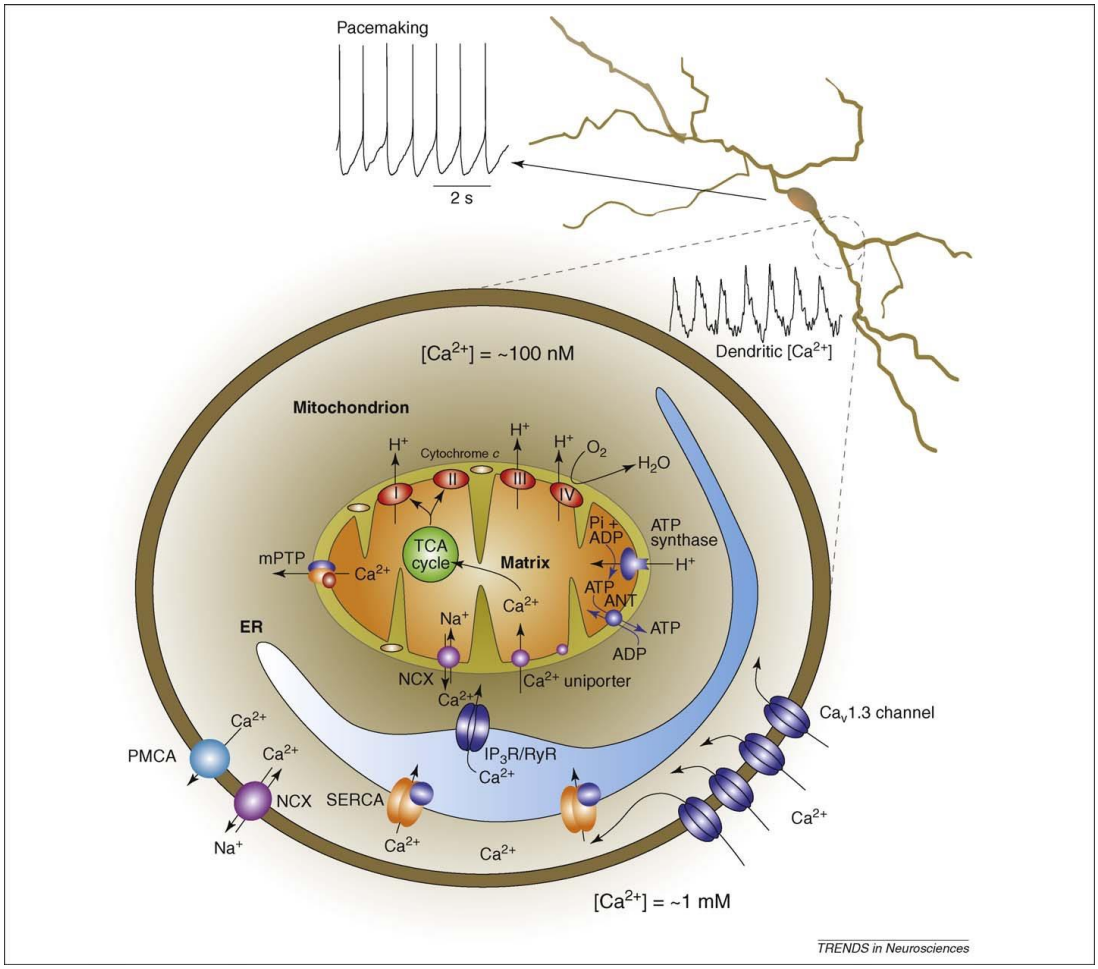

Fig 5.From: C. Chan et al. (2009). DOI: 10.1016/j.tins.2009.01.006250.

As distinctive as the physiological phenotype is the electrical activity of SNpc DA neurons. This activity is a consequence of the calcium oscillation in the dendrites of the neurons and is modulated by a complex and intricate interplay of distinct ion channels, transporters, and receptors. It is crucial for presynaptic and somatodendritic dopamine release, and hence for all dopamine-mediated functions[251]. The electric activity of DA neurons is further modulated

by dopamine, creating a negative feedback loop, by activation of the G-protein coupled K^+ channels (GIRK2) via dopamine auto-receptors of the D2-type (D2-AR).

4.3 Electrophysiological PD studies in animal models

Even though PD animal models do not optimally resemble all the characteristics of the disease, many studies have been performed to better understand the pathophysiology of dopaminergic neurons before the neurodegeneration.

A rotenone rat model was described as causing a syndrome that replicates both neuropathological findings and the behavioral symptoms of PD. Von Wrangel and colleagues[185] were able to reproduce PD specific motor phenotypes and selective loss of DA neurons in the SNpc. Interestingly, the study reveals that the loss of dopaminergic neurons after exposure to rotenone creates a specific electrophysiological phenotype on the connected neurons of the striatum:

- STN neurons discharged with a significantly higher firing rate
- STN neurons discharged with significantly more bursts per minute in the rotenone treated group
- STN neurons discharged with a highly entropic firing pattern

This study suggests that the loss of connection between two groups of neurons that are normally related can cause alterations in their activity causing hyper-activation and hyper-bursting behavior. These are known to generate stress and alter the functionality of the cells.

In another study, a mouse model with LRRK2 G2019S knock-in mutation was developed. LRRK2–G2019S mice generate abnormally elevated excitatory activity and altered spine morphology in dorsal striatal spiny projection neurons that is kinase dependent, a gain-of-abnormal activity that is outside the normal role of LRRK2 function. This paper confirms the previous data showing an alteration in the electrical and physiological activity of neurons connected with DA neurons. The hyperactivity and disorganization of the synapsis are phenotypes directly caused by PD related mutation[252].

MitoPark mice are a recently developed genetic model of PD that lacks the gene for mitochondrial transcription factor A in dopaminergic neurons. Using a MitoPark mouse, Branch and colleagues[253] investigated the activity of DA neurons in brain slices in order to obtain insight of the specific behavior of these cells before neurodegeneration. This model mimics many distinct characteristics of PD including progressive and selective loss of SNpc DA neurons, motor deficits that are improved by L-DOPA and development of inclusion bodies[210]. Using patch clamp technique, they were able to demonstrate multiple examples of declining functionality in single dopaminergic neurons across a range of ages; in particular

they show the disruption of the pacemaker activity, an increase in firing rate and a reduction in the firing peak and amplitude. DA neurons in the MitoPark mice also show a disruption in the presynaptic and postsynaptic vesicle systems, especially related to dopamine. All of these characteristics are consistent with the PD phenotype.

4.4 Human studies

One of the main goals of neuroscientists is to find the quickest, least invasive and most accurate way to obtain and automatize an early diagnosis of neurological diseases using molecular, structural and functional neuroimaging modalities[254]. Known examples exist for Alzheimer's disease[255–257], epilepsy[258], alcoholism[259], attention-deficit hyperactivity disorder[260] and major depressive disorder[261]. Searching for applications of these techniques for the early diagnosis of PD is a natural next step. Positron emission tomography (PET), functional magnetic resonance imaging(fMRI)[262,263], transcranial sonography[264], magnetoencephalography[265] or single-photon emission computed tomography are currently used to examine the dopaminergic system of the brain of PD patients to understand the pathophysiology. To identify alterations in early PD's patient brains, researchers try to find disorganization in the brains functional or effective connectivity[266]. Functional connectivity is defined as a temporal correlation between spatially remote neurophysiological events, whereas effective connectivity is defined as the influence that one neuronal system exerts over another[267]. It has been demonstrated that cases of PD combined with dementia are often correlated with a disruption of both functional and effective connectivity in the cortex[268]. Another symptom associated with PD is depression, which has been shown to be connected with disrupted functional connectivity between the median cingulate cortex and the precuneus, prefrontal cortex, and cerebellum[269].

There are many other examples that demonstrate altered connectivity between brain areas causing PD motor and non-motor symptoms. A recent publication proved, for the first time, a substantial change in the dynamic connectivity of PD patients' brains. Jinhee Kim and colleagues analyzed 31 PD patients and 23 healthy, age-matched controls and they observed two discrete connectivity configurations:

a. a more frequent, sparsely connected within-network state (State I), and

b. a less frequent, more strongly interconnected between-network state (State II).

Interestingly, patients with PD show a significant decrease in the occurrence of the sparsely connected State I (-12.62%), while the expression of the more strongly interconnected State II increased by the same amount. This phenotype seems to correlate with the clinical severity of PD symptoms and suggests a reduction in functional segregation among networks. The paper also describes a higher variability in PD network global efficiency and abnormal global integration of brain networks. These phenotypes confirm that the connectivity of a PD brain

is more vulnerable and displays higher susceptibility to stress and is overall more likely to display degeneration[270].

5. iPSC disease modelling and calcium imaging

As discussed previously, it is not yet known the extent to which neurodegeneration in PD results from intrinsic or cell-autonomous mechanisms, or whether non-neuronal cell types such as astrocytes or microglia play important roles in this process. The use of iPS cell technology, which allows the generation of different cell types from the same patient, makes possible the investigation of the impact of cell types other than DA neurons, for the first time. One of the main issues for modeling pathologies in vitro is the difficulty in obtaining the relevant cell type and producing an abundant number of differentiated cells to study early signs of neurodegeneration and test therapeutic treatments. To do this, we used a previously published protocol[216] that mimics the stages and processes of ventral midbrain DA neuron maturation, whilst applying an appropriate combination of growth factors and signaling molecules to develop this area of the brain *in vitro*.

Having successfully differentiated the iPSC to A9 DA neurons, those susceptible to neurodegeneration in PD, using calcium imaging techniques we can study the dynamic and functional behavior of these cells over a defined period of time that precedes the morphological degeneration. The data collected with this technique allow us to examine and visualize the evolution of connectivity in the A9 DA neuron cell culture and highlight the differences in functional behavior between the cell lines derived from PD and age-matched controls.

OBJECTIVES

Using iPSC derived from PD patients, we have created a proven *in vitro* model of the pathological phenotypes of PD[217]. Being able to reproduce PD phenotypes in a controlled environment gives us a unique opportunity to study the steps that precede neurodegeneration. We know from the literature that PD develops over the course of 20 years or more and that PD patients go through a period in which the DA neurons start to degenerate but no outward signs and symptoms are displayed. During this period the small percentage of DA neurons that are still not affected by the disease are capable of maintaining the physiological duties of the SNpc. This suggests that while some DA neurons are dysfunctional others are still healthy and are affected later.

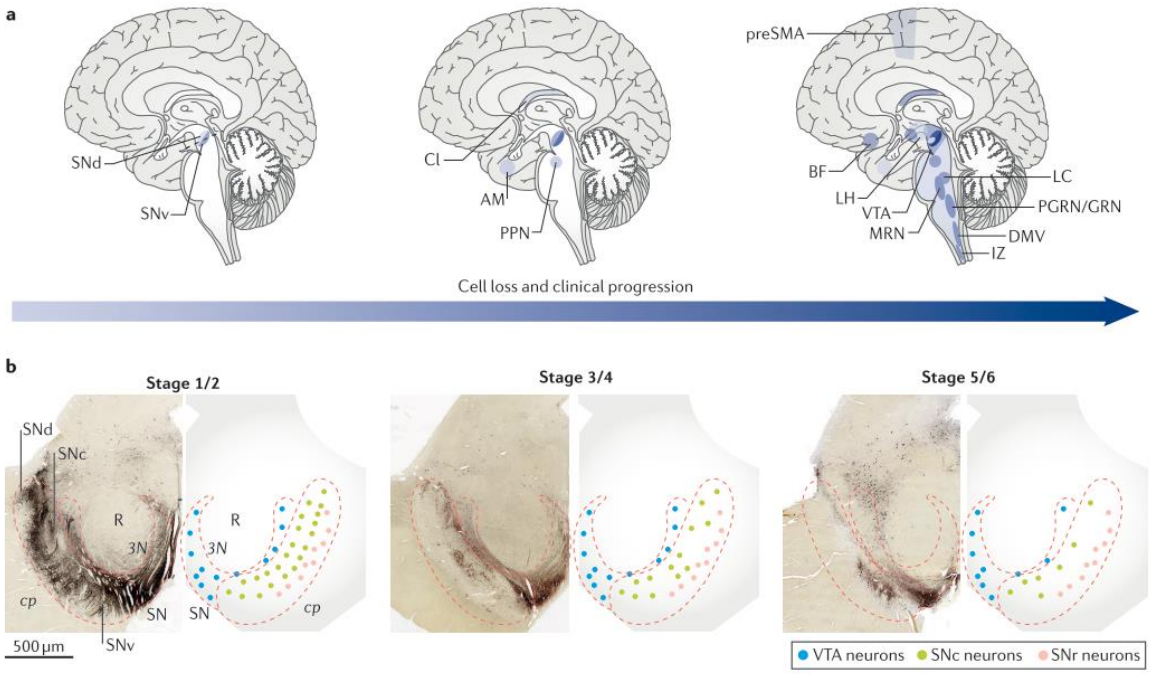

Fig 6. from D.Surmeier et al. (2017). DOI: 10.1038/nrn.2016.178.

Our model demonstrates the major neurodegenerative events, such as the synuclein accumulation and the selective loss of DA neurons *in vitro.* This allows us to undertake a comprehensive and multidimensional investigation to study this early phase of the disease where functional degeneration has started but is not yet systemic or symptomatic. The goals of this study are:

1. To identify early functional alterations in DA neurons differentiated from PD patient-specific iPSC:

    a. establish a robust cell culture system to derive human midbrain specific progenitor cells in order to obtain ventral midbrain dopaminergic neurons;

    b. study the spontaneous functional behavior of ventral midbrain DA neurons from PD patient specific lines compared to controls;

    c. individuate biological and molecular targets connected with functional impairment applying a gene expression profiling technique.

2. To investigate whether DA neurons degeneration in PD is truly a cell-autonomous phenomenon, or whether it is influenced by an altered cross talk between ventral midbrain DA neurons and glial cells.

MATERIALS and METHODS

1. iPSC information

We used 6 iPSC lines previously generated and characterized in our laboratory, as previously described[217,271]. These comprise one iPSC line obtained from a healthy donor (SP11) and two other lines obtained from Parkinson's disease patients carrying the LRRK2 G2019S mutation (SP12 and SP13). From these original lines, isogenic controls, differing in the presence of the LRRK2 G2019S mutation, were obtained by correcting the mutation to the SP12 iPSC line and by knocking-in one mutant allele into the *wild type* SP11 control iPSC line. Two *Tyrosine Hydroxylase* reporter iPSC lines were also generated by gene editing from the same parental SP11 and SP12 iPSC lines.

Table 4. Information on PD patients, controls and iPSC lines used in this study

Status	Code	Sex	Age	Age of onset	Family history	Mutation
Controls	SP11#1	F	48			
	SP11#1 TH	F	48			
	SP12#3 ED	F	63	49	Yes	LRRK2 (Corrected)
	SP13#4 ED	F	68	57	Yes	LRRK2 (Corrected
Mutants	SP12#3	F	63	49	Yes	LRRK2
	SP13#4	F	68	57	Yes	LRRK2
	SP12#3 TH	F	63	49	Yes	LRRK2

2. General cell culture protocols

2.1 iPSC

As described by Sanchez Danes et al.[271] a biopsy of keratinocytes or fibroblasts from PD patients and aged matched controls were cultured in serum-free low calcium medium and reprogrammed using a 1:1:1 mix of retro-viruses encoding FLAG-tagged OCT4, SOX2 and KLF4. A specific medium was used to select the reprogrammed cells composed by KO-DMEM (Invitrogen) supplemented with 20% KO-Serum Replacement (Invitrogen), 2 mM Glutamax (Invitrogen), 50 mM β-mercaptoethanol (Invitrogen), non-essential amino acids (Cambrex) and 10ng/ml βFGF (Peprotech). The selected cells acquired pluripotency

features. The cells were maintained at 37ºC, 5% CO_2 and the medium was changed every day. After 45/60 days, colonies that resemble iPCS morphology were manually picked and plated on top of human fetal fibroblast for at least 10 passages in order to remove the residual virus. Stock of iPSCs on feeder layers were cryopreserved and stored as a backup. After 10 passages on the feeder layer, iPSCs were manually passed on top of Matrigel coated plates and maintained in mTeSR™ medium to preserve the pluripotency. Another 5 passages, using Accutase enzyme, were carried out to adapt the iPSC to Matrigel condition. All the experiments were done using Matrigel adapted iPSC. These lines were characterized fully for pluripotency in the previous cited paper.

3. Evaluation and amelioration of neuronal generation protocols and NPCS

We tested multiple different protocols that could be used to obtain an enriched culture of DA neurons as these are the neuronal population that is most relevant for the study of PD.

Crucial for the aim of my project was to have a feeder's free culture to allow us proper usage of the calcium imaging assay.

The best working protocol to generate DA neurons is derived from the one published by Kriks et al[216]. I set up and adapted the protocol to our line and cell culture conditions.

3.1 Generation of ventral midbrain precursors from monolayer

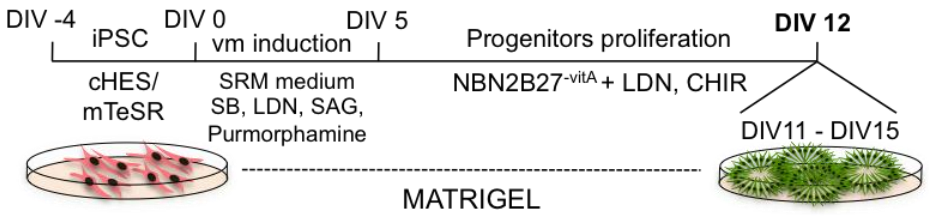

Fig 7. Schematic representation of the first steps of the floorplate protocol that we used to differentiate iPSC into ventral midbrain specific DA NPCs.

Kriks et al. have developed a new protocol based on the neurodevelopmental steps that happen during the embryogenesis *in vivo*. This protocol is based on culturing iPSC in

conditioned medium HES or mTeSR commercial medium until they reach 80% confluence. Then ventral midbrain induction is forced by switching to SRM medium (KO-DMEM, 15% KO serum, 1%P/S, 1% glutamine, 1% NEAA, 0,1% beta mercaptoethanol) with SB Tocris 1614 (selective inhibitor of the grow factor TGF-β), LDN193189, Stemgent 04-0074 (BMP inhibitor) to inhibit the dual SMAD pathway, SAG and Purmorphamine, Calbiochem 540220 (SHH pathway activators) to induce neuroepithelial stem cells formation and proliferation. Next the medium is changed to Neurobasal with 1% P/S, 1% N2 and 2% B27-VitA and CHIR99021, Stemgent 04-0004 (CHIR), a potent GSK3B inhibitor known to strongly activate WNT signaling that induces LMX1A in FOXA2 ventral midbrain dopaminergic neuron precursors. We used this combination to induce dopaminergic differentiation of midNESC, with some modifications. We fix in PFA 4% (paraformaldehyde) culture the cells for 11, 12, 13, 14, 15 day to check the best co-localization between FoxA2 and Lmx1A.

3.2 Generation of ventral midbrain precursors from embryoid bodies

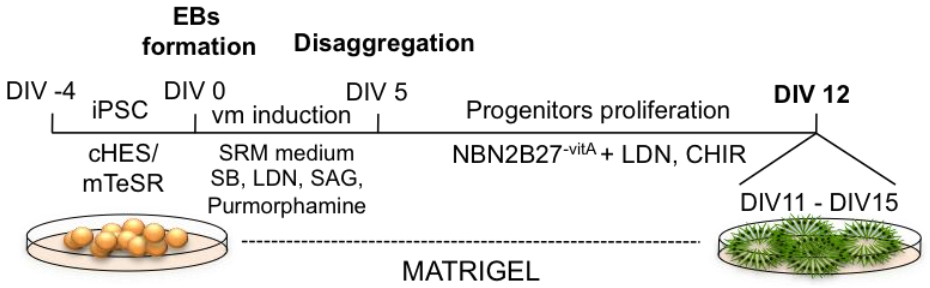

Fig 8. Schematic representation of the first steps of the alternative protocols that we apply to generate ventral midbrain specific DA NPCs

In parallel we tested another protocol published by A. Kirkeby and derived from Kriks's protocol. We performed this test to verify if this method allows us to obtain a greater population of vmDA neurons. We used the same medium, which we use for the monolayer floorplate protocol. Instead of plating the iPSC as a monolayer this protocol required the formation of EBs (embryoid bodies). These are cultured for 5 days in suspension, and then selected neural structures were disaggregated and plated. Following the precursor generation we fix in PFA4% the culture at D11 to D15, and verify again the best co-expression of FoxA2 and Lmx1A. This protocol showed a lower efficiency and was not used further in the study.

4. Generation of DA neurons using monolayer progenitors

4.1 Non edited lines: CTR (SP11#1), PD1 (SP12#3) and PD2 (SP13#4)

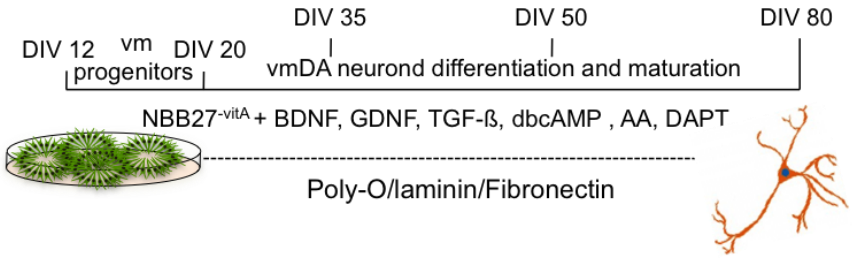

Fig 11. Schematic representation of the last steps of the floorplate protocol that we used to differentiate NPCs into ventral midbrain DA neurons.

After generating and characterizing the ventral midbrain DA precursors, these cells were cultured in Neurobasal medium, 1% P/S and 2% B27-VitA with neurotrophic factors: the transforming growth factor family (TGFβ2/3) Peprotech (Poulsen et al., 1994; Roussa et al., 2009); members of the neurotrophin family, such as brain-derived neurotrophic factor (BDNF) Peprotech (Frim et al., 1994; Hyman et al., 1991); glial cell-line-derived neurotrophic factor (GDNF) Peprotech (Akerud et al., 2001; Arenas et al., 1995; Beck et al., 1995; Choi-Lundberg et al., 1997; Gash et al., 1996; Kordower et al., 2000; Lin et al., 1993; Rosenblad et al., 1998; Tomac et al., 1995); and other compounds such as AA (ascorbic acid) known to increase the expression of genes involved in neurogenesis, maturation, and neurotransmission (Neuroreport. 2004 Aug 26;15(12): 1959-63. Ascorbic acid responsive genes during neuronal differentiation of embryonic stem cells. Shin DM1, Ahn JI, Lee KH, Lee YS, Lee YS.); DAPT Tocris 2634, γ-secretase inhibitor (Notch inhibitor); dbcAMP Calbiochem, dibutyryl cyclic adenosine monophosphate, known to increase neuronal survival and differentiation.

At D20 the precursors were split into wells previously coated with Poly Ornithine (15 ug/ml left in it overnight and washed 3 times in DPBS), human Laminin (1 µg/mL filtered and left overnight) and Fibronectine (2 µg/mL left in overnight); all of which were diluted in DPBS. The number of cells plated for each well is important because it influences the survival of the culture (100,000 cells in 24 well plates and $1*10^6$ cells in 6 well plates). The neurons were plated using the center-plating technique.

Cells were differentiated for 15, 30 and 60 days (D35, D50 and D80), fixed in PFA 4% and characterized for ventral midbrain DA specific markers like TH, Girk2 (G-protein in DAn), DAT (dopamine transporter) and FoxA2 (transcriptional activator for DAn differentiation) and

mature neuron markers like MAP2. Other neural markers were tested: 5-HT, GABA, Calbindin and GFAP to verify if there was contamination from other neural populations.

5. TALENTs and CRISPR/Cas9 edited lines generation: Isogenic line isoPD1 (SP12#3) and isoPD2 (SP13#4)

For correcting the LRRK2 G2019S mutation, iPSC from PD1 (SP12#3) and PD2 (SP13#4) were gene-edited using TALENs. iPSC are grown to confluence in 10cm plates. 2-4 hours before the gene editing procedure they are treated with 10 µM Y-27632 (RI; Miltenyi-Biotech). After two to three hours, iPSC were disaggregated to small clumps using Accutase (eBiosciences), re-suspended in ice-cold cHES medium supplemented with RI and containing 15 µg of each TALEN monomer-coding plasmids and 30 µg HDR donor template and placed in an electroporation cuvette. Cells were electroporated with a Gene Pulser Xcell electroporation system (BioRad) set to 250 V and 500 µF (time constant should be between 10 and 14 milliseconds). After being pulsed, the cell suspensions were seeded in 10 cm plates coated with Matrigel containing RI-supplemented cHES medium. 72 hours post-transfection, 50 µg/mL G-418 (Melford Laboratories Ltd.) treatment was initiated and maintained for 2 weeks until resistant colonies attained enough size to be screened. At that moment, half of each resistant colony was manually picked and site-specific integration was verified by means of PCR and Sanger sequencing assessed gene correction. The clones were expanded, cryopreserved and karyotyped.

5.1 TH reporter lines

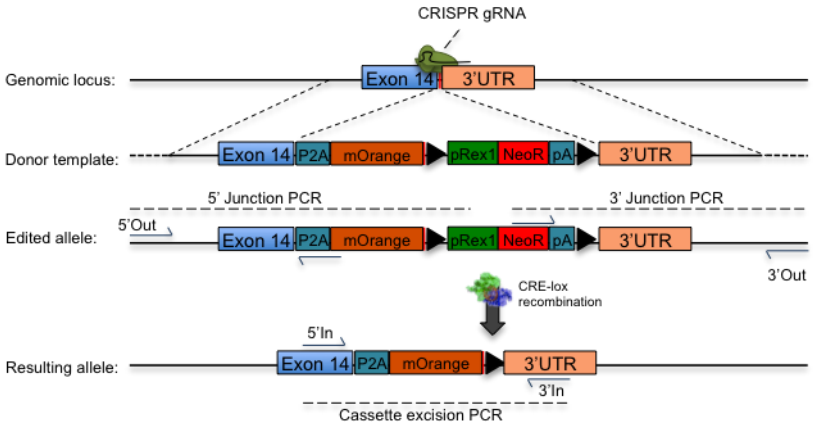

Fig 15. Scheme describing the recombination steps during the editing process. Blue arrows represent the primers used for the PCR screening procedure. Black triangles represent LoxP sites surrounding the selection cassette.

We edited CTR (SP11#1) and PD1 (SP12#3) lines with CRISPR/Cas9 plasmid pSpCas9(BB)-2A-GFP (PX458)[272] obtained from Addgene (#48138). The original pCbh promoter was exchanged for the full-length pCAGGS promoter in order to achieve higher expression levels in iPSC. Custom guide RNAs were cloned into the BbsI sites as annealed oligos.

For the TH donor template, homology arms were amplified from genomic DNA and verified by Sanger sequencing. Resulting sequences matched those of the reference genome GRCh38. They were inserted into the KpnI-ApaI (5'HA) and SpeI-XbaI (3'HA) sites of pBS-SK(-). P2A peptide was added to mOrange, with the primers used to amplify the gene, and the PCR product was inserted into the ApaI-XhoI sites of the pBS-5'HA-3'HA plasmid. Finally, pRex1-Neo-SV40 was inserted between the XhoI and SpeI of the previous plasmid.

For the generation of TH reporter iPSC cell lines, iPSC are grown to confluence in 10cm plates and co-transfected with 6 µg of CRISPR/Cas9 plasmid and 9 µg HDR template using FuGENE HD (Promega) at a 1:3 DNA to reagent ratio. 72 hours post-transfection, 50 µg/mL G-418 (Melford Laboratories Ltd.) treatment was initiated and maintained for 2 weeks until resistant colonies attained enough size as to be screened. The colonies that contain the genetic reporter are selected and we proceed with the excision of the selection cassette. Edited iPSC are transfected with CRE recombinase-expressing plasmid (gifted from Dr. Michel Sadelain - Sloan Kettering Institute; Addgene plasmid #27546). 48 hours post-transfection, cells were singularized and seeded at clonal density on a feeder layer of irradiated human fibroblasts. Once colonies attained a certain size they were picked and cultured in independent matrigel-coated wells. Cells were sampled and checked for cassette excision by PCR and Sanger sequencing. Those clones in which the cassette was excised were expanded, cryopreserved and karyotyped.

5.2 TALENTs and Crispr/Cas9 edited lines differentiation

DA neurons were generated from the edited lines (both isogenic and TH reporter) using the same protocol described above with minor modifications. We noticed that these cells were more likely to die during the differentiation, so we decided to change little details during the first step of precursor generation and the final step of DA neuron differentiation and maturation to increase the survival and the ventral midbrain differentiation efficiency.

Briefly, instead of switching the medium abruptly we gradually passed from SRM medium to NBN2B27^{-VitA} during D5 to D9 of progenitor induction. We maintained CHIR in the medium until D20 and we split the progenitors using Rock inhibitor (Miltenyi). The next day, half of the medium was changed and from that day on CHIR was removed.

As well as the previous non edited lines, at D20 the precursors were split into wells previously coated with Poly Ornithine (15 ug/ml left in it overnight and washed 3 times in DPBS), human Laminin (1 µg/mL filtered and left overnight) and Fibronectine (2 µg/mL left in overnight); all of which were diluted in DPBS.

Neurons were differentiated for 15, 30 and 60 days (D35, D50 and D80), fixed in PFA 4% and characterized for ventral midbrain specific markers like TH, Girk2 (G-protein in DAn), DAT (dopamine transporter) and FoxA2 (transcriptional activator for DAn differentiation), and mature neurons markers like MAP2.

6. Immunocytochemistry

iPSC in distinct stages of differentiation were used to characterize protein expression using immunocytochemistry. All the cultures were fixed with 4% PFA for 15 minutes, washed three times with DPBS for 15 minutes, then washed with TBS1x (low Triton protocol for vesicles specific antibodies) or with TBS1+ (with 0.3% Triton for standard protein immunocytochemistry) 3 times for 15 minutes and then blocked for 2 hours with TBS+ with 0.1% Donkey Serum with 0.3% Triton or 0.01% Triton depending on the normal or low Triton protocol. Primary antibodies were incubated for 48 hours at 4ºC. After 48 hours incubation with the primary antibody, samples were washed with TBS 1x/TBS+ for 15 minutes three times. Then the blocking was repeated for 1 hour at room temperature followed by 2 hours incubation with the secondary antibodies (all at a dilution of 1:200). The samples were washed with TBS 1x for 15 minutes three times and then incubated with nuclear staining DAPI (Invitrogen, dilution 1:5000 in TBS1x) for 10 minutes. After washing twice the DAPI with TBS1x samples were mounted with PVA:DABCO, dried for 2 hours at room temperature and stored at 4ºC until imaged. Samples were imaged using an SP5 confocal microscope (Leica®) and analyzed with FIJI® Just ImageJTM®. The following antibodies were used:

Table 5: Information on primary antibodies used in this study

Antibody	Species	Reference	Dilution	Low Triton
MAP2	anti-Rabbit	Santa Cruz sc-20172	1:1000	NO
GIRK2	anti-Rabbit	Sigma P8122	1:40	NO
FOXA2	anti-Mouse	R&D Systems (AF2400)	1:250	NO
LMX1A	anti-Rabbit	Millipore (AB10533)	1:1000	NO
Engrailed (D-20)	anti-Goat	Santa Cruz (sc-46101)	1:200	NO
Nestin	anti-Rabbit	Chemicon (AB5922)	1:250	NO
α-synuclein	anti-Mouse	BD, 610787	1:500	SI
TH	anti-Sheep	Pel-Freez, P60101-0	1:500	NO
TH	anti-Rabbit	Santa Cruz, sc-14007	1:250	NO
DAT	anti-Rat	Chemicon (MAB369)	1:300	YES
RFP	anti-Rabbit	Abcam (ab34771)	1:400	NO

Table 6: Information on secondary antibodies used in this study

Antibody	Species	Product Code
Alexa Fluor 488	anti-Mouse IgG	Jackson 715-545-150
Cy3	anti-Rabbit IgG	Jackson 711-165-152
DyLight 649	Anti-Mouse	Jackson 706-495-148
Alexa Fluor 647	anti-Sheep	Jackson 713-605-147
Cy3	anti-Rat IgG	Jackson 712-165-153
Cy™2 AffiniPure Donkey	Anti-Rabbit IgG (H+L)	Jackson 711-225-152
Cy™3 AffiniPure Donkey	Anti-Mouse IgG (H+L)	Jackson 715-165-151

7. Neurite quantification

The images were analyzed using the program NeuronJ® to quantify the length and differentiate the type of neurite for both TH+ and MAP2+ cells. For each neuron, primary, secondary and tertiary neurites were highlighted and classified in the program and each trace was automatically measured and organized in order to obtain information for each single cell. An average of 5 images with 10 neurons in each image at each timepoint was quantified for TH+ analysis. 5 images with 5 neurons in each image at each timepoint were used to extract the MAP2+ data.

8. Calcium imaging

We used calcium imaging[224,225,273,274] to evaluate the differences in spontaneous activity between healthy and PD neurons. Calcium imaging allows the monitoring of a large population of neurons, simultaneously and non-invasively, which makes it particularly suitable for whole network analyses. Living neurons were incubated for 30 minutes in a solution that contained 3ml of recording medium (EM, consisting of 128 mM NaCl, 1 mM CaCl2, 1 mM MgCl2, 45 mM sucrose, 10 mM glucose, and 0.01 M Hepes; treated to pH 7.4) and 4 µg/ml of the cell-permeant calcium sensitive dye Fluo-4-AM. At the end of incubation, we washed the culture with 2 ml of fresh EM to remove residual free Fluo-4. This medium was then discarded to place 4 ml of fresh EM, the final medium for actual recordings. The culture dish was mounted on a Zeiss inverted microscope equipped with a CMOS camera (Hamamatsu Orca Flash 2.8) and an arc lamp for fluorescence. Grey scale images of neuronal activity were acquired at intervals of 20 frame per second and a spatial resolution of 4.40 µm/pixel. Images had a size of 960 × 720 pixels with 256 gray-scale levels. The latter settings provided a final field of view of 2.8x2.1 mm that contained between 300 and 700 neurons. Cells were imaged in bright field and then for 15/30-minute recordings using Hokawo® software[275]. Next, calcium fluorescence traces were retrieved using customized software based on MatLab® First, a manual selection of Regions of Interest (ROIs) was

carried out to track the activity of cells that had prototypical neuronal morphology. After analyzing the recording, further post-processing allowed the removal of fluorescence traces not corresponding to stereotyped neuronal firing (either non differentiated cells or glia). Data was finally averaged among the minimum 2 replicates of each time-point. Hence, our results are based on a population of at least 500 neurons per time-point.

Thanks to this program if was possible to obtain all the different information to analyze the behavior of the neurons:

- Clumps and unclear ROIs were excluded,
- Peaks of calcium fluorescence,
- Video of the registration,
- Percentage of active neurons.

8.1 Data analysis

In order to reconstruct the neurons' activation sequence, we first isolated a particular bursting event from the rest of the sequence. Next, for the fluorescence signal of each neuron, we carried out two linear fits: one fit of the data points preceding the firing and another one of the points encompassing the fast increase in fluorescence. The crossing point of the two lines provided the activation time of the neuron. This process was repeated for all neurons, and the final activation time dataset was ordered to reconstruct the neurons' firing sequence.

8.2 Network dynamics

We represented the overall neuronal fluorescence activity of each experiment as a raster plot in which each neuronal calcium transient, or burst, is plotted as a dot against its initiation time. The collective activity of a large set of neurons can be summarized, allowing for the fast identification of particular ensemble dynamics such as synchronization in the form of hyper-bursting or low-amplitude oscillations.

8.3 Global network activity

We investigated the collective activity of the whole set of studied experiments by analyzing their neuronal firing sequences. We summed all the firing events occurring in a sliding window of 1s in length (20 frames) and normalized the count by the number of neurons analyzed in each experiment (corresponding to selected ROIs), allowing for the computation of the Global Network Activity (GNA) of each experiment.

8.4 Extreme events

After computing GNA, we selected the maxima of each GNA trace that had a predefined prominence. In this sense, a point was considered a maximum peak if it has the maximal value and was preceded (to the left) by a value lower than a threshold amplitude delta. We extracted the statistics of GNA amplitudes and considered extreme events to be those maxima displaying amplitudes above the average GNA level plus one standard deviation. We calculated the z-score for each extreme as:

$$z = \frac{x - \mu}{\sigma}$$

- x is the value of the maxima,
- μ is the average maxima height and
- σ is the standard deviation of the distribution of maxima.

We considered extreme events to be those peaks with a z-score above 0.96. After considering these peaks, we computed the ratio of extreme events by dividing the number of peaks matching our criteria by the overall number of peaks found. We also computed the

frequency of extreme events by dividing the number of extreme events found by the time duration of the experiment in minutes.

8.5 Neuronal networking and functional analysis

To better understand the functional connections between each active neuron we identified causal relationships between neuronal firings using measures that identify the flow of information between two firing sequences. Besides, we analyzed the functional organization of all networks in terms of its fitness to models of hierarchical structures, as explained below.

8.5.1 Effective connectivity analysis

The sequences of neuronal activations give us the information about the degree of causal influence between any pair of cells in the network. If the firing of a neuron *j* concurrently follows the firing of a neuron *i*, the principle of causality establishes an increased probability that the activity of *i* induces the activity of *j*. The likelihood of this relationship is weighted based on the frequency of occurrence along the observational time. Such algorithm provides the effective connectivity between neurons in a network.

8.5.2 Closeness to free scale distribution

We hypothesized a scale-free organization of functional networks in the cultures and computed how much the retrieved topology diverged from our hypothesis. The model we used is an extension of the Barabási and Albert algorithm [276]called *Initial Attractiveness* model, which reads:

$$p_k = C(k + A)^{-\gamma}.$$

In this model, three parameters control the degree of distribution of a network p_k in order for it to display a low degree cut-off, resembling some of the distributions we found in our analyses. *A* is the *initial attractiveness* parameter, which indicates whether the network is in the random network regime (high *A*) or scale-free (low *A*). Besides, an exponent γ larger than 3 (which particularly corresponds to the standard Barabási-Albert model) is indicative of a random network organization. Finally, C provides the 'steepness' of the probability

function in a log-log representation. We fitted our data to this model using the least square error method[277] and computed the coefficient of determination R^2 [278]. An R^2 value close to 1 denoted a close fit between data and model, whereas a low R^2 value represented a bad fit between data and model. Since our model generates hierarchical topologies known to be characteristic of neuronal networks, we classified our cultures as being topologically organized if their functional organization fitted a hierarchical model of degree of distribution and disorganized otherwise.

9. Molecular biology

9.1 DNA and RNA extraction

9.1.1 DNA extraction

Genomic DNA was extracted from cells to verify the correct insertion of the specific plasmid in the appropriate locus during the gene editing technique. To obtain genomic DNA Ethanol/NaAc precipitation protocol was used. Cells were plated in 96 well plate for the screening, gently detached from the plate with 30μl of Accutase and 70μl of cHES. 50μl of the cell suspension was re-plated and 50μl were placed in another 96 well plates with the V bottom and used for genomic DNA extraction and gene editing screening. The rest of the cells were re-plated to maintain the colony and be able to identify it if the editing was correct.

The cells suspension was centrifuged at 1200rpm for 10 minutes to collect the cells on the bottom of the well without breaking them. After discarding the medium, 50μl of lysis buffer (PBS with Proteinase K 50ug/mL and 1.7 uM of SDS) was added in each well and incubated over night at 55ºC. The next day 10μl of NaAc 3M and 40μl of isopropanol were added in each well. The plate was then vortexed and centrifuged at maximum speed for 15 minutes. The supernatant was discarded and the pellet washed with 100μl of Ethanol 70%. A second centrifugation at maximum speed for 15 minutes was done and the ethanol was removed. The pellet was resuspended in 30μl Eluition Buffer (EA) Quiagen and used for PCR and Sanger sequencing.

Plasmid DNA extractions from bacterial culture were obtained following the protocol of the Quiagen Mini Kit.

9.1.2 RNA extraction

RNA extraction was performed using the TRIZOL protocol. To optimize the extraction, cells were quantified and re-suspended in TRIZOL at a volume of 5×10^6 cells / 1ml TRIZOL. The

cell suspension was incubated in TRIZOL at room temperature for five minutes and then 200μl chloroform / 1mL TRIZOL were added. The eppendorf was vortexed for 15 seconds, and left at room temperature for 2-3 minutes. From this step on, the samples were maintained in ice in order to inhibit the RNAse enzymes physiologically present in the cells. Next, we centrifuged the sample at 12,000rpm for 15 minutes at 2-8 ºC. The centrifugation allows the sample to separate into three phases visible within the tube. We transferred the aqueous phase (top) that contains the RNA to a fresh tube, being careful not to contaminate the solution with the other phases. Contamination will be obvious by the presence of any flakes or unclear liquid.

500ul isopropanol /1ml TRIZOL (previously used) was added to the new tube and incubated in ice for 10 minutes so the RNA could precipitate. The samples were centrifuged at 12,000rpm for 10 minutes at 2-8ºC. The supernatant was removed and the pellet was washed with 500μl 80% EtOH. The samples were centrifuged again at 7,500rpm for 5 minutes at 2-8ºC. After removing the supernatant it's important to allow the remaining Ethanol to air dry for 2-3 minutes. Dissolve the pellet in RNAse free water from Quiagen.

These samples were used to generate cDNA and perform qPCR to characterize the ventral midbrain dopaminergic neurons culture.

9.1.3 RNA extraction for gene expression profile with nanoString nCounter

To perform gene expression profile analysis RNA was extracted from D50 DA neurons using RNEasy mini kit from Qiagen. Briefly cells were washed with DPBS, lifted with a scraper and collected in a DPBS suspension. The cells were quickly centrifuged for 15 seconds to avoid any membrane rupture and the supernatant was removed. The cells were disrupted by adding 350μl Buffer RLT Plus. The cells were vortexed for at least 1 minute in order to obtain a homogeneous lysate. The homogenized lysate was transferred into a gDNA Eliminator spin column placed in a 2ml collection tube, centrifuged for 30 seconds and the flow-through with the RNA was saved. 350μl of 70% Ethanol was added and up to 700 μl of the sample, including any precipitate that may have formed, was transferred to an RNeasy spin column placed in a 2ml collection tube. The column was centrifuged several times and washed with different buffers to ensure the purification of the RNA. The RNA conserved in the filter of the column was eluted using RNAse free water (40μl) and stored at -20ºC.

9.2 PCR

In our standard PCR protocol we mix all the components in a PCR thin walled 0.2ml tube with a final volume of 50µl or less. All the reagents were thawed on ice. The reagents were added in the following order: water, buffer, dNTPs, $MgCl^2$, template primers, Taq polymerase. The reaction tube was gently mixed by tapping and briefly centrifuged to settle tube contents. Negative and positive controls were prepared, the first without template DNA, the second with a template of known size and appropriate primers. The result of the PCR was analyzed by electrophoresis gel.

Table 7: PCR mix components

Component	Final Concentration/Amount
Water	To 50 µl
Buffer	2 X Or 5x
Taq Polymerase	0.05 Units/µl
dNTPs	100 µm
$MgCl^2$	0.1-0.5 Mm
Forward Primer	0.1-0.5 µm
Reverse Primer	0.1-0.5 µm
Template	Depending on the concentration

Table 8: PCR termocycler steps

Step	Temp	Time	# of cycles
Initial Denaturation	94°C	5 min	
Denaturation	94°C	30 sec	
Primer Annealing	Tm of primers-5°C	45 sec	30-35
Extension	72°C	1 min per kb	
Final Extension	72°C	5 min	

9.3 rtPCR

The isolation of total mRNA was performed using a Quiagen RNA mini kit. One microgram was used to synthesize cDNA with the SuperScript III Reverse Transcriptase Synthesis Kit (Invitrogen). Quantitative RT-PCR analyses were done in triplicate on 50ng with Platinum

Syber Green qPCR Super Mix (Invitrogen) in an ABI Prism 7000 thermo-cycler (Applied Biosystems). All results were normalized to GAPDH.

9.4 Sample preparation for gene expression profile with nanoString nCounter

All the steps were done in ice and using the nCounter nanoString reagent for Neuropathology panel. The master mix for the hybridization process was prepared by mixing hybridization buffer and reporter CodeSet.

A dilution of 10µg/µl for each RNA to be analyzed was prepared and maintained in ice. For each sample a tube was prepared with 5µl of RNA (10µg/µl) and 8µl of master mix. 2µl of Capture ProbeSet was added in each tube and the hybridization process was started using a PCR machine at 65ºC for at least 16 hours. After this step, the samples were maintained at 4ºC.

Once the hybridization process was completed the hybridized RNA was loaded in the neuropathology cartridge and the data were available 24 hours later.

9.5 ROSALIND bioinformatics analysis

Read Distribution percentages, violin plots, identity heatmaps, and sample MDS plots were generated as part of the QC step. The limma R library[279] was used to calculate fold changes and p-values. Clustering of genes for the final heatmap of differentially expressed genes was done using the PAM (Partitioning Around Medoids) method using the fpc R library[280,281] that takes into consideration the direction and type of all signals on a pathway, the position, role and type of every gene, etc. Functional enrichment analysis of pathways, gene ontology, domain structure and other ontologies was performed using HOMER[282]. Several database sources were referenced for enrichment analysis, including Interpro[283], NCBI[284], KEGG[285–287], MSigDB[288], REACTOME[289], WikiPathways[290] Enrichment was calculated relative to a set of background genes relevant for the experiment.

RESULTS

1. Generation and characterization of neural progenitor cells (NPCs)

Many existing differentiation protocols have a basic DA neuron phenotype (TH-positive cells) as the target, but more recent protocols tend to be designed for obtaining DA neurons of a specific DA subtype such as A9 DA neurons (TH/GIRK2-TH/DAT-TH/FoxA2 double-positive neurons). Even though we can reproduce early developmental morphogenic stimuli and differentiate neural progeny from human pluripotent stem cells, many of the cells derived from human iPSC remain immature. Differentiation to a specific cell type is unavoidably accompanied by contamination with other cell types. Defining the stages and processes of DA neuron maturation has an important impact on the cell integration, migration and differentiation in transplantation studies. Identifying an appropriate combination of growth factors and signaling molecules that mimic as closely as possible the development of the human brain is also an important area of investigation.

We checked our dopaminergic progenitors at different time points to verify the co-expression of LMX1A and FOXA2 (Figure 17)

We obtained the best co-localization staining at D12 so we decided to check the expression of the other known markers of ventral midbrain fate at this stage. Both the controls and LRRK2-PD lines show a correct expression of the progenitors' markers. From D0 to D12 iPSC were cultured in a specification medium that helped them to reach the ventral midbrain fate.

From D12 to D20 the progenitors were cultured in a maturation medium with neurotrophic factors that accelerates their maturation. No differences were found between controls and LRRK2-PD progenitors (Figure 18).

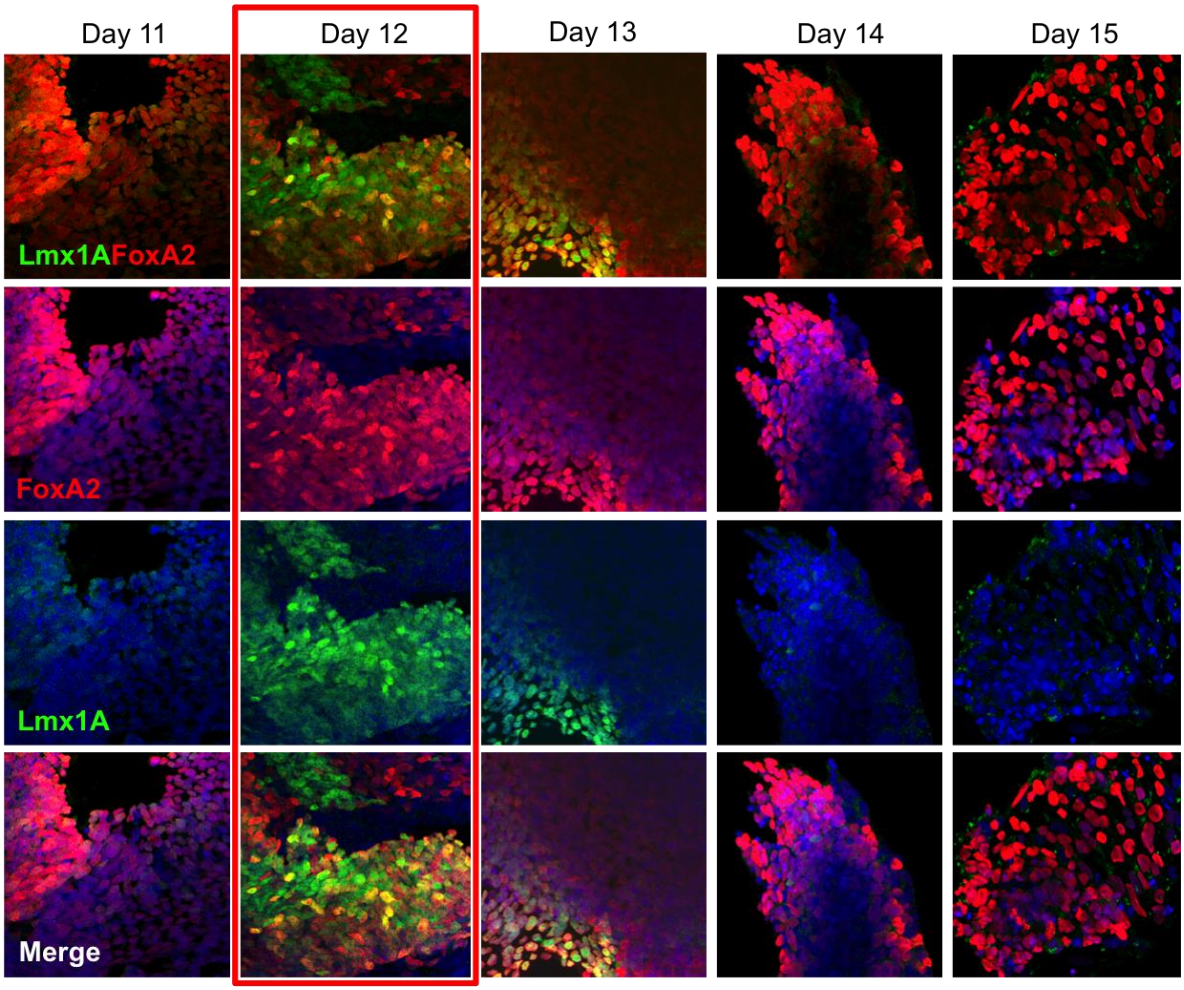

Fig 17: **Timeline of DA progenitors stained for FOXA2 and LMX1A**. Immunocytochemistry of CTR SP11#1 DA progenitors at different timepoints of differentiation (Day 11, 12, 13, 14 and 15) stained for FOXA2, LMX1A and DAPI. The experiment highlights the best co-localization time of the two ventral midbrain markers at day 12.

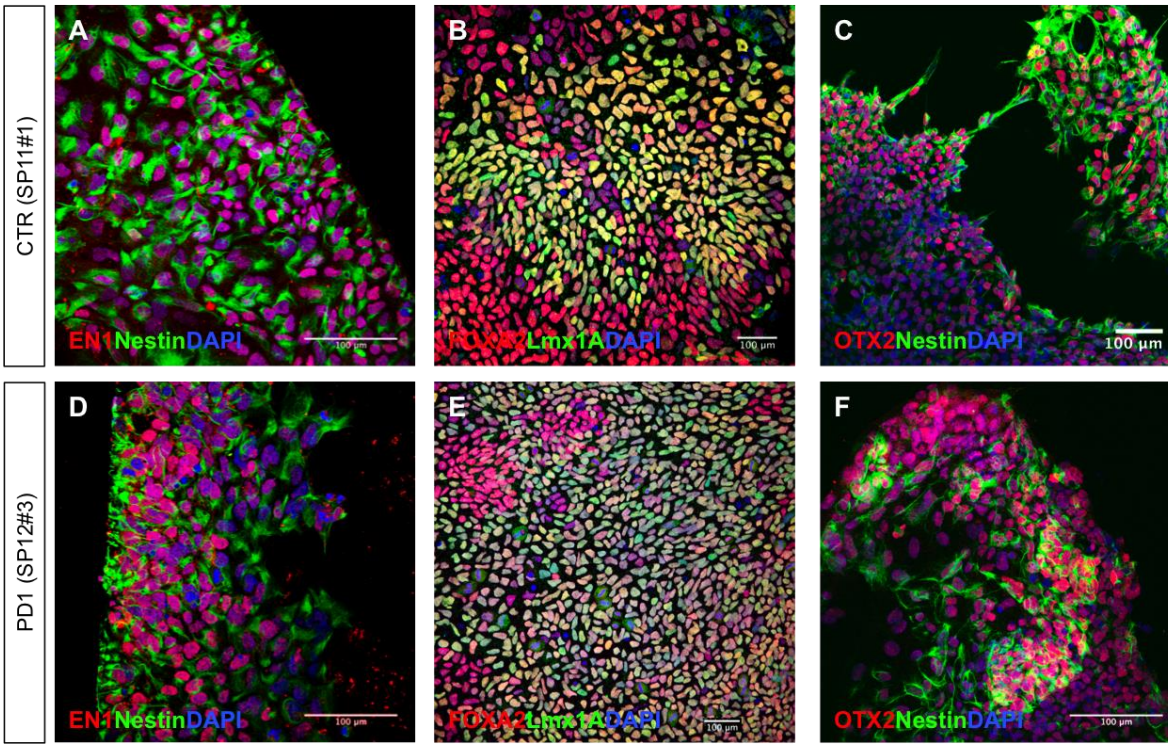

Fig. 18: **Characterization of D12 DA progenitors.** Immunocytochemistry of DA progenitors of CTR SP11#1 and PD1 SP12#3 at D12 of the differentiation process. The experiments show a consistent expression in both lines of ventral midbrain specific markers such as EN1, FOXA2, LMX1A and OTX2.

2. Generation and characterization of DA neurons

At D20 the progenitors were placed on top of cover glass coated with a combination of polyornithine, laminin and fibronectin: proteins which reinforce the neuronal differentiation. From this day on the neurons are maintained in maturation medium with neurotrophic factors for 15, 30 and 60 days (D35, D50 and D80).

At D50 of the differentiation process, the DA neurons derived from ventral midbrain NPCs were analyzed using immunocytochemistry (ICC), in order to obtain a complete characterization of the cultures. All the differentiated lines were tested for neuronal markers including MAP2 (indicating mature neurons), TH (indicating dopaminergic neurons), Calbindin (indicating interneurons A10) and 5-HT (indicating serotonergic neurons). This showed:

a. a full commitment towards mature neurons (~90% of MAP2/DAPI),

b. a high expression of TH (30-35% of TH/DAPI),

c. no markers for GFAP astrocytes,

d. episodic appearance of other types of neurons. (Figure 19).

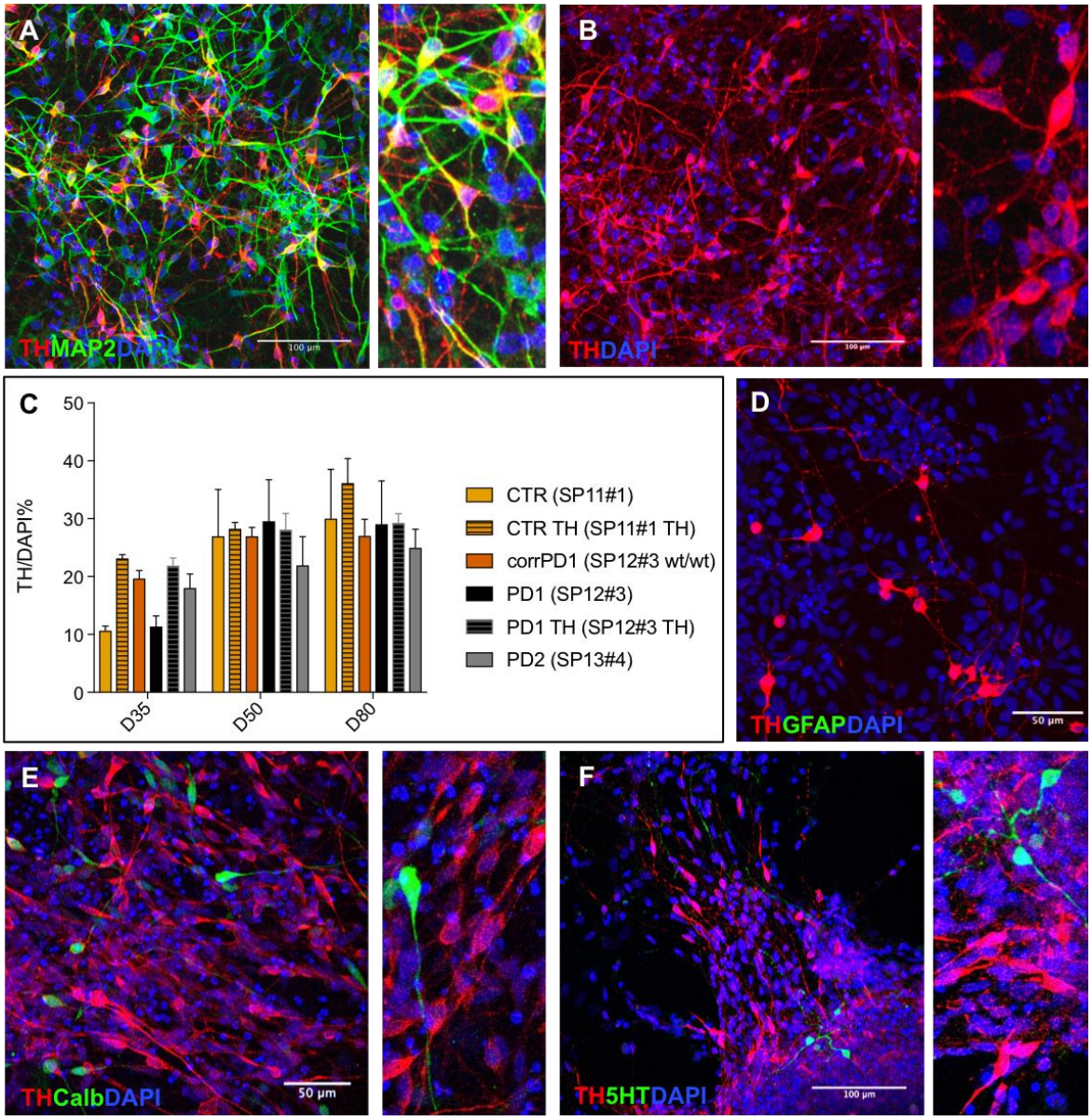

Fig. 19: **Characterization of D50 DA- enriched neuronal culture.** Immunocytochemistry of control SP11#1 neurons at D50. Representative images of a D50 cuture stained for (A) MAP2 co-expressed with TH, dopaminergic specific marker. (B) TH dopaminergic marker with the relative quantification in each differentiated line (C), (D) TH and GFAP marker of astrocytes always absent from the culture, (E) TH and Calbindin, markers of A10 interneurons, and (F) TH and 5HT marker of serotonergic neurons.

Markers for midbrain DA neurons (FOXA2, GIRK2) and their quantification (Figure 20) confirm the commitment of the culture toward a ventral midbrain dopaminergic fate. DAT dopamine transporter marker, Synapsin1 marker for synaptic vesicles and PSD95 markers for post synaptic vesicle were used to confirm the capability of our neuronal culture to create

synaptic connections and consequently to be able to functionally create networks (Figure 21).

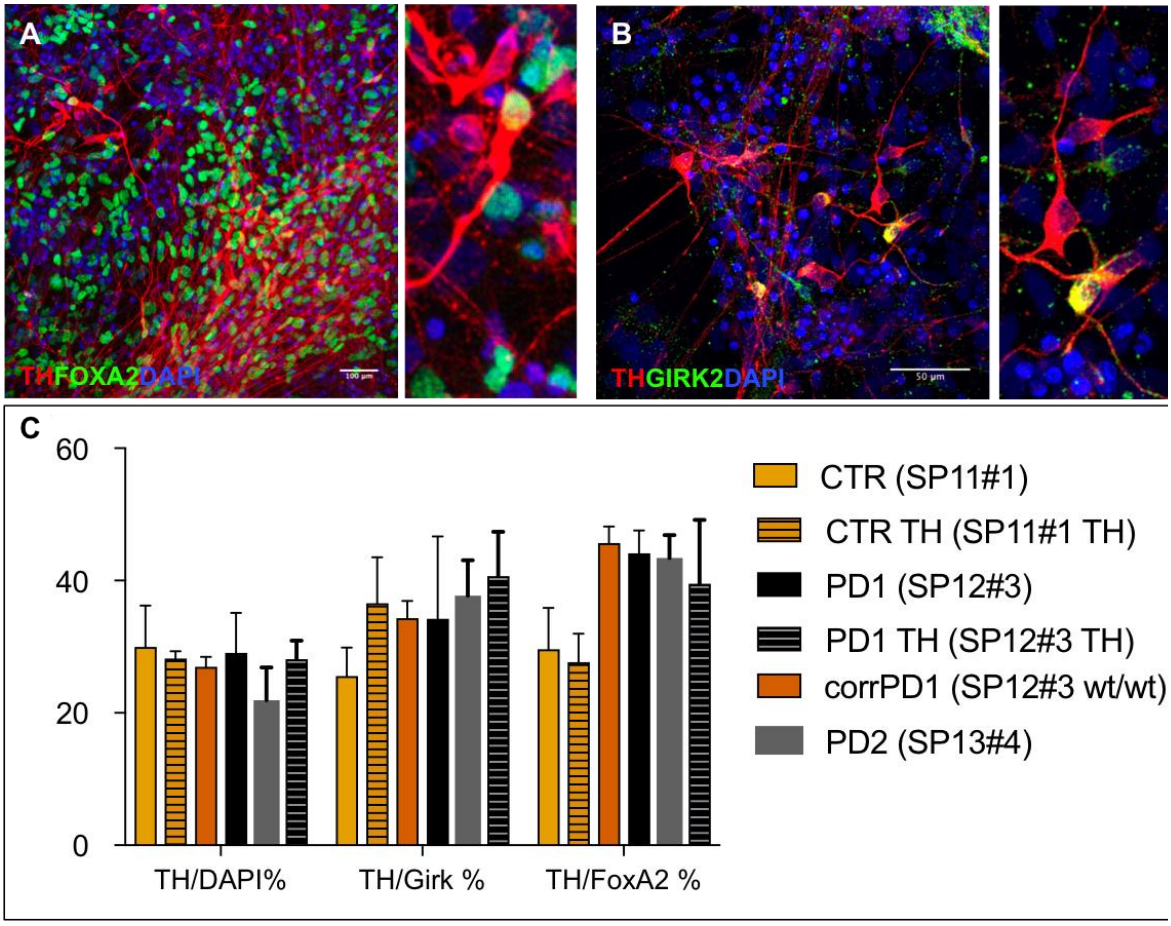

Fig. 20: **Commitment of the DA neurons toward A9.** Representative images of a D50 cuture stained for (A) TH and FOXA2 and (B) TH and GIRK with the relative quantification for each line used in the study (C).

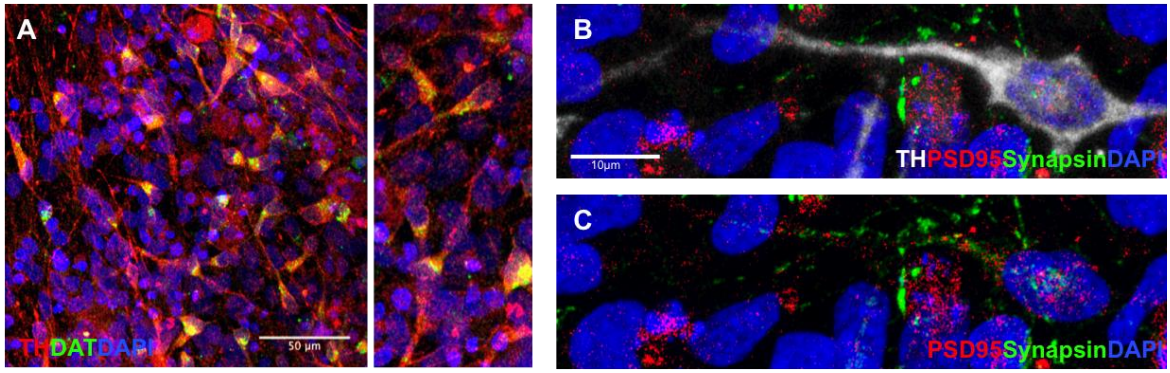

Fig.21: **Expression of functional proteins in DA neurons**. Representative images of D50 culture stained for (A) TH and DAT dopamine transportes specific marker of mature dopaminergic neurons and (B) TH, PSD 95 post-synaptic protein and synapsin, presynaptic protein.

We recorded neuronal functional activity at D35, D50 and D80 and saw no degeneration of the DA neurons at these stages. To confirm this we quantified the number of dopaminergic neurons for each timepoint and saw that between D35 and D50 there was an increase in the DA neuron numbers due to the ongoing differentiation process in the culture, while between D50 and D80 the number of DA neurons remain unchanged meaning that the population was stable and no major neurodegenerative events occurred. The main variability between lines was observed at D35, an early stage of differentiation. Here, control and PD1 lines showed about 10% TH/DAPI positive cells, whereas the rest of the lines showed closer to 20%. At D50 and D80, considered late stages of differentiation, all lines showed a similar TH/DAPI ratio (between 30-35%).

The absence of neurodegeneration was crucial for our functional experiments since we wanted to assess early functional alterations that happen before the neurodegeneration and the selective dopaminergic death.

Maintaining our neurons in culture for a very long period (D120) we were able to reproduce the PD phenotype of specific DA neuron death in the PD lines, confirming the efficacy of the model (Figure 22).

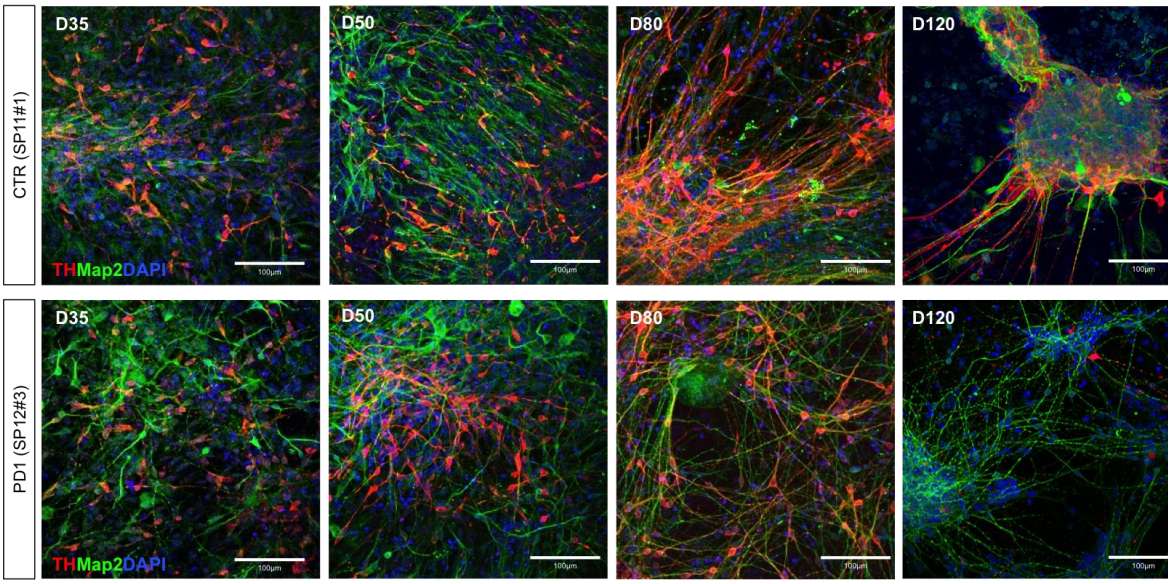

Fig.22: **DA expression in CTR and PD lines.** Representative images of neuronal culture form CTR and PD1 lines at different time points (D35-D50-D80-D120) show selective loss of DA neurons exclusively in the PD line.

3. PD DA neurons show synuclein accumulation after culturing without neurotrophic factors

Comparing the neurons derived from the two PD lines with the neurons derived from the controls, when cultured with neurotrophic factors for 30 days of differentiation, no differences were observed in the expression of dopaminergic marker (TH).

In order to verify the appearance of PD-related phenotypes, at D35 we removed neurotrophic factors from the cultures for 15 days, stressing the culture condition. The absence of neurotrophic factors reduced the efficiency of dopaminergic neuron differentiation in both cultures (control and PD lines), which did not exceed 15% of TH positive cells, whilst the cultures with neurotrophic factors confirmed the data obtained in the previous experiments (30-35% TH positive cells). At D50, the PD lines cultured without the neurotrophic factors showed an accumulation of α-syn, which is not present in the neurons derived from a control line (Figure 23).

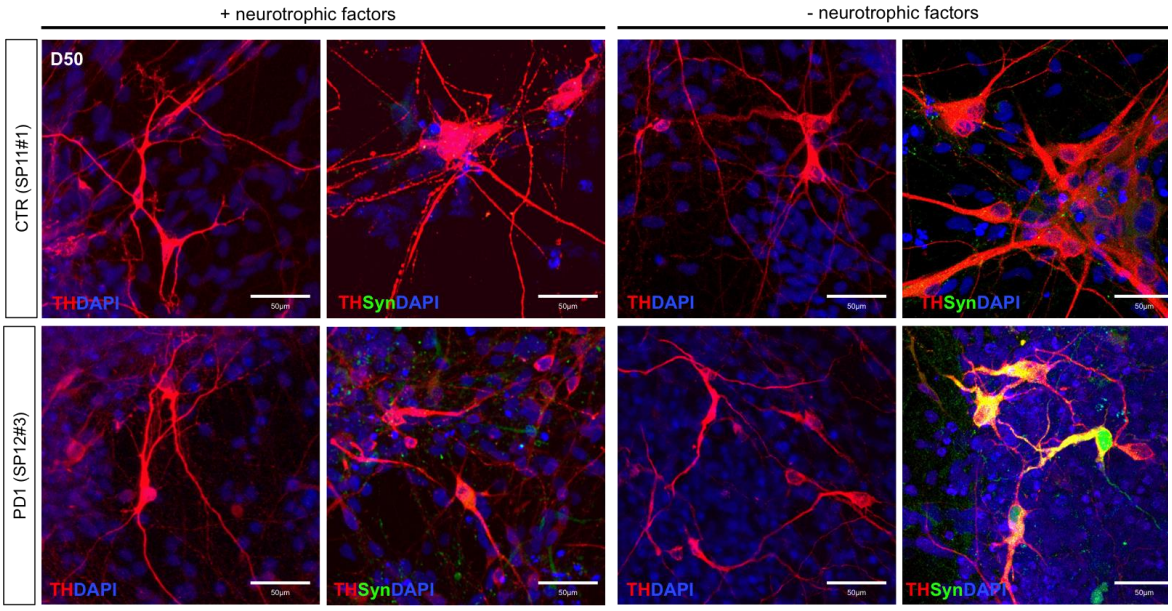

Fig. 23: **α-syn specifically accumulate in PD DA neurons.** Representative images of neuronal culture form CTR and PD1 lines ad D50 of differentiation cultures with and without factors show how similar morphology and protein expression in the 2 lines when cultured with neurotrophic factors. Removing the factors cause a specific accumulation of α-syn in DA neurons derived from the PD lines.

4. Control neurons show oscillatory behavior

We used calcium imaging to monitor spontaneous activity in the neuronal cultures at D35, D50 and D80. About 1,000 regions of interest (ROIs) were manually selected and their fluorescence time evolution extracted (Fiigure 24 A-B). Sharp increases in the fluorescence traces (Figure 24 C), revealed neuronal activations, which were analyzed to extract the onset times of action potentials. The raster plots (Figure 25 B-C) illustrate the global network dynamics of the cultures. Neurons fired either independently or in concurrence with other neurons, with large neuronal co-activations comprising the entire network.

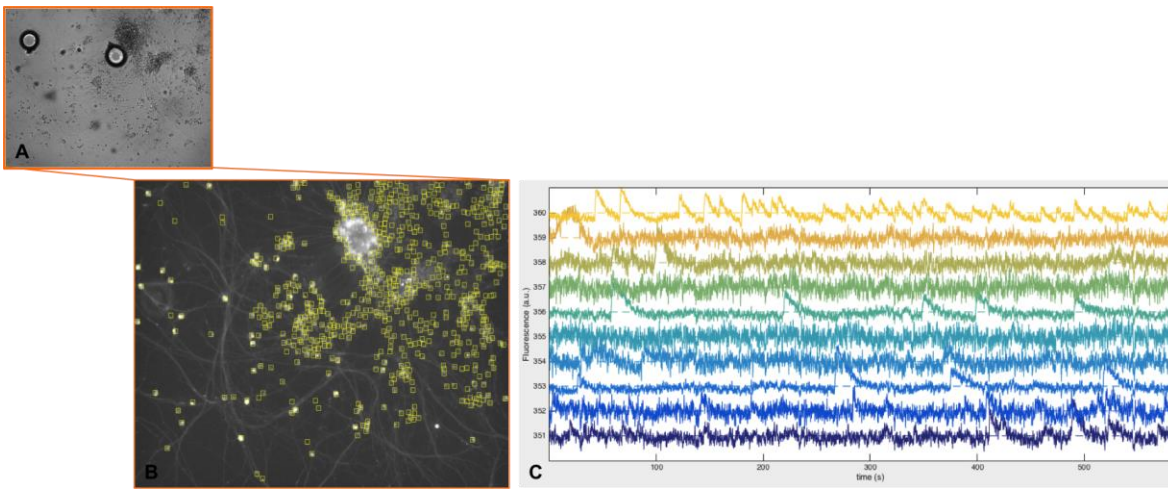

Fig.24: **Diagram of calcium imaging analysis. (A)** Live images in bright field and the corresponding Fluo-4 AM (B) fluorescent signal of differentiated neurons (D50) during calcium imaging, yellow squares identify the manually selected ROIs (diameter 10um). (C) Calcium traces of selected neurons (ROIs) neurons confirm electrophysiological activity.

To provide a quantification of the network average activity by time, we used the Global Network Activity (GNA) measure, defined as the number of neuronal activations in a time window of 1 second. Our overall analysis of the GNA showed that all studied cell lines exhibited a progressive increase of activity during maturation (Figure 25 A). Control lines were characterized by a persistent dynamic in which small sized activations coexisted with larger, full network ones. We consider this behavior as “oscillatory behavior” in which the cells demonstrate a persistent sparse activation.

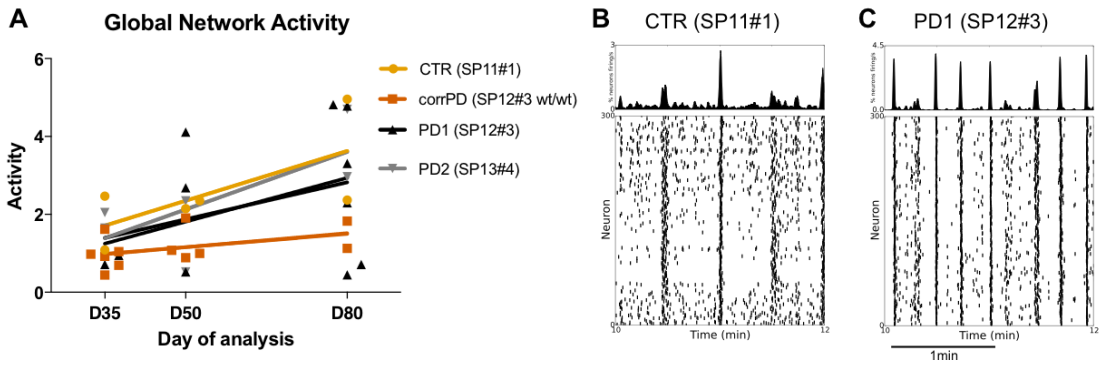

Fig. 25: **Dynamic characterization of the DA neurons.** (A) Average GNA for all experiments at different maturation days. Minimum number of independent experiments: n=2. (Coefficients of determination for linear regressions: CTR-SP11 R2:0.9238; isoPD1-SP12 wt/wt R2: 0.999; PD1-SP12 R2: 0.4942; PD2-SP13 R2: 0.6006). (B-C) Raster plot representation of the activity of control cultures at D80. Each plot represents 2 minutes of recording. Scale bar 1 min.

The GNA analysis demonstrated the first dynamic difference between the control and PD lines.

5. PD neurons show hyper activated, hyper synchronous behavior

PD lines displayed a two-state dynamic, completely different to the oscillatory behavior used to describe the dynamic of the controls. A two-state dynamic is characterized by strong synchronous events combined with quiescent intervals. Since the rate of activity increase was similar in all lines (PD and control), we hypothesized that the structure of collective activations, and not average individual neuronal activity, was the key feature of the malfunctioning behavior. Control and PD neurons show distinctive GNA patterns, suggesting the existence of intrinsically different network mechanisms in the two systems, resulting in a markedly different collective behavior (Figure 26 A-B).

To quantify these differences, we analyzed the amplitude of the GNA events and extracted those that exceeded one standard deviation from the mean, categorizing them as ‘extreme events’. The ratio between these extreme events and all observed events is shown in Figure 26 C and the frequency of occurrence of extreme events is shown in Figure. 26 D. Data shows that PD lines tend to exhibit stronger and more frequent extreme events than control lines. We can conclude that PD lines display an abnormally high synchronous dynamic, particularly at late stages of maturation.

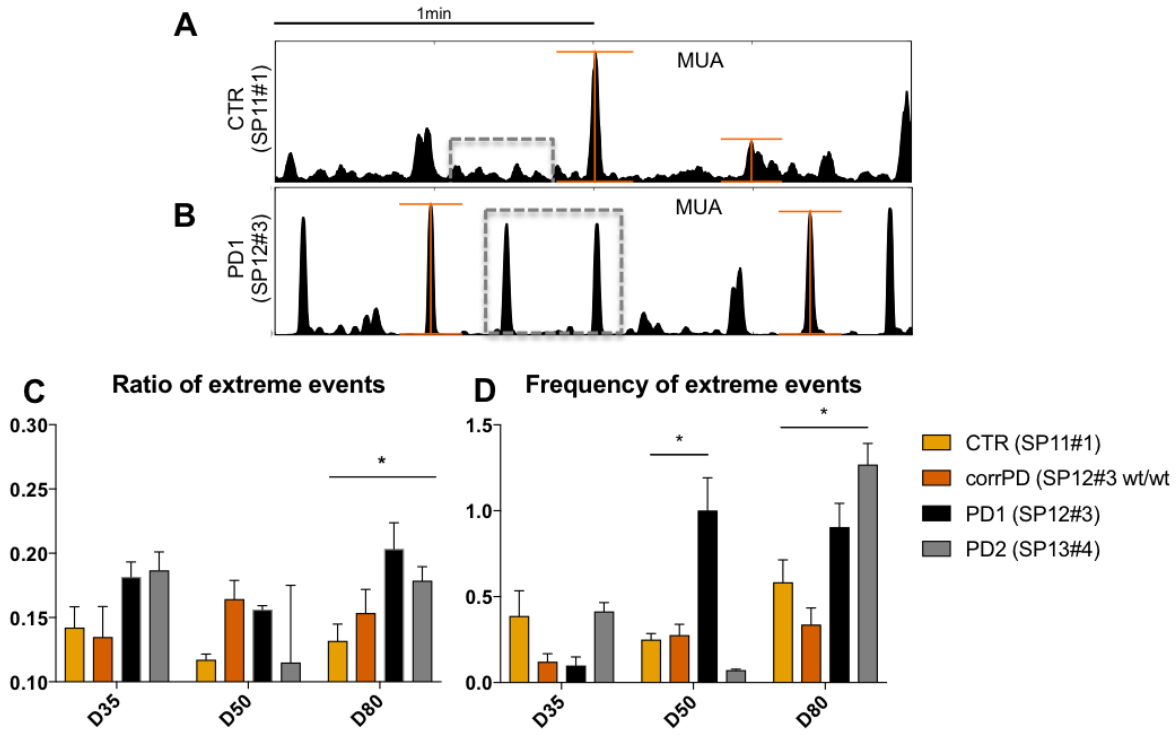

Fig. 26: **Characterization of the oscillatory mixed mode and hyper synchronous dynamic behavior of CTR and PD neuronal culture.** Examples of GNA for (A) control (CTR SP11) and (B) Parkinson Disease (PD1 SP12) experiments (D80). The orange bars indicate different network bursts amplitudes. The dashed grey lines show the dominating dynamics for the two experiments, i.e. low amplitude oscillations for CTR and high amplitude bursts for PD1. (C) Ratio of extreme events for all experiments at different maturation days (Multiple t-test analysis p-Value: 0.0354). (D) Frequency of extreme events for all experiments at different maturation days. (Multiple t-test analysis p-Value D50: 0.01; p-Value D80: 0.0047).

6. Control neurons form a dynamically mature network during the differentiation time

After the dynamic characterization of our lines, our data demonstrates that the global activity of controls and PD lines is substantially different. To show that the dynamic differences are matched to functional alterations, we studied the neuronal culture behavior in more detail. We considered the data at D50 and D80, which corresponds to intermediate and late stages of neuronal differentiation. The exclusion of D35 from the analysis is justified by the great variability of the culture at this stage of maturation due to the presence of numerous progenitors that were not fully differentiated into neurons.

The analysis was performed using time delays[224] to compute the functional connectivity among all pairs of active neurons in a given network. A representative functional network for the control line is provided in Figure 27 A-B, showing only the top 20% of functional connections for clarity. The distribution of functional connections (number of neurons with a given connectivity degree, *k*) averaged over all measurements of the control, is provided in

Figure 27 C. The shape of the distribution reflects the topology of the network. A least-squares fit of the data in log-log scale produced a linear relationship between the connectivity degree *k* and its statistical occurrence. This relationship indicates that there is not a characteristic connectivity degree in the network, and that a large number of low-degree neurons coexist with fewer high-degree neurons.

Controls display a log-log scaling relationship represented by a straight line. This is a fingerprint for scale-free systems, in which interactions among the system's elements coexist at different scales. In the control networks this signifies that neurons participate in co-activations of different sizes, from few neurons to the entire network, a behavior that concords with the low ratio of extreme events observed.

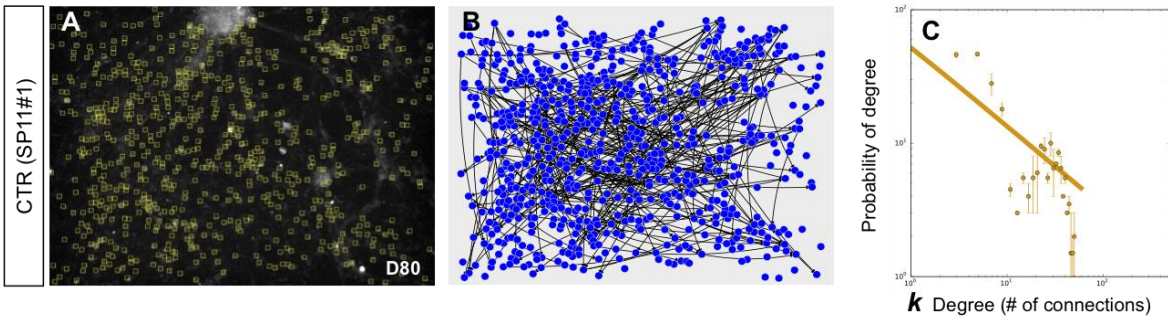

Fig. 27: **Functional characterization of CTR neuronal networks.** (A) Image of Fluo-4 AM fluorescent signal from CTR differentiated neurons (D80) with the corresponding extracted functional network (B)**.** (C) Distribution of degree, or number of functional connections, for all the control experiments at day 80. In log-log scale, the probability of a neuron of having a particular degree is linearly correlated with the degree itself, showing a predominance of low degree over high degree, which is indicative of scale-free arrangements.

7. PD neurons do not create a mature network and show impairment in functionality

Analyzing the functional connectivity traits of the PD lines we see that the least-squares fit provides a flat curve with a cut-off at large connectivity degree *k* (Figure 28). This is markedly different from the control lines. This distribution suggests the existence of neurons with different connectivity degrees but no logical relation between them. No network was created by this system, so the functional activity is much poorer than displayed in the control lines. Although there is variability in the connectivity degrees of the neurons, the overall distribution is smaller compared to control lines. The richness in connectivity and network dynamics, typical of the control, is lost in the PD lines, with neurons in the network often locked in extreme scenarios of full synchrony or full silence.

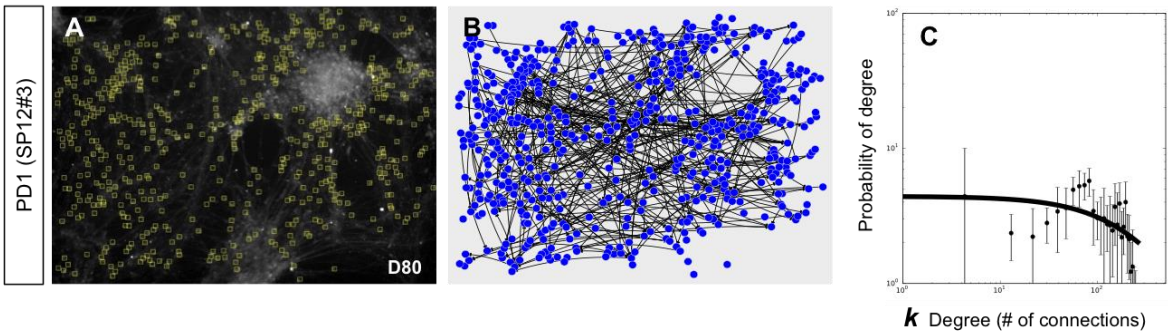

Fig. 28: **Functional characterization of PD neuronal networks** (A) Image of Fluo-4 AM fluorescent signal from PD1 differentiated neurons (D80) with the corresponding extracted functional network (B)**.** Distribution of degrees for all PD1 experiments. In this case, the power-law fit of the distribution does not show a linear trend in log-log scale.

8. Control neurons show scale-free functional behavior

A characteristic of scale-free networks is a straight power law relationship between the number of connections and the number of hubs (in this case neurons)[276,291–293]. Scale-free distribution in a neuronal network is generally considered an indicator of physiologically healthy behavior. The low number of highly connected neurons means that the average importance of any given neuron to the network is low. Randomly removing one neuron from the network has little to no negative effect on the overall network performance as other neurons are able reconstruct the lost connections.

We examined the connectivity of our iPSC-derived neuronal networks, plotting the data against a standard scale-free network model to verify the strength of the networks. We compared our results at D50 and D80 against the standard Barabási-Albert model of scale-free network behavior to calculate how close they are to ideal scale-free distribution. A higher value R^2 (Figure 29) indicates a strong correlation between our experimental data and the model. The control lines resulted in similar, high R^2 values for the two time points (D50 and D80) suggesting a scale-free distribution synonymous of healthy neuronal network functionality.

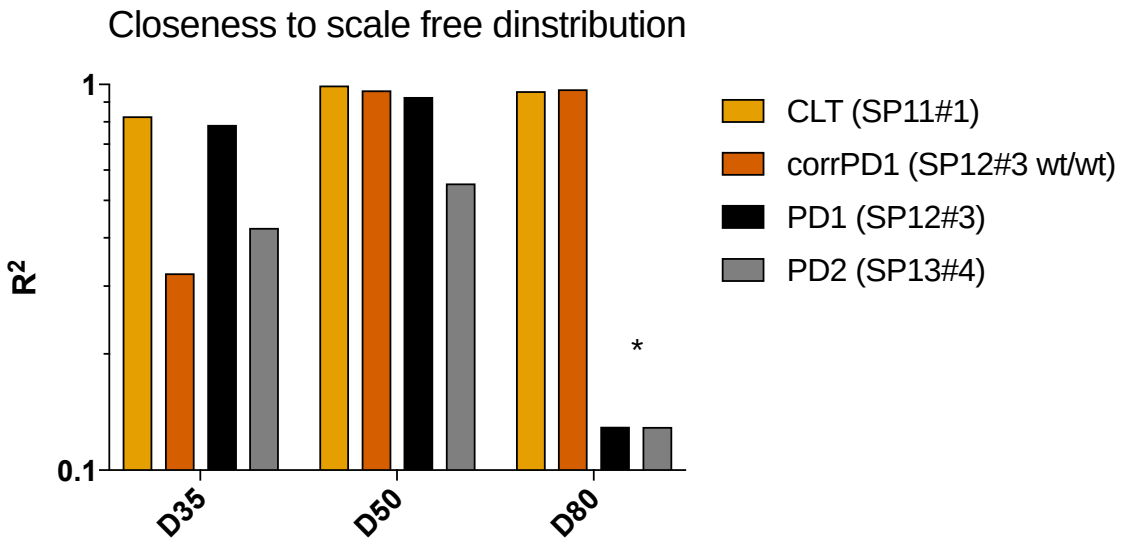

Fig. 29: **Closeness to scale free distribution.** Parameter that indicate how similar to scale free distribution are the experimental degree distributions both from CTR and PD lines at different timepoints (2 way ANOVA analysis, p-Value <0,1).

9. PD neurons show impairment in network functionality

The neuronal networks derived from PD lines show a different behavior, distinct from the scale-free distribution that we consider a sign of healthy network functionality. The R^2 values of the PD lines (Figure 29) clearly show the PD1 network concorded with the control networks at D50 but dramatically departed from the control lines by D80, signaling the onset of functional alterations. The PD2 network has already partially diverged from the healthy behavior at D50, a result that hints at a more aggressive progression of functional alterations in this line.

This result strongly suggests that the LRRK2 mutation undermines the development of scale-free neuronal networking to such an extent that it disrupts the collective activity and functional organization of the circuits. This has a negative impact on the fault tolerance of the neuronal network and increases the likelihood of a connectivity failure.

10. Control DA neurons display a normal subpopulation dynamic

To investigate the origin of the functional impairment that we described in PD lines at late stages of maturation, we took advantage of the genetic TH-reporter tool[294] created in our

lab. We generated a genetic reporter construct that could robustly and reliably label DA neurons by using a genome-editing technology to knock-in a P2A-mOrange adjacent to the last exon of the *TH* gene. We chose mOrange because it is one of the brightest monomeric fluorescent proteins available[295]. The designed CRISPR/Cas9 guide RNA spacer sequence overlapped the *TH* gene stop codon, avoiding retargeting of properly edited alleles (see methods). At D50 of the differentiation process, cells were live imaged (Figure 30 A) and fixed to confirm the fidelity of the reporter. Immunofluorescence analysis of the fluorescent neurons revealed an absolute correlation between mOrange signal and both TH- and mRFP1- immunoreactivity (mOrange is a mRFP1 derivative) (Figure 30 B). Conversely, the MAP2-positive neurons that were negative for TH were also negative for mOrange (Figure 30 C), confirming the specificity of the transgene in reproducing the endogenous TH expression pattern.

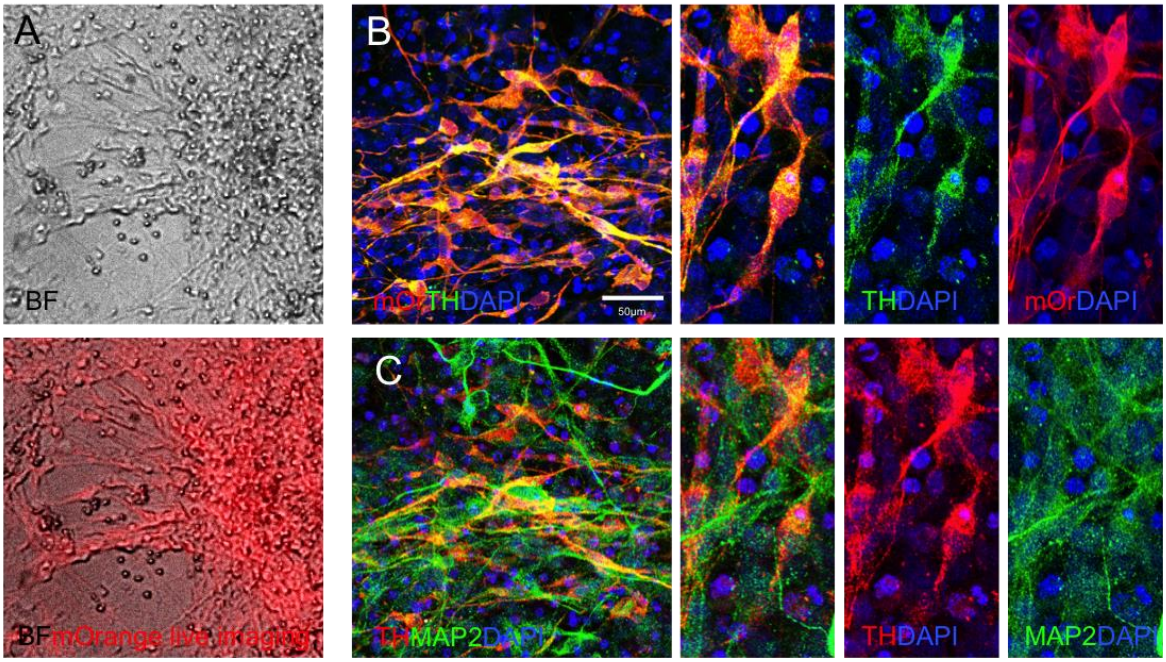

Fig. 30: **Characterization of DA neurons derived from TH reporter line.** (A) Differentiation towards floorplate DA neurons gives rise to fluorescent cells (BF mOrange-LIVE imaging). (B) Representative image of D50 Dopaminergic neurons co- express TH (green) and mOrange (red) and (C) pan-neuronal MAP2 (green) and reporter-derived mOrange (red) staining. This confirming the presence of MAP2 positive mOrange/TH negative cells. Scale bar: 50um. Number of independent experiments n = 3

The genetic reporter tool allows us to identify TH and non-TH neuronal populations in the networks and analyze their functional characteristics separately.

In Figure 31 we see the 2 neuronal layers, one corresponding to TH neurons (red) and another one corresponding to non-TH neurons (blue) (Figure 31 B). An inspection of the activity patterns for the control lines reveals that the two subpopulations exhibit different collective

dynamics. The non-TH subpopulation is characterized by a persistent activity; whereas the TH population shows a two-state dynamic that combines synchronous events with quiescent intervals (Figure 32 A). TH and non-TH activity ratios for the control were similar at D50 and D80 (Figure 32 C). To complete the functional analysis, we investigated the functional connectivity of the two subpopulations and explored the closeness of the inferred distributions to scale-free. The non-TH connectivity degree distribution was highly similar to a scale-free network, while the TH distribution departed from it (Figure 32 D). These distinct functional traits among populations were maintained through development and suggest that the non-TH neurons are responsible for building the scale-free network whilst the TH neurons have little impact.

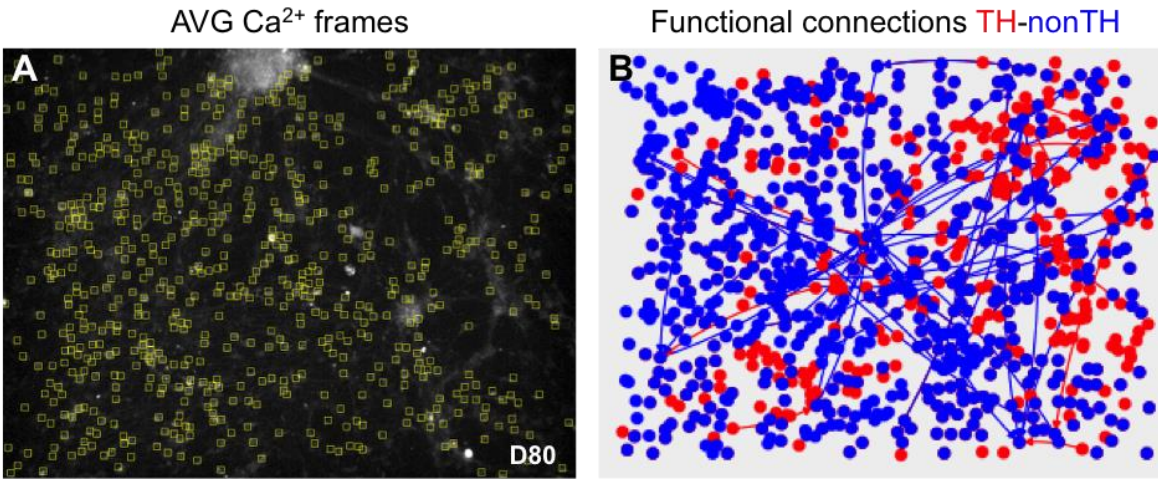

Fig. 31: **Grafic representation of ROI used to plot functional connection between TH and non TH neurons.** Analysis of dynamics of TH+ and non TH+ neurons. (A) Image of Fluo-4 AM fluorescent signal from CTR differentiated neurons (D80) with the correspondent extracted functional network indicating the position of TH+ neurons, in red, and non TH+ neurons, in blue

11. PD TH neurons display abnormal subpopulation dynamic that affects the network behavior

As mentioned before, the PD lines display a two-state dynamic. Using the TH-reporter, we verified that this dynamic is common to both subpopulations, with a clear abundance of extreme events (Figure 32 B). The activity ratio in PD lines switched from TH dominated at D50 to non-TH dominated at D80 (Figure 32 C). These results show an abnormal dynamic in the subpopulations in PD networks, with a reversal in leadership of TH and non-TH subpopulations during differentiation.

In the PD neuronal network organization, at D50, the TH distribution was the closest to a scale-free behavior, while the non-TH departed from it. By D80, both distributions lose their similarity to scale-free network behavior (Figure 32 D). These results reveal that

network communicability and information flow in PD networks is substantially different to our controls, and that this affects both TH and non-TH neurons throughout differentiation.

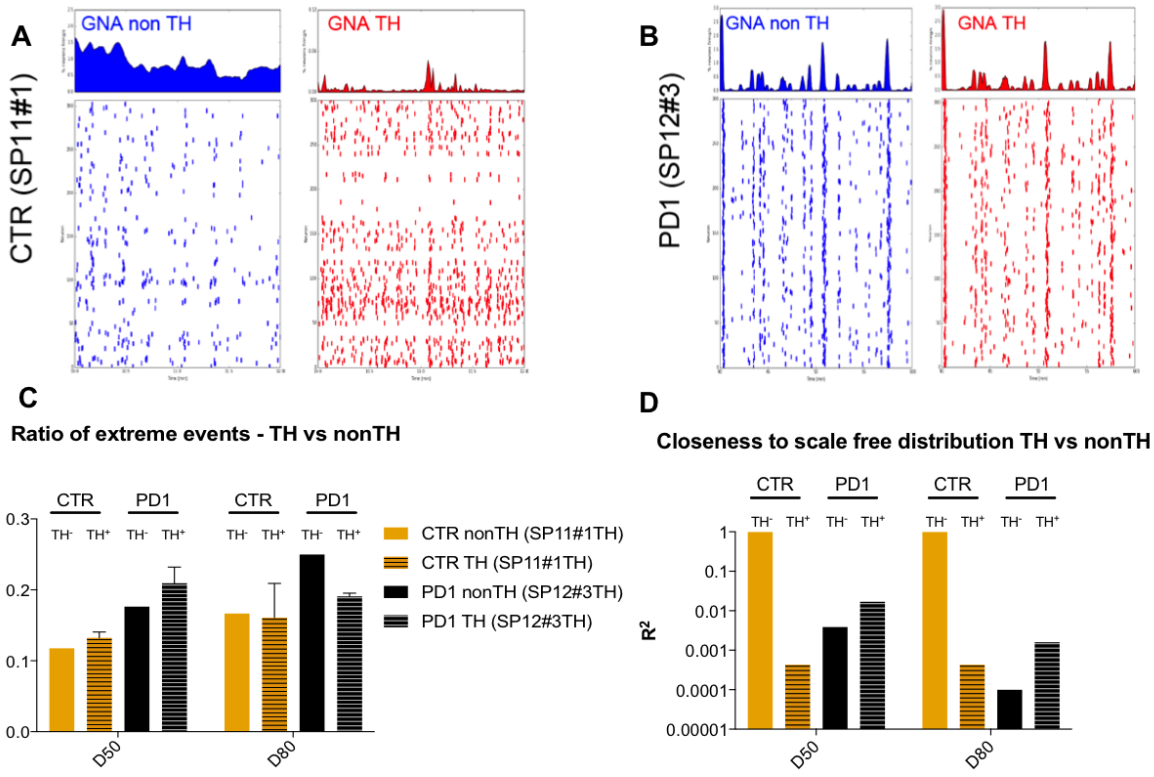

Fig. 32: **Dynamic characterization of TH and non TH neurons.** (A-B) Raster plots of TH+ and non TH+ neurons for both CTR-TH (SP11-TH) and PD1-TH (SP12-TH) lines. (C) Ratio of extreme events for each subpopulation of neurons at two late maturation days (D50 and D80). (D) Closeness to scale free distribution indicating the goodness of fit between experimental degree distributions and a power-law distribution generation model (2 way ANOVA analysis, p-Value <0,1) for each subpopulation of neurons at two late maturation days (D50 and D80).

12. PD TH neurons have short neurites compared to control

To investigate the causes of alteration in the network dynamic and functionality of PD neurons we checked a known PD phenotype already described with our model: the retraction of the neurites. We tested this hypothesis using an *in silico* model designed by Dr. Malagarriga, under the supervision of Prof. Jordi Soriano. Our mathematical simulation reproduces the functional behavior of the control neurons' network. We used experimental data to display the ROIs in the field (Figure 33 A), randomly distributing the correct ratio of DA, excitatory and inhibitory neurons

(Figure 33 B). With this model, we were able to reproduce the behavior of the control neurons, characterized by a strong background activity, or small coordinated activations, in combination with sporadic full-synchrony episodes.

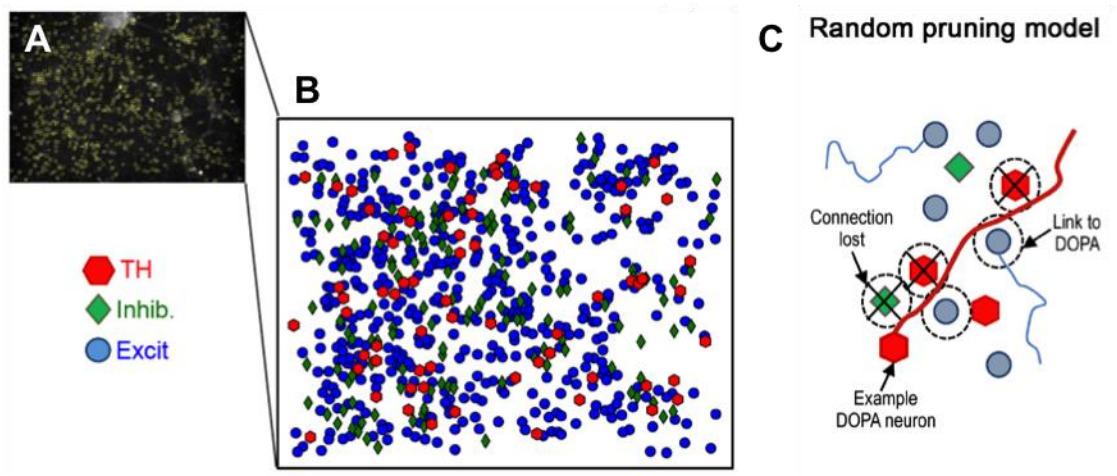

Fig.33: **Numerical *in silico* simulations of CTR and PD1 lines.** (A) Image of Fluo-4 AM fluorescent signal from CTR differentiated neurons (D80) used for posterior numerical simulation. (B) Random neuronal positions were assigned to excitatory (blue circles), inhibitory (green diamonds) and dopaminergic neurons (red hexagons). (C) Random pruning algorithm, through which random connections to the dopaminergic subpopulation are removed.

Using our *in silico* model we simulated the loss of neurites as a reduction of 80% in the connectivity probability of the TH population (Figure 33 C). When a minimum of 10% of the TH neurons are affected the network moves towards on exceedingly synchronous state, typical of the PD phenotype (Figure 34).

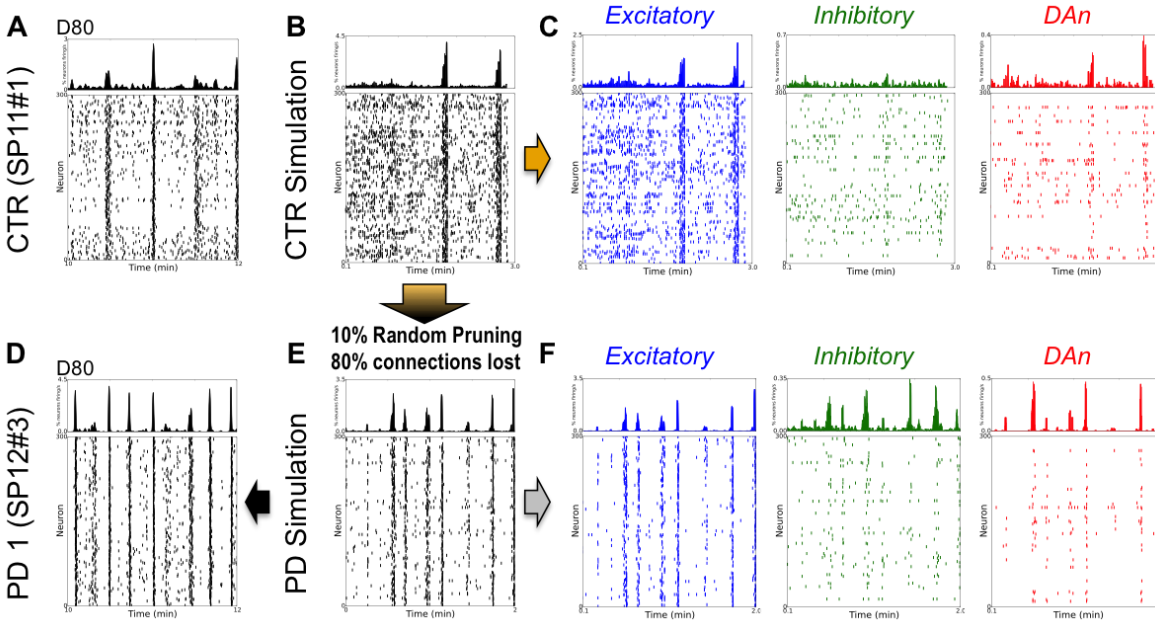

Fig. 34: **Raster plot representing the *in silico* simulation of CTR and PD conditions.** (A) Experimental raster plot for a CTR culture at D80 and a simulated counterpart (B). Simulations were fitted to experimental data in order to display similar dynamic. (C) Raster plots of each neuronal subtype for simulated CTR. (D) Experimental raster plot for a PD1 culture at D80 and its simulated counterpart (E). The best matching dynamics for the simulated PD1 culture were obtained after applying a random pruning of a 80% of connections onto a 10% of the dopaminergic subpopulation. (F) Raster plots of each neuronal subtype for simulated PD1.

To confirm this hypothesis in our biological culture, we examined neurite density in the control and PD neurons at D50 and D80. We observed a much lower number of TH neurites in the PD lines. The deficit was already present at D50 and accentuated at D80 (Figure 35 A). This result was consistent among all the experimental instances. Additionally, the number of neurites increased in the DA control populations during development while it decreased in PD lines, indicating a progressive worsening of network structure for the latter (Figure 35 B). We also analyzed the number of neurites in MAP2+ neurons in both lines and no significant differences were observed (Figure 35 C). Taken together, these results prove that the dynamic and functional deficits of PD lines are localized in the TH subpopulation, and that these cells experience a gradual structural failure in the form of neurite loss.

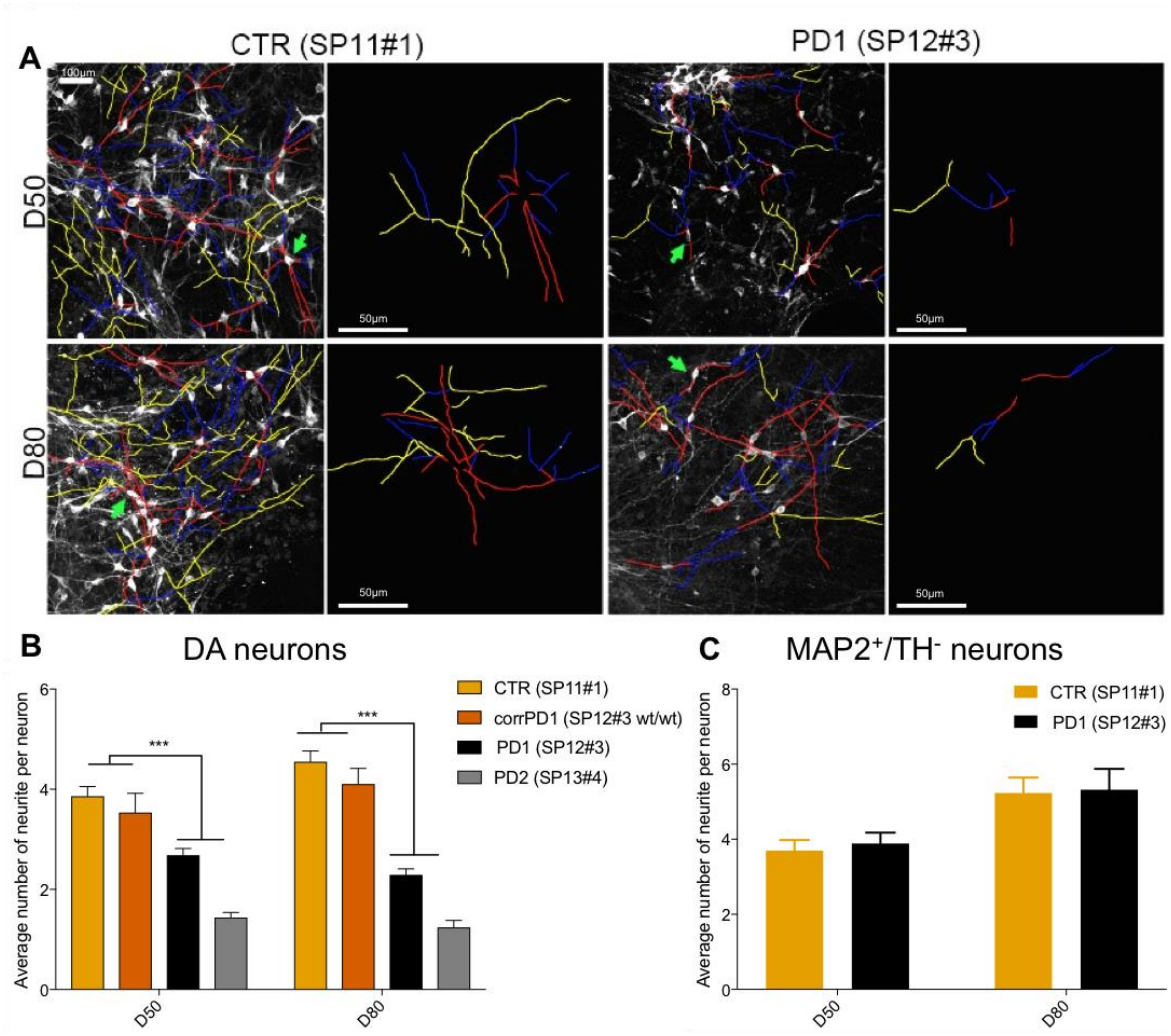

Fig. 35: **Neurite quantification to corroborate the data of the *in silico* model.** (A) CTR (SP11) and PD1 (SP12) TH+ neurons are tracked to determine the number and the structure of the neurite at D50 and D80 (scale bar: 50um). (B) The quantification of the number of TH neurites shows significant differences between CTR and PD1 both at D50 and D80 while no difference were found when analyzing $MAP2^{+}/TH^{-}$ neurons (C). Multiple t test analisis p-Value D50 ($<0.01*10^{4}$) and D80 ($<0.01*10^{3}$). Number of independent experiments n = 3.

13. Gene expression profile analysis reveals little difference in biological and molecular pathways

Our experiments have demonstrated that in PD DA neurons higher synchronicity leads to a general alteration of the network. Using the biophysical model developed in collaboration with Dr. Malagarriga, we simulated the experimental alteration and verified that a known feature of $LRRK2^{G2019S}$ DA neurons, neurite arborization, was a cause of the functional alteration that we were able to describe in our PD *in vitro* culture.

We then used our *in vitro* model to take a step backwards and examine the biological and molecular behavior before the functional alteration manifests. We analyzed the culture at D50, when the data suggests that the functional alteration has not yet developed fully, using gene expression profile analysis to identify possible deregulations in pathways that can be connected to the altered functionality.

To address this question, we generated 3 independent biological replicates of ventral midbrain DA neurons from 5 different lines: 1 control, 2 PD lines (PD1 and PD2) and the relative 2 corrected isogenic lines. At D50 we harvested the cells and performed RNA extraction. The RNA obtained was then processed by nanoString machine in order to individuate the gene expression profile of each line using a commercial gene panel related to neuropathology. We analyzed the raw data using ROSALIND bioinformatics[296] developed by OnRamp BioInformatics, Inc. (San Diego, CA).

The ROSALIND program revealed that our iPSC-derived neurons do not show more than 1.5-2% difference in the genomic expression profile of each line (Figure 36 A). Our analysis focused on differentially expressed genes, selected with a pAdjValue of 0.05 and a fold change $\leq$-2 and $\geq$ 2. Within these strict selection criteria, we were unable to highlight any gene related to LRRK2 PD and isogenic PD (Figure 36 B). This confirms the validity of the *in vitro* model and the robustness of the differentiation protocol and shows that the functional phenotype is not due to macroscopic neurodegenerative conditions.

Future investigation could relax the strict selection criteria and examine small, specific changes in the gene expression which can be connected to the functional alterations. Small deregulations in these pathways could be used for drug screening and as early biomarkers to identify the disease.

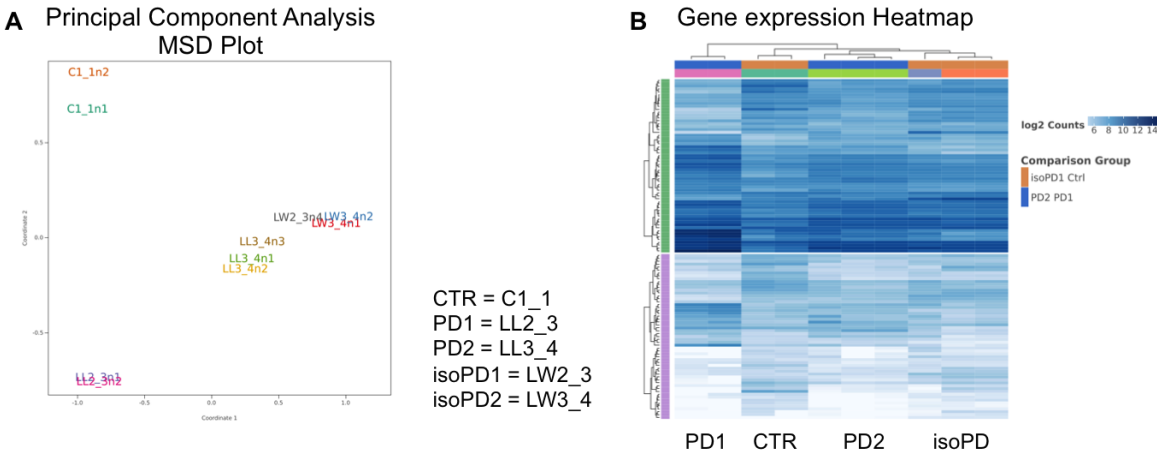

Fig.36. **Gene expression profile analysis of D50 DA neurons.** A. Principal component analysis describe a 1.5-2% difference in the genomic expression profile of each line. B. Gene expression heatmap show little difference between CTR, PD and isogenic D50 DA neurons confirming the robustness of our *in vitro* protocol.

14. Isogenic PD LRRK2^{G2019S} show an overall less active dynamic but a full recovery in functional behavior and neurite length

Using isogenic lines is important for our investigation as it gives us insight into the penetrance of the mutation and its direct involvement in the different aspects of the disease's pathogenesis. We know from the literature that the LRRK2^{G2019S} mutation has a pathogenesis indistinguishable from idiopathic forms of PD. Molecularly this mutation is mostly associated with common PD cellular phenotypes such as autophagy dysfunctions, signaling impairment and mitochondrial pathological phenotypes. In our cell model, the isogenic PD lines were able to recover from the phenotypes that we described in the PD lines. Isogenic PD lines partially recovered their dynamic activity. They show a consistent progression in neuronal calcium activity during the 3 different time points analyzed but they never reach the level of activation of the control or PD lines (Figure 24 A). The isogenic neurons show an oscillatory behavior typical of the control lines and noticeably different from the hyper active, hyper-synchronous behavior of the PD lines (Figure 25 B-C). The functional behavior of the isogenic neurons was similar to the control lines and displayed a high closeness to scale-free behavior (Figure 29). The isogenic PD DA neurons fully recover their neurite length, similar to the control DA neurons and never show neurodegeneration typical to the PD lines (Figure 35).

Discussion

For this study, we have efficiently differentiated 6 iPSC lines into DA neurons and monitored their functional activity using calcium imaging assay. The first step of production of the correct type of neurons is not trivial. iPSC technology offers us a great opportunity to investigate systemic and complex diseases, especially neurological diseases. With previous methods it was very difficult to directly study the molecular mechanisms and pathophysiological stages of the disease, but we are now able to derive specific neuronal cell types directly from patients.

For studying PD, it is important to generate A9 ventral midbrain DA neurons. This specific cell type gives us the confidence that the phenotypes we are observing and describing are directly and accurately connected with the disease and not an artifact of the *in vitro* model. (FIND PAPERS). Our differentiation process resulted in ~35% A9 ventral midbrain DA neurons which gives us confidence that we are reproducing consistent and robust data, describing the first phases of the pathophysiology of PD.

We have confidence in the model because:

Our iPSC lines were already used to demonstrate PD related phenotypes and we reproduced and validated this;

Our cultures consistently express DA-specific progenitors and mature DA-specific markers;

We used a reporter line that allows us to identify DA neurons (TH^+) and differentiate them from the non DA neurons (TH^-).

Having validated our neuronal culture, we carried out in-depth functional analysis using calcium imaging to identify early signs that can be used to predict morphological neurodegeneration and death of the DA specific neurons.

All of our neuronal cultures were active and displayed calcium spikes during the different analysis time points. Each line grows their overall activity from D35 to D80 and we notice an evolution in the dynamic of each line. Focusing on the intrinsic characteristics of the dynamic activity of the neuronal cultures, we were able to identify two distinct patterns of activity: controls lines display a mixed mode, oscillatory activity while PD lines display a two-state dynamic, characterized by hyper-active and hyper-synchronous behavior, with strong bursting events combined with intervals of almost no activity.

Based on this observed behavior, we carried out functional network analysis and demonstrated that:

Mixed mode, oscillatory behavior is related to a scale-free distribution of the neuronal network, and correlates with healthy functional connections between the neurons;

The ‘all-or-none’ hyper-active hyper-synchronous behavior of the diseased neurons diverges from a scale-free distribution of the neuronal network and is a sign of altered functional connectivity between neurons.

Using genetic TH reporter lines, we were able to focus on just the DA population of our neuronal culture. Our analysis shows that, in healthy conditions, DA neurons never overrule the non-DA neurons in organizing the network behavior, they remain integrated and function in line with the general network activity.

PD DA neurons, on the contrary, already dictate the neuronal network activity at the first stage of functional analysis (D50), spreading the hyper-synchronous dynamic to the non-DA neurons and altering the network by D80.

These data are sustained by the literature which describes an increase in a “strongly interconnected between-network” state in PD patients. This means that PD patients, like our *in vitro* PD neuronal networks, lose the capability of creating long distance, modulated and organized oscillatory connections and diverge into a hyper-active hyper-connected state. This state suggests a lack of regulation, with the network missing the physiological crosstalk and modulation that normally organize the neuronal connections. The PD neuronal network dynamic has a clear fingerprint that can be use as guidance to develop early diagnostic tests. We demonstrated that this dynamic is connected with the loss of neurite arborization, a known PD phenotype, confirming the authenticity of the model. We were also able to identify a potential therapeutic window during which some of the neurons are functionally affected but no neuronal loss has occurred and morphological neurodegeneration is not happening.

The next challenge is to translate these *in vitro* data into clinical applications.

More in-depth characterization of the model and its applicability to biomarker discovery and drug screening could follow 2 different approaches:

Organoids and 3D complex cultures

As mentioned before cellular neuroscience mainly rely on *in vitro* animal models[297], *ex vivo* brain slices[298] and *in vitro* 2D cultures. These different experimental conditions show limitations in understanding the complexity of the biology, chemist and physic underlying the basic processes that happen in the brain. *In vivo* animal model cannot reproduce the human cognitive abilities at the cellular level and fail into reproduce human relevant data

and clinical features[299]. Brain slices are too sensitive to axotomy and this limitation creates artifacts and variability inducing neuronal death[300,301]. 2D *in vitro* culture allow the investigation of basic cellular and functional neuronal network data but lack the *in vivo* complexity and microenvironment, do not resemble the architecture typical of a 3D complex system[302].

3D brain organoids, new tissue engineering technology derived from stem cells, are able to overcome the previously described limitation and offer new opportunities in brain modeling[303–305].3D brain organoids have already been used to model early-onset neurologic disease variants such as early-onset AD[306]. 3D brain organoids derived from early-onset familial AD (fAD) patients showed AD phenotypes including β-amyloid aggregation, hyper-phosphorylated Tau (pTau), and endosome abnormalities[307]. These data suggest that brain organoids have the great potential to expand our knowledge of physiological and pathological features, not just for neurodevelopmental diseases but also for the neurodegenerative ones. They may allow higher order investigation of mechanisms and functionality and their 3D nature means that they can also give new insights into cell-to-cell interaction, modelling distinct brain regions and their specific connections. 3D-iPSC-based brain organoid models enable researchers to analyze molecular and pharmacological effects in a complex tissue system, functioning as a drug screening platform. We can go further using the great efficiency of the current protocols to generate organoids that can be used as a personalized medicine tool if iPSC are derived from specific patients. Furthermore, 3D-cultured organoids remain viable for much longer than 2D-cultured neurons, as long as nutrients and oxygen are sufficiently supplied. Therefore, the 3D culture system provides an exciting platform for exploring pathogenesis caused by long-term neurotoxicant exposure and chronic cellular response.

The interaction between non-neuronal cell populations and neuronal function has become one of the most useful features that can be modeled by 3D brain organoids. More efficient culture techniques that increase the complexity of the neural and non-neural population are under study, coupled with imaging and functional assay that are needed to ameliorate this potentially powerful tool. To date the main limitation of brain organoids is that most neurodegenerative diseases manifest at a late developmental stage and the lack of vasculature structures in organoids may prevent them from developing full physiological/pathological maturation. Vascularization is essential for neuronal progenitor differentiation in the subventricular zone during late development[308]. This limits PD modelling because degeneration of nigrostriatal projection neurons is the primary cause of PD symptoms, and vascularization is an essential first step to begin the enormous task of modelling a functional nigrostriatal circuit in a culture setting. Techniques have been developed to address the lack of vascularization such as building a vascular microenvironment with microfluidic chambers, further mimicking the physiological niche that promotes neurogenesis[309–311]. In the tissue scaffold created by the microfluidic chambers, pre-capillary networks were built by co-culture of pericytes and early vascular cells derived from iPSCs[312,313]. This approach was able to facilitate the generation of physiologically relevant vascular networks for neurogenesis. Using a combination of these new techniques, perfusion-based human iPSC-derived 3D brain organoid platforms can

make our *in vitro* model even more realistic and effective in understanding the pathophysiology underlying neurodegenerative diseases.

Artificial Intelligence

Artificial intelligence (AI) techniques can be applied in translational and wide approaches for the study of neurodegenerative disorders.

The main characteristic of AI techniques that make them suitable to biological research and development is their efficiency in handling large data sets. Pairing AI techniques such as deep learning with mathematical *in silico* models allows us to produce and analyze vast numbers of scenarios, working out which parts are statistically relevant and might be applied in the biomedical field without needing to experimentally test all possible combinations.

AI is already being applied in diagnostic processes, making them faster and less susceptible to errors. AI can recognize common patterns in fMRI, DAT or PET brain scan datasets allowing for a much faster identification of anomalies than traditional methods[314].

We can use AI to help with the identification of potential drugs and biological targets that would lead to better treatments. AI can be used to analyze and disassemble the functional behavior of each drug molecule, allowing us to re-purpose them into new treatments for other type of diseases and reexamine previously failed molecules that may have more success in different therapeutic areas.

The application of AI to personalized medicine can create a new form of healthcare based on personal genetic and physiological conditions. Personalized drug molecules, able to deliver targeted therapies that are tailored to each patient can be designed. This will help us to better understand the basic molecular cause of neurodegenerative processes, guiding the direction for new more advanced cures.

CONCLUSIONS

- Ventral midbrain dopaminergic neurons (DAn) were efficiently generated from induced pluripotent stem cells (iPSC) representing healthy individuals (Ctrl) and LRRK2 associated PD patients.

- LRRK2 PD and Ctrl DAn formed complex networks that showed evident signs of functional maturation over time.

- PD neuronal networks developed a dynamically abnormal hypersynchrony, in contrast with healthy or gene-edited isogenic PD networks that presented an oscillatory-mixed mode.

- The functional connectivity of the controls displays a log-log scaling relationship represented by a straight line. This is a fingerprint for scale-free systems, in which interactions among the system's elements coexist at different scales. In the control networks this signifies that neurons participate in co-activations of different sizes, from few neurons to the entire network, a behavior that concords with the low ratio of extreme events observed.

- On the contrary the functional connectivity traits of the PD lines using the least-squares fit shows a flat curve with a cut-off at large connectivity degree. This distribution suggests the existence of neurons with different connectivity degrees but no logical relation between them. No network was created by this system, so the functional activity is much poorer than displayed in the control lines.

- Using dopaminergic neuron lineage tracing we demonstrate that in the control the non-TH neurons are responsible for building the scale-free network whilst the TH neurons have little impact.

- Analyzing the behavior of TH and non-TH neurons in the PD lines we see an abnormal dynamic in the subpopulations of PD networks, with a reversal in leadership of TH and non-TH subpopulations during differentiation. These results reveal that network communicability and information flow in PD networks is substantially different to our controls, and that this affects both TH and non-TH neurons throughout differentiation.

- The generation of an *in silico* model based on our experimental data suggests that one of the primary causes of the functional alteration is the random pruning of TH neurites. To confirm this hypothesis in our biological culture, we examined neurite density in the control and PD neurons at D50 and D80. We observed a much lower number of TH neurites in the PD lines. The deficit was already present at D50 and accentuated at D80 while the number of neurites in MAP2+/TH- neurons showed no significant differences.

- Gene expression profile analysis revealed that our iPSC-derived neurons do not show more than 1.5-2% difference in the genomic expression profile of each line suggesting no clear difference in the gene expression between controls, LRRK2 PD and isogenic PD. This confirms the validity of the in vitro model and the robustness of the differentiation protocol and shows that the functional phenotype is not due to macroscopic neurodegenerative conditions.

- Thus, our results identify early alterations in PD neuronal function that predate the onset of neuron degeneration and highlight the extraordinary window of opportunity that iPSC-based experimental models provide into pre-symptomatic assessment of chronic degenerative diseases.

BIBLIOGRAPHY

1. Parkinson, J. An essay on the Shaking Palsy. *Arch. Neurol.* **20**, 441–445 (1969).
2. Hughes, A. J., Daniel, S. E., Kilford, L. & Lees, A. J. Accuracy of clinical diagnosis of idiopathic Parkinson's disease: A clinico-pathological study of 100 cases. *J. Neurol. Neurosurg. Psychiatry* **55**, 181–184 (1992).
3. Cummings, J. L. Intellectual Impairment in Parkinson's Disease: Clinical, Pathologic, and Biochemical Correlates. *J. Geriatr. Psychiatry Neurol.* **1**, 24–36 (1988).
4. Hughes, T. A. *et al.* A 10-year study of the incidence of and factors predicting dementia in Parkinson's disease. *Neurology* **54**, 1596–602 (2000).
5. Aarsland, D., Andersen, K., Larsen, J. P. & Lolk, A. Prevalence and Characteristics of Dementia in Parkinson Disease. *Arch. Neurol.* **60**, 387 (2003).
6. Aarsland, D. *et al.* The effect of age of onset of PD on risk of dementia. *J. Neurol.* **254**, 38–45 (2007).
7. Cersosimo, M. G. *et al.* Gastrointestinal manifestations in Parkinson's disease: prevalence and occurrence before motor symptoms. *J. Neurol.* **260**, 1332–1338 (2013).
8. Lee, V. M.-Y. *et al.* α-Synuclein in Lewy bodies. *Nature* **388**, 839–840 (2002).
9. Goedert, M., Spillantini, M. G., Del Tredici, K. & Braak, H. 100 years of Lewy pathology. *Nature Reviews Neurology* **9**, 13–24 (2013).
10. Marsden, C. D. Neuromelanin and Parkinson's disease. *J. Neural Transm. Suppl.* **19**, 121–41 (1983).
11. Surmeier, D. J., Obeso, J. A. & Halliday, G. M. Selective neuronal vulnerability in Parkinson disease. *Nature Reviews Neuroscience* **18**, 101–113 (2017).
12. Lundblad, M., Decressac, M., Mattsson, B. & Bjorklund, A. Impaired neurotransmission caused by overexpression of -synuclein in nigral dopamine neurons. *Proc. Natl. Acad. Sci.* **109**, 3213–3219 (2012).
13. Crowther, R. A., Hasegawa, M., Spillantini, M. G., Jakes, R. & Goedert, M. -Synuclein in filamentous inclusions of Lewy bodies from Parkinson's disease and dementia with Lewy bodies. *Proc. Natl. Acad. Sci.* **95**, 6469–6473 (2002).
14. Collaborators, G. B. of D. S. 2013 *et al.* Global, regional, and national incidence, prevalence, and years lived with disability for 301 acute and chronic diseases and injuries in 188 countries, 1990–2013: a systematic analysis for the Global Burden of Disease Study 2013. *Lancet* **386**, 743–800 (2015).
15. Schapira, A. H. V. Etiology of Parkinson's disease. *Neurology* **66**, S10–S23 (2006).
16. Shojaee, S. *et al.* Genome-wide Linkage Analysis of a Parkinsonian-Pyramidal Syndrome Pedigree by 500 K SNP Arrays. *Am. J. Hum. Genet.* **82**, 1375–1384 (2008).
17. Fonzo, A. D. *et al.* FBXO7 mutations cause autosomal recessive, early-onset parkinsonian- pyramidal syndrome. *Neurology* **72**, 240–245 (2009).
18. Nichols, W. C. *et al.* Genetic screening for a single common LRRK2 mutation in familial Parkinson's disease. *Lancet* **365**, 410–412 (2005).
19. Ramirez, A. *et al.* Hereditary parkinsonism with dementia is caused by mutations in ATP13A2, encoding a lysosomal type 5 P-type ATPase. *Nat. Genet.* **38**, 1184–1191 (2006).
20. Valente, E. M. *et al.* Hereditary early-onset Parkinson's disease caused by mutations in PINK1. *Science (80-.).* **304**, 1158–1160 (2004).
21. Bonifati, V. *et al.* Mutations in the DJ-1 gene associated with autosomal recessive early-onset parkinsonism. *Science (80-.).* **299**, 256–259 (2003).
22. Kitada, T. *et al.* Mutations in the parkin gene cause autosomal recessive juvenile parkinsonism. *Nature* **392**, 605–608 (1998).
23. Vilarino-Guell, C. *et al.* VPS35 mutations in parkinson disease. *Am. J. Hum. Genet.* **89**, 162–167 (2011).

24. Zimprich, A. *et al.* Mutations in LRRK2 cause autosomal-dominant parkinsonism with pleomorphic pathology. *Neuron* **44**, 601–607 (2004).

25. Paisán-Ruíz, C. *et al.* Cloning of the gene containing mutations that cause PARK8-linked Parkinson's disease. *Neuron* **44**, 595–600 (2004).

26. Singleton, B. *et al.* α-Synuclein Locus Triplication Causes Parkinson's Disease. *Science (80-.).* **302**, 841 (2003).

27. Polymeropoulos, M. H. *et al.* Mutation in the α-synuclein gene identified in families with Parkinson's disease. *Science (80-.).* **276**, 2045–2047 (1997).

28. Lee, Y.-T. C., Hsu, S.-T. D., Cloud Lee, Y.-T. & Danny Hsu, S.-T. Familial Mutations and Post-translational Modifications of UCH-L1 in Parkinson's Disease and Neurodegenerative Disorders. *Curr. Protein Pept. Sci.* **18**, 733–745 (2016).

29. Calabrese, V. *et al.* Aging and Parkinson's Disease: Inflammaging, neuroinflammation and biological remodeling as key factors in pathogenesis. *Free Radical Biology and Medicine* **115**, 80–91 (2018).

30. Powers, R. *et al.* Metabolic investigations of the molecular mechanisms associated with Parkinson's disease. *Metabolites* **7**, (2017).

31. Haaxma, C. A. *et al.* Gender differences in Parkinson's disease. *J. Neurol. Neurosurg. Psychiatry* **78**, 819–24 (2007).

32. Georgiev, D., Hamberg, K., Hariz, M., Forsgren, L. & Hariz, G. M. Gender differences in Parkinson's disease: A clinical perspective. *Acta Neurologica Scandinavica* **136**, 570–584 (2017).

33. Ben-Shlomo, Y. The epidemiology of Parkinson's disease. *Baillieres. Clin. Neurol.* **6**, 55–68 (1997).

34. Schwarzschild, M. A. *et al.* Diet, Urate, and Parkinson's Disease Risk in Men. *Am. J. Epidemiol.* **167**, 831–838 (2008).

35. Ascherio, A. & Schwarzschild, M. A. The epidemiology of Parkinson's disease: risk factors and prevention. *The Lancet Neurology* **15**, 1257–1272 (2016).

36. Thacker, E. L. *et al.* Recreational physical activity and risk of Parkinson's disease. *Mov. Disord.* **23**, 69–74 (2008).

37. Pan-Montojo, F. & Reichmann, H. Considerations on the role of environmental toxins in idiopathic Parkinson's disease pathophysiology. *Translational Neurodegeneration* **3**, 10 (2014).

38. Sacks, O. The origin of "Awakenings". *Br. Med. J. (Clin. Res. Ed).* **287**, 1968–9 (1983).

39. Jang, H., Boltz, D. A., Webster, R. G. & Smeyne, R. J. *Viral parkinsonism*. *Biochimica et Biophysica Acta - Molecular Basis of Disease* **1792**, 714–721 (Elsevier, 2009).

40. Boltz, D. *et al.* Highly pathogenic H5N1 influenza virus can enter the central nervous system and induce neuroinflammation and neurodegeneration. *Proc. Natl. Acad. Sci.* **106**, 14063–14068 (2009).

41. Höglinger, G. U. *et al.* Chronic systemic complex I inhibition induces a hypokinetic multisystem degeneration in rats. *J. Neurochem.* **84**, 491–502 (2003).

42. Ferrante, R. J., Schulz, J. B., Kowall, N. W. & Beal, M. F. F. Systemic administration of rotenone produces selective damage in the striatum and globus pallidus, but not in the substantia nigra. *Brain Res.* **753**, 157–162 (1997).

43. Spillantini, M. G. *et al.* Progression of Parkinson's Disease Pathology Is Reproduced by Intragastric Administration of Rotenone in Mice. *PLoS One* **5**, e8762 (2010).

44. Pal, A. *et al.* Environmental toxins trigger PD-like progression via increased alpha-synuclein release from enteric neurons in mice. *Sci. Rep.* **2**, 898 (2012).

45. Levy, L. S., Capleton, A. C., Rushton, L., Rumsby, P. C. & Brown, T. P. Pesticides and Parkinson's Disease—Is There a Link? *Environ. Health Perspect.* **114**, 156–164 (2005).

46. Walker, R. W., Hand, A., Jones, C., Wood, B. H. & Gray, W. K. The prevalence of Parkinson's disease in a rural area of North-East England. *Park. Relat. Disord.* **16**, 572–575 (2010).

47. Polymeropoulos, M. H. *et al.* Mapping of a gene for Parkinson's disease to chromosome 4q21-q23. *Science (80-.).* **274**, 1197–1199 (1996).

48. Lee, V. M.-Y. *et al.* α-Synuclein in Lewy bodies. *Nature* **388**, 839–840 (2002).

49. Kingdom, U. □-Synuclein in filamentous inclusions of Lewy bodies from Parkinson's. *Neurobiol. Commun. by Max F. Perutz, Med. Res. Counc.* **95**, 6469–6473 (1998).

50. Ibáñez, P. *et al.* Causal relation between α-synuclein gene duplication and familial Parkinson's disease. *Lancet* **364**, 1169–1171 (2004).

51. Yoshino, H. *et al.* Clinical heterogeneity of α-synuclein gene duplication in Parkinson's disease. *Ann. Neurol.* **59**, 298–309 (2005).

52. Farrer, M. *et al.* Comparison of Kindreds with Parkinsonism and α-Synuclein Genomic Multiplications. *Ann. Neurol.* **55**, 174–179 (2004).

53. Hoenicka, J. *et al.* The new mutation, E46K, of α-synuclein causes parkinson and Lewy body dementia. *Ann. Neurol.* **55**, 164–173 (2004).

54. Rajput, A. H. *et al.* Alpha-synuclein p.H50Q, a novel pathogenic mutation for Parkinson's disease. *Mov. Disord.* **28**, 811–813 (2013).

55. Dürr, A. *et al.* G51D α-synuclein mutation causes a novel Parkinsonian-pyramidal syndrome. *Ann. Neurol.* **73**, 459–471 (2013).

56. Sheerin, U. M. *et al.* Screening for VPS35 mutations in Parkinson's disease. *Neurobiol. Aging* **33**, 838.e1-838.e5 (2012).

57. Sharma, M. *et al.* A multi-centre clinico-genetic analysis of the VPS35 gene in Parkinson disease indicates reduced penetrance for disease-associated variants. *J. Med. Genet.* **49**, 721–726 (2012).

58. Yang, N. *et al.* Systematically analyzing rare variants of autosomal-dominant genes for sporadic Parkinson's disease in a Chinese cohort. *Neurobiology of Aging* (2018). doi:10.1016/j.neurobiolaging.2018.11.012

59. Obara, Y. & Ishii, K. Transcriptome Analysis Reveals That Midnolin Regulates mRNA Expression Levels of Multiple Parkinson's Disease Causative Genes. *Biol. Pharm. Bull. Pharm. Bull.* **41**, 20–23 (2017).

60. Iqbal, Z. & Toft, M. CHCHD2 and Parkinson's disease. *Lancet Neurol.* **14**, 680–681 (2015).

61. Zhou, W. *et al.* PD-linked CHCHD2 mutations impair CHCHD10 and MICOS complex leading to mitochondria dysfunction. *Hum. Mol. Genet.* (2018). doi:10.1093/hmg/ddy413

62. Imai, Y., Meng, H., Shiba-Fukushima, K. & Hattori, N. Twin CHCH Proteins, CHCHD2, and CHCHD10: Key Molecules of Parkinson's Disease, Amyotrophic Lateral Sclerosis, and Frontotemporal Dementia. *Int. J. Mol. Sci.* **20**, 908 (2019).

63. Funayama, M. *et al.* A new locus for Parkinson's disease (PARK8) maps to chromosome 12p11.2-q13.1. *Ann. Neurol.* **51**, 296–301 (2002).

64. Hasegawa, K. *et al.* Familial parkinsonism: Study of original Sagamihara PARK8 (I2020T) kindred with variable clinicopathologic outcomes. *Park. Relat. Disord.* **15**, 300–306 (2009).

65. Healy, D. G. *et al.* Phenotype, genotype, and worldwide genetic penetrance of LRRK2-associated Parkinson's disease: a case-control study. *Lancet Neurol.* **7**, 583–590 (2008).

66. Pezzoli, G. *et al.* Comprehensive analysis of the LRRK2 gene in sixty families with Parkinson's disease. *Eur. J. Hum. Genet.* **14**, 322–331 (2005).

67. Ross, O. A. *et al.* Association of LRRK2 exonic variants with susceptibility to Parkinson's disease: A case-control study. *Lancet Neurol.* **10**, 898–908 (2011).

68. Ferreira, M. & Massano, J. An updated review of Parkinson's disease genetics and clinicopathological correlations. *Acta Neurol. Scand.* **135**, 273–284 (2017).

69. Khan, N. L. *et al.* Progression of nigrostriatal dysfunction in a parkin kindred: an [18F]dopa PET and clinical study. *Brain* **125**, 2248–56 (2002).

70. Lohmann, E. *et al.* How much phenotypic variation can be attributed to *parkin* genotype? *Ann. Neurol.* **54**, 176–185 (2003).

71. Kay, D. M. *et al.* Heterozygous *parkin* point mutations are as common in control subjects as in Parkinson's patients. *Ann. Neurol.* **61**, 47–54 (2007).

72. Lincoln, S. J. *et al.* Parkin variants in North American Parkinson's disease: Cases and controls. *Mov. Disord.* **18**, 1306–1311 (2003).

73. Annesi, G. *et al.* DJ-1 mutations and parkinsonism-dementia-amyotrophic lateral sclerosis complex. *Ann. Neurol.* **58**, 803–807 (2005).

74. Abou-Sleiman, P. M., Healy, D. G., Quinn, N., Lees, A. J. & Wood, N. W. The role of pathogenicDJ-1 mutations in Parkinson's disease. *Ann. Neurol.* **54**, 283–286 (2003).

75. Nuytemans, K., Theuns, J., Cruts, M. & Van Broeckhoven, C. Genetic etiology of Parkinson disease associated with mutations in the SNCA, PARK2, PINK1, PARK7, and LRRK2 genes: a mutation update. *Hum. Mutat.* **31**, 763–780 (2010).

76. Wilson, G. R. *et al.* Mutations in RAB39B cause X-linked intellectual disability and early-onset Parkinson disease with α-synuclein pathology. *Am. J. Hum. Genet.* **95**, 729–35 (2014).

77. Lesage, S. *et al.* Loss-of-function mutations in RAB39B are associated with typical early-onset Parkinson disease. *Neurol. Genet.* **1**, e9 (2015).

78. Stephenson, S. E. M. *et al.* The emerging role of Rab GTPases in the pathogenesis of Parkinson's disease. *Mov. Disord.* **33**, 196–207 (2018).

79. Edvardson, S. *et al.* A Deleterious Mutation in DNAJC6 Encoding the Neuronal-Specific Clathrin-Uncoating Co-Chaperone Auxilin, Is Associated with Juvenile Parkinsonism. *PLoS One* **7**, e36458 (2012).

80. Olgiati, S. *et al.* DNAJC6 Mutations Associated with Early-Onset Parkinson's Disease. *Ann. Neurol.* **79**, 244–256 (2016).

81. Köroğlu, Ç., Baysal, L., Cetinkaya, M., Karasoy, H. & Tolun, A. DNAJC6 is responsible for juvenile parkinsonism with phenotypic variability. *Park. Relat. Disord.* **19**, 320–324 (2013).

82. Rogaeva, E. *et al.* A Multicenter Study of Glucocerebrosidase Mutations in Dementia With Lewy Bodies. *JAMA Neurol.* **70**, 727 (2013).

83. Lesage, S. & Brice, A. Parkinson's disease: From monogenic forms to genetic susceptibility factors. *Human Molecular Genetics* **18**, R48–R59 (2009).

84. Ballard, C. *et al.* Glucocerebrosidase mutations and neuropsychiatric phenotypes in Parkinson's disease and Lewy body dementias: Review and meta-analyses. *Am. J. Med. Genet. Part B Neuropsychiatr. Genet.* **177**, 232–241 (2017).

85. Gan-Or, Z. *et al.* The age at motor symptoms onset in LRRK2-associated Parkinson's disease is affected by a variation in the MAPT locus: A possible interaction. *J. Mol. Neurosci.* **46**, 541–544 (2012).

86. Chen, X. *et al.* The melanoma-linked "redhead" MC1R influences dopaminergic neuron survival. *Ann. Neurol.* **81**, 395–406 (2017).

87. Tienari, P. J. *et al.* A Rare Truncating Mutation in ADH1C (G78Stop) Shows Significant Association With Parkinson Disease in a Large International Sample. *Arch. Neurol.* **62**, 74 (2005).

88. Feng, Y., Jankovic, J. & Wu, Y. C. Epigenetic mechanisms in Parkinson's disease. *Journal of the Neurological Sciences* **349**, 3–9 (2015).

89. Matsumoto, L. *et al.* CpG demethylation enhances alpha-synuclein expression and affects the pathogenesis of Parkinson's disease. *PLoS One* **5**, e15522 (2010).

90. Emamzadeh, F. N. & Surguchov, A. Parkinson's disease: Biomarkers, treatment, and risk factors. *Frontiers in Neuroscience* **12**, 612 (2018).

91. Przedborski, S. The two-century journey of Parkinson disease research. *Nat. Rev. Neurosci.* **18**, 251–259 (2017).

92. Harris, H. & Rubinsztein, D. C. Control of autophagy as a therapy for neurodegenerative disease. *Nature Reviews Neurology* **8**, 108–117 (2012).

93. Martinez-Vicente, M. *et al.* Dopamine-modified α-synuclein blocks chaperone-mediated autophagy. *J. Clin. Invest.* **118**, 777–778 (2008).

94. International Parkinson Disease Genomics Consortium *et al.* Imputation of sequence variants for identification of genetic risks for Parkinson's disease: a meta-analysis of genome-wide association studies. *Lancet (London, England)* **377**, 641–649 (2011).

95. Chung, C. Y., Koprich, J. B., Siddiqi, H. & Isacson, O. Dynamic Changes in Presynaptic and Axonal Transport Proteins Combined with Striatal Neuroinflammation Precede Dopaminergic Neuronal Loss in

a Rat Model of AAV -Synucleinopathy. *J. Neurosci.* **29**, 3365–3373 (2009).

96. Ihara, M. *et al.* Sept4, a Component of Presynaptic Scaffold and Lewy Bodies, Is Required for the Suppression of α-Synuclein Neurotoxicity. *Neuron* **53**, 519–533 (2007).

97. Chinta, S. J., Mallajosyula, J. K., Rane, A. & Andersen, J. K. Mitochondrial alpha-synuclein accumulation impairs complex I function in dopaminergic neurons and results in increased mitophagy in vivo. *Neurosci. Lett.* **486**, 235–239 (2010).

98. Wareski, P. *et al.* Mutant A53T α-Synuclein Induces Neuronal Death by Increasing Mitochondrial Autophagy. *J. Biol. Chem.* **286**, 10814–10824 (2011).

99. Chen, L. *et al.* Oligomeric α-synuclein inhibits tubulin polymerization. *Biochem. Biophys. Res. Commun.* **356**, 548–553 (2007).

100. Lee, M. K. *et al.* Accumulation of Toxic -Synuclein Oligomer within Endoplasmic Reticulum Occurs in -Synucleinopathy In Vivo. *J. Neurosci.* **32**, 3301–3305 (2012).

101. Brundin, P. & Melki, R. Prying into the Prion Hypothesis for Parkinson's Disease. *J. Neurosci.* **37**, 9808–9818 (2017).

102. Scheckel, C. & Aguzzi, A. Prions, prionoids and protein misfolding disorders. *Nature Reviews Genetics* **19**, 405–418 (2018).

103. Braak, H. *et al.* Staging of brain pathology related to sporadic Parkinson's disease. *Neurobiol. Aging* **24**, 197–211 (2003).

104. Youle, R. J. *et al.* REVIEW Mitochondrial Fission, Fusion, and Stress. *Science (80-.).* **337**, 1062–1065 (2012).

105. Perier, C. & Vila, M. Mitochondrial biology and Parkinson's disease. *Cold Spring Harb. Perspect. Med.* **2**, a009332 (2012).

106. Wood, N. W. *et al.* PINK1-Associated Parkinson's Disease Is Caused by Neuronal Vulnerability to Calcium-Induced Cell Death. *Mol. Cell* **33**, 627–638 (2009).

107. Sheng, Z. H. & Cai, Q. Mitochondrial transport in neurons: Impact on synaptic homeostasis and neurodegeneration. *Nature Reviews Neuroscience* **13**, 77–93 (2012).

108. Borland, M. K. *et al.* Chronic, low-dose rotenone reproduces lewy neurites found in early stages of Parkinson's disease, reduces mitochondrial movement and slowly kills differentiated SH-SY5Y neural cells. *Mol. Neurodegener.* **3**, 21 (2008).

109. Sano, H. Biochemistry of the extrapyramidal system. *Parkinsonism and Related Disorders* **6**, 3–6 (2000).

110. Ehringer, H. & Hornykiewicz, O. Verteilung Von Noradrenalin Und Dopamin (3-Hydroxytyramin) Im Gehirn Des Menschen Und Ihr Verhalten Bei Erkrankungen Des Extrapyramidalen Systems. *Klin. Wochenschr.* **38**, 1236–1239 (1960).

111. Lees, A. J., Hardy, J. & Revesz, T. Parkinson's disease. *Lancet* **373**, 2055–2066 (2009).

112. Hegarty, S. V., Sullivan, A. M. & O'Keeffe, G. W. Midbrain dopaminergic neurons: A review of the molecular circuitry that regulates their development. *Dev. Biol.* **379**, 123–138 (2013).

113. Cerri, S., Siani, F. & Blandini, F. Investigational drugs in Phase I and Phase II for Levodopa-induced dyskinesias. *Expert Opinion on Investigational Drugs* **26**, 777–791 (2017).

114. Caviness, J. N. Presymptomatic Parkinson's disease: The Arizona experience. *Parkinsonism Relat. Disord.* **18**, S203–S206 (2011).

115. Wey, S.-P. *et al.* Correlation of Parkinson Disease Severity and 18 F-DTBZ Positron Emission Tomography. *JAMA Neurol.* **71**, 758 (2014).

116. Antonini, A. *et al.* Axonal damage and loss of connectivity in nigrostriatal and mesolimbic dopamine pathways in early Parkinson's disease. *NeuroImage Clin.* **14**, 734–740 (2017).

117. Kordower, J. H. *et al.* Disease duration and the integrity of the nigrostriatal system in Parkinson's disease. *Brain* **136**, 2419–2431 (2013).

118. Oliveira, L. M. A. *et al.* Elevated α-synuclein caused by SNCA gene triplication impairs neuronal differentiation and maturation in Parkinson's patient-derived induced pluripotent stem cells. *Cell Death Dis.* **6**, (2015).

119. Gilks, W. P. *et al.* A common LRRK2 mutation in idiopathic Parkinson's disease. *Lancet* **365**, 415–416 (2005).

120. Di Fonzo, A. *et al.* A frequent LRRK2 gene mutation associated with autosomal dominant Parkinson's disease. *Lancet* **365**, 412–415 (2005).

121. Lin, L. *et al.* Molecular Features Underlying Neurodegeneration Identified through In Vitro Modeling of Genetically Diverse Parkinson's Disease Patients. *Cell Rep.* **15**, 2411–2426 (2016).

122. Antoniou, N. *et al.* Defective synaptic connectivity and axonal neuropathology in a human iPSC-based model of familial Parkinson's disease. *Proc. Natl. Acad. Sci.* **114**, E3679–E3688 (2017).

123. Cotzias, G. C., Papavasilious, P. S. & Gellene, R. Modification of parkinsonism: chronic treatment with levadopa. *N. Engl. J. Med.* **280**, 337–345 (1969).

124. Levine, C. B. *et al.* Diagnosis and treatment of Parkinson's disease: a systematic review of the literature. *Evid. Rep. Technol. Assess. (Summ).* 1–4 (2003).

125. Huang, L. *et al.* β-asarone and levodopa coadministration increases striatal levels of dopamine and levodopa and improves behavioral competence in Parkinson's rat by enhancing dopa decarboxylase activity. *Biomed. Pharmacother.* **94**, 666–678 (2017).

126. Du, J. J. & Chen, S. Di. Current nondopaminergic therapeutic options for motor symptoms of parkinson's disease. *Chinese Medical Journal* **130**, 1856–1866 (2017).

127. Gibbons, A. S., Neo, J., Dean, B., Scarr, E. & Udawela, M. Cholinergic connectivity: it's implications for psychiatric disorders. *Front. Cell. Neurosci.* **7**, 55 (2013).

128. Joyner, A. L., Liu, A. & Millet, S. Otx2, Gbx2 and Fgf8 interact to position and maintain a mid–hindbrain organizer. *Curr. Opin. Cell Biol.* **12**, 736–741 (2000).

129. Rhinn, M. *et al.* Sequential roles for Otx2 in visceral endoderm and neuroectoderm for forebrain and midbrain induction and specification. *Development* **125**, **845**–**8**, 845–856 (1998).

130. Wassarman, K. M. *et al.* Specification of the anterior hindbrain and establishment of a normal mid/hindbrain organizer is dependent on Gbx2 gene function. *Development* **124**, 2923–34 (1997).

131. Placzek, M. & Briscoe, J. The floor plate: Multiple cells, multiple signals. *Nature Reviews Neuroscience* **6**, 230–240 (2005).

132. Kabanova, A. *et al.* Temporal-spatial changes in Sonic Hedgehog expression and signaling reveal different potentials of ventral mesencephalic progenitors to populate distinct ventral midbrain nuclei. *Neural Dev.* **6**, 29 (2011).

133. Brown, A., Machan, J. T., Hayes, L. & Zervas, M. Molecular organization and timing of Wnt1 expression define cohorts of midbrain dopamine neuron progenitors in vivo. *J. Comp. Neurol.* **519**, 2978–3000 (2011).

134. McKay, R. D. G. *et al.* Wnt antagonism of Shh facilitates midbrain floor plate neurogenesis. *Nat. Neurosci.* **12**, 125–131 (2009).

135. Lin, W. *et al.* Foxa1 and Foxa2 function both upstream of and cooperatively with Lmx1a and Lmx1b in a feedforward loop promoting mesodiencephalic dopaminergic neuron development. *Dev. Biol.* **333**, 386–396 (2009).

136. Burbach, J. P. H. *et al.* A second independent pathway for development of mesencephalic dopaminergic neurons requires Lmx1b. *Nat. Neurosci.* **3**, 337–341 (2002).

137. Andersson, E. K. I., Irvin, D. K., Ahlsiö, J. & Parmar, M. Ngn2 and Nurr1 act in synergy to induce midbrain dopaminergic neurons from expanded neural stem and progenitor cells. *Exp. Cell Res.* **313**, 1172–1180 (2007).

138. Perlmann, T. *et al.* Specific and integrated roles of Lmx1a, Lmx1b and Phox2a in ventral midbrain development. *Development* **138**, 3399–3408 (2011).

139. Andersson, E. *et al.* Identification of intrinsic determinants of midbrain dopamine neurons. *Cell* **124**, 393–405 (2006).

140. Hanaway, J., McConnell, J. A. & Netsky, M. G. Histogenesis of the substantia nigra, ventral tegmental area of Tsai and interpeduncular nucleus: An autoradiographic study of the mesencephalon in the rat. *J. Comp. Neurol.* **142**, 59–73 (1971).

141. Poirier, L. J., Giguère, M. & Marchand, R. Comparative morphology of the substantia nigra and ventral tegmental area in the monkey, cat and rat. *Brain Res. Bull.* **11**, 371–97 (1983).

142. Arenas, E., Denham, M. & Villaescusa, J. C. How to make a midbrain dopaminergic neuron. *Development* **142**, 1918–1936 (2015).

143. Albin, R. L., Young, A. B. & Penney, J. B. The functional anatomy of basal ganglia disorders. *Trends Neurosci.* **12**, 366–375 (1989).

144. Hawkes, C. H., Del Tredici, K. & Braak, H. Parkinson's disease: A dual-hit hypothesis. *Neuropathology and Applied Neurobiology* **33**, 599–614 (2007).

145. Dijkstra, A. A. *et al.* Stage-dependent nigral neuronal loss in incidental Lewy body and Parkinson's disease. *Mov. Disord.* **29**, 1244–1251 (2014).

146. Shill, H. A. *et al.* Unified staging system for Lewy body disorders: correlation with nigrostriatal degeneration, cognitive impairment and motor dysfunction. *Acta Neuropathol.* **117**, 613–634 (2009).

147. Burnett, M. *et al.* Incidental Lewy Body Disease and Preclinical Parkinson Disease. *Arch. Neurol.* **65**, 1074–1080 (2008).

148. Kramer, M. L. & Schulz-Schaeffer, W. J. Presynaptic -Synuclein Aggregates, Not Lewy Bodies, Cause Neurodegeneration in Dementia with Lewy Bodies. *J. Neurosci.* **27**, 1405–1410 (2007).

149. Orme, T., Guerreiro, R. & Bras, J. The Genetics of Dementia with Lewy Bodies: Current Understanding and Future Directions. *Current Neurology and Neuroscience Reports* **18**, (2018).

150. Quinn, N. *et al.* Parkin Disease. *JAMA Neurol.* **70**, 571 (2013).

151. Kingsbury, A. E. *et al.* Brain stem pathology in Parkinson's disease: An evaluation of the Braak staging model. *Mov. Disord.* **25**, 2508–2515 (2010).

152. Dugger, B. N. & Dickson, D. W. Cell type specific sequestration of choline acetyltransferase and tyrosine hydroxylase within Lewy bodies. *Acta Neuropathol.* **120**, 633–639 (2010).

153. Roberts, H. L. & Brown, D. R. Seeking a mechanism for the toxicity of oligomeric α-synuclein. *Biomolecules* **5**, 282–305 (2015).

154. Winner, B. *et al.* Accumulation of oligomer-prone α-synuclein exacerbates synaptic and neuronal degeneration in vivo. *Brain* **137**, 1496–1513 (2014).

155. Consiglio, A. *et al.* In vivo demonstration that -synuclein oligomers are toxic. *Proc. Natl. Acad. Sci.* **108**, 4194–4199 (2011).

156. Rusconi, R. *et al.* Brain propagation of transduced α-synuclein involves non-fibrillar protein species and is enhanced in α-synuclein null mice. *Brain* **139**, 856–870 (2016).

157. Rusconi, R. *et al.* Neuron-to-neuron α-synuclein propagation in vivo is independent of neuronal injury. *Acta Neuropathol. Commun.* **3**, (2015).

158. Schapira, A. H. V. Mitochondrial pathology in Parkinson's disease. *Mt. Sinai J. Med.* **78**, 872–881 (2011).

159. Beilina, A. & Cookson, M. R. Genes associated with Parkinson's disease: regulation of autophagy and beyond. *Journal of Neurochemistry* **139**, 91–107 (2016).

160. Cookson, M. R. DJ-1, PINK1, and their effects on mitochondrial pathways. *Mov. Disord.* **25**, S44–S48 (2010).

161. Heo, J. Y. *et al.* DJ-1 null dopaminergic neuronal cells exhibit defects in mitochondrial function and structure: Involvement of mitochondrial complex i assembly. *PLoS One* **7**, e32629 (2012).

162. Funayama, M. & Hattori, N. CHCHD2 and Parkinson's disease—Authors' reply. *Lancet Neurol.* **14**, 682–683 (2015).

163. Pacelli, C. *et al.* Elevated Mitochondrial Bioenergetics and Axonal Arborization Size Are Key Contributors to the Vulnerability of Dopamine Neurons. *Curr. Biol.* **25**, 2349–2360 (2015).

164. Zharikov, A. D. *et al.* ShRNA targeting α-synuclein prevents neurodegeneration in a Parkinson's disease model. *J. Clin. Invest.* **125**, 2721–2735 (2015).

165. Bean, B. P. The action potential in mammalian central neurons. *Nature Reviews Neuroscience* **8**, 451–465 (2007).

166. Putzier, I., Kullmann, P. H. M., Horn, J. P. & Levitan, E. S. Cav1.3 Channel Voltage Dependence, Not Ca2+ Selectivity, Drives Pacemaker Activity and Amplifies Bursts in Nigral Dopamine Neurons. *J. Neurosci.* **29**, 15414–15419 (2009).

167. Kondapalli, J. *et al.* Oxidant stress evoked by pacemaking in dopaminergic neurons is attenuated by DJ-1. *Nature* **468**, 696–700 (2010).

168. Votyakova, T. V. & Reynolds, I. J. ΔΨm-dependent and -independent production of reactive oxygen species by rat brain mitochondria. *J. Neurochem.* **79**, 266–277 (2001).

169. Wong, E. & Cuervo, A. M. Autophagy gone awry in neurodegenerative diseases. *Nature Neuroscience* **13**, 805–811 (2010).

170. Burke, W. J. *et al.* Neurotoxicity of MAO Metabolites of Catecholamine Neurotransmitters: Role in Neurodegenerative Diseases. *Neurotoxicology* **25**, 101–115 (2004).

171. Hastings, T. G. The role of dopamine oxidation in mitochondrial dysfunction: Implications for Parkinson's disease. *Journal of Bioenergetics and Biomembranes* **41**, 469–472 (2009).

172. Burbulla, L. F. *et al.* Dopamine oxidation mediates mitochondrial and lysosomal dysfunction in Parkinson's disease. *Science (80-.).* **357**, 1255–1261 (2017).

173. Brimblecombe, K. R., Gracie, C. J., Platt, N. J. & Cragg, S. J. Gating of dopamine transmission by calcium and axonal N-, Q-, T- and L-type voltage-gated calcium channels differs between striatal domains. *J. Physiol.* **593**, 929–946 (2015).

174. Rao, R. V & Bredesen, D. E. Misfolded proteins, endoplasmic reticulum stress and neurodegeneration. *Current Opinion in Cell Biology* **16**, 653–662 (2004).

175. Ritchie, C. M. & Thomas, P. J. Alpha-synuclein truncation and disease. *Health (Irvine. Calif).* **04**, 1167–1177 (2012).

176. Dauer, W. & Przedborski, S. Parkinson's Disease: Mechanisms and Models. *Neuron* **39**, 889–909 (2003).

177. Xicoy, H., Wieringa, B. & Martens, G. J. M. The SH-SY5Y cell line in Parkinson's disease research: a systematic review. *Molecular Neurodegeneration* **12**, 1–11 (2017).

178. Lázaro, D. F., Pavlou, M. A. S. & Outeiro, T. F. Cellular models as tools for the study of the role of alpha-synuclein in Parkinson's disease. *Experimental Neurology* **298**, 162–171 (2017).

179. Gubellini, P. & Kachidian, P. Animal models of Parkinson's disease: An updated overview. *Revue Neurologique* **171**, 750–761 (2015).

180. Vingill, S., Connor-Robson, N. & Wade-Martins, R. Are rodent models of Parkinson's disease behaving as they should? *Behavioural Brain Research* **352**, 133–141 (2018).

181. Costa, G. *et al.* MPTP-induced dopamine neuron degeneration and glia activation is potentiated in MDMA-pretreated mice. *Mov. Disord.* **28**, 1957–1965 (2013).

182. Chiueh, C. C. *et al.* Neurochemical and behavioral effects of 1-methyl-4-phenyl-1,2,3,6-tetrahydropyridine (MPTP) in rat, guinea pig, and monkey. *Psychopharmacol. Bull.* **20**, 548–53 (1984).

183. Glajch, K. E., Fleming, S. M., Surmeier, D. J. & Osten, P. Sensorimotor assessment of the unilateral 6-hydroxydopamine mouse model of Parkinson's disease. *Behav. Brain Res.* **230**, 309–316 (2012).

184. Nandipati, S. & Litvan, I. Environmental exposures and Parkinson's disease. *Int. J. Environ. Res. Public Health* **13**, (2016).

185. Alam, M. *et al.* The rotenone-induced rat model of Parkinson's disease: Behavioral and electrophysiological findings. *Behav. Brain Res.* **279**, 52–61 (2015).

186. Betarbet, R. *et al.* Chronic systemic pesticide exposure reproduces features of Parkinson's disease. *Nat. Neurosci.* **3**, 1301–1306 (2000).

187. Rajput, A. H. & Uitti, R. J. Paraquat and Parkinson's disease. *Neurology* **37**, 1820 (1987).

188. Day, B. J., Patel, M., Calavetta, L., Chang, L.-Y. & Stamler, J. S. A mechanism of paraquat toxicity involving nitric oxide synthase. *Proc. Natl. Acad. Sci.* **96**, 12760–12765 (2002).

189. Thiruchelvam, M. *et al.* Age-related irreversible progressive nigrostriatal dopaminergic neurotoxicity in the paraquat and maneb model of the Parkinson's disease phenotype. *Eur. J. Neurosci.* **18**, 589–600 (2003).

190. Granado, N. *et al.* Persistent MDMA-induced dopaminergic neurotoxicity in the striatum and substantia nigra of mice. *J. Neurochem.* **107**, 1102–1112 (2008).

191. Morrow, B. A., Roth, R. H., Redmond, D. E. & Elsworth, J. D. Impact of methamphetamine on dopamine neurons in primates is dependent on age: Implications for development of Parkinson's disease. *Neuroscience* **189**, 277–285 (2011).

192. Visanji, N. P. *et al.* α-Synuclein-Based Animal Models of Parkinson's Disease: Challenges and Opportunities in a New Era. *Trends in Neurosciences* **39**, 750–762 (2016).

193. Hatami, A. & Chesselet, M. F. Transgenic rodent models to study alpha-synuclein pathogenesis, with a focus on cognitive deficits. *Curr. Top. Behav. Neurosci.* **22**, 303–330 (2014).

194. Van der Perren, A., Van den Haute, C. & Baekelandt, V. Viral Vector-based models of Parkinson's disease. *Curr. Top. Behav. Neurosci.* **22**, 271–301 (2014).

195. Tofaris, G. K. Pathological Changes in Dopaminergic Nerve Cells of the Substantia Nigra and Olfactory Bulb in Mice Transgenic for Truncated Human -Synuclein(1-120): Implications for Lewy Body Disorders. *J. Neurosci.* **26**, 3942–3950 (2006).

196. Xiong, Y., Dawson, T. M. & Dawson, V. L. Models of LRRK2-associated parkinson's disease. in *Advances in Neurobiology* **14**, 163–191 (NIH Public Access, 2017).

197. Volta, M. & Melrose, H. LRRK2 mouse models: dissecting the behavior, striatal neurochemistry and neurophysiology of PD pathogenesis. *Biochem. Soc. Trans.* **45**, 113–122 (2017).

198. Giaime, E. *et al.* Age-Dependent Dopaminergic Neurodegeneration and Impairment of the Autophagy-Lysosomal Pathway in LRRK-Deficient Mice. *Neuron* **96**, 796-807.e6 (2017).

199. Yun, S. P. *et al.* Block of A1 astrocyte conversion by microglia is neuroprotective in models of Parkinson's disease. *Nat. Med.* **24**, 931–938 (2018).

200. Lee, Y. *et al.* PINK1 Primes Parkin-Mediated Ubiquitination of PARIS in Dopaminergic Neuronal Survival. *Cell Rep.* **18**, 918–932 (2017).

201. Van Rompuy, A.-S., Lobbestael, E., Van der Perren, A., Van den Haute, C. & Baekelandt, V. Long-Term Overexpression of Human Wild-Type and T240R Mutant Parkin in Rat Substantia Nigra Induces Progressive Dopaminergic Neurodegeneration. *J. Neuropathol. Exp. Neurol.* **73**, 159–174 (2014).

202. Rousseaux, M. W. C. *et al.* Progressive dopaminergic cell loss with unilateral-to-bilateral progression in a genetic model of Parkinson disease. *Proc. Natl. Acad. Sci.* **109**, 15918–15923 (2012).

203. Sørensen, D. M. *et al.* Parkinson disease related ATP13A2 evolved early in animal evolution. *PLoS One* **13**, e0193228 (2018).

204. Bento, C. F., Ashkenazi, A., Jimenez-Sanchez, M. & Rubinsztein, D. C. The Parkinson's disease-associated genes ATP13A2 and SYT11 regulate autophagy via a common pathway. *Nat. Commun.* **7**, (2016).

205. Gonzalez-Reyes, L. E. *et al.* Sonic Hedgehog Maintains Cellular and Neurochemical Homeostasis in the Adult Nigrostriatal Circuit. *Neuron* **75**, 306–319 (2012).

206. Kadkhodaei, B. *et al.* Nurr1 Is Required for Maintenance of Maturing and Adult Midbrain Dopamine Neurons. *J. Neurosci.* **29**, 15923–15932 (2009).

207. Nordström, U. *et al.* Progressive nigrostriatal terminal dysfunction and degeneration in the engrailed1 heterozygous mouse model of Parkinson's disease. *Neurobiol. Dis.* **73**, 70–82 (2015).

208. van den Munckhof, P. Pitx3 is required for motor activity and for survival of a subset of midbrain dopaminergic neurons. *Development* **130**, 2535–2542 (2003).

209. Baiguera, C. *et al.* Late-onset Parkinsonism in NFκB/c-Rel-deficient mice. *Brain* **135**, 2750–2765 (2012).

210. Ekstrand, M. I. & Galter, D. The MitoPark Mouse - An animal model of Parkinson's disease with impaired respiratory chain function in dopamine neurons. *Park. Relat. Disord.* **15**, S185-8 (2009).

211. Friedman, L. G. *et al.* Disrupted Autophagy Leads to Dopaminergic Axon and Dendrite Degeneration and Promotes Presynaptic Accumulation of -Synuclein and LRRK2 in the Brain. *J. Neurosci.* **32**, 7585–7593 (2012).

212. Taylor, T. N., Alter, S. P., Wang, M., Goldstein, D. S. & Miller, G. W. Reduced vesicular storage of

catecholamines causes progressive degeneration in the locus ceruleus. *Neuropharmacology* **76**, 97–105 (2014).

213. Calatayud, C., Carola, G., Consiglio, A. & Raya, A. *Modeling the genetic complexity of Parkinson's disease by targeted genome edition in iPS cells*. *Current Opinion in Genetics and Development* **46**, 123–131 (2017).

214. Zeltner, N. & Studer, L. Pluripotent stem cell-based disease modeling: Current hurdles and future promise. *Current Opinion in Cell Biology* **37**, 102–110 (2015).

215. Beard, C. *et al.* Parkinson's Disease Patient-Derived Induced Pluripotent Stem Cells Free of Viral Reprogramming Factors. *Cell* **136**, 964–977 (2009).

216. Kriks, S. *et al.* Dopamine neurons derived from human ES cells efficiently engraft in animal models of Parkinson's disease. *Nature* **480**, 547–51 (2011).

217. Sánchez-Danés, A. *et al.* Disease-specific phenotypes in dopamine neurons from human iPS-based models of genetic and sporadic Parkinson's disease. *EMBO Mol. Med.* **4**, 380–395 (2012).

218. Nguyen, H. N. *et al.* LRRK2 mutant iPSC-derived da neurons demonstrate increased susceptibility to oxidative stress. *Cell Stem Cell* **8**, 267–280 (2011).

219. Reinhardt, P. *et al.* Genetic correction of a lrrk2 mutation in human iPSCs links parkinsonian neurodegeneration to ERK-dependent changes in gene expression. *Cell Stem Cell* **12**, 354–367 (2013).

220. Xie, Y. Z., Zhang, R. X. & Zhang, @bullet R X. Neurodegenerative diseases in a dish: the promise of iPSC technology in disease modeling and therapeutic discovery. *Neurol. Sci.* **36**, 21–27 (2014).

221. Cooper, O. *et al.* Pharmacological rescue of mitochondrial deficits in iPSC-derived neural cells from patients with familial Parkinson's disease. *Sci. Transl. Med.* **4**, 141ra90 (2012).

222. Csöbönyeiová, M., Danišovič, Ľ. & Polák, Š. Induced pluripotent stem cells for modeling and cell therapy of Parkinson's disease. *Neural Regeneration Research* **11**, 727–728 (2016).

223. WHO. The top 10 causes of death. *Media centre* (2011). Available at: https://www.who.int/news-room/fact-sheets/detail/the-top-10-causes-of-death. (Accessed: 5th March 2019)

224. Tibau, E., Valencia, M. & Soriano, J. Identification of neuronal network properties from the spectral analysis of calcium imaging signals in neuronal cultures. *Front. Neural Circuits* **7**, 199 (2013).

225. Takahashi, N., Sasaki, T., Usami, A., Matsuki, N. & Ikegaya, Y. Watching neuronal circuit dynamics through functional multineuron calcium imaging (fMCI). *Neurosci. Res.* **58**, 219–225 (2007).

226. Desmet, A. S., Cirillo, C., Tack, J., Vandenberghe, W. & Berghe, P. Vanden. Live calcium and mitochondrial imaging in the enteric nervous system of parkinson patients and controls. *Elife* **6**, 1–17 (2017).

227. Neher, E. & Sakaba, T. Multiple Roles of Calcium Ions in the Regulation of Neurotransmitter Release. *Neuron* **59**, 861–872 (2008).

228. Zucker, R. S. Calcium- and activity-dependent synaptic plasticity. *Curr. Opin. Neurobiol.* **9**, 305–313 (1999).

229. Lyons, M. R. & West, A. E. Mechanisms of specificity in neuronal activity-regulated gene transcription. *Progress in Neurobiology* **94**, 259–295 (2011).

230. Berridge, M. J., Bootman, M. D. & Roderick, H. L. Calcium signalling: Dynamics, homeostasis and remodelling. *Nature Reviews Molecular Cell Biology* **4**, 517–529 (2003).

231. Berridge, M. J. Neuronal Calcium Signaling. *Neuron* **21**, 13–26 (1998).

232. Ridgway, E. B. & Ashley, C. C. *CALCIUM TRANSIENTS IN SINGLE MUSCLE FIBERS*. **29**, (1967).

233. Shimomura, O., Johnson, F. H. & Saiga, Y. Extraction, Purification and Properties of Aequorin, a Bioluminescent Protein from the Luminous Hydromedusan,Aequorea. *J. Cell. Comp. Physiol.* **59**, 223–239 (2005).

234. Tsien, R. Y., Pozzan, T. & Rink, T. J. Calcium homeostasis in intact lymphocytes: Cytoplasmic free calcium monitored with a intracellularly trapped fluorescent indicator. *J. Cell Biol.* **94**, 325–334 (1982).

235. Neher, E. The use of fura-2 for estimating ca buffers and ca fluxes. *Neuropharmacology* **34**, 1423–1442 (1995).

236. Heim, R. *et al.* Fluorescent indicators for Ca2+based on green fluorescent proteins and calmodulin. *Nature* **388**, 882–887 (2002).

237. Looger, L. L. & Griesbeck, O. Genetically encoded neural activity indicators. *Current Opinion in Neurobiology* **22**, 18–23 (2012).

238. Rochefort, N. L. & Konnerth, A. Genetically encoded Ca2+sensors come of age. *Nat. Methods* **5**, 761–762 (2008).

239. Smith, S. J. & Augustine, G. J. Calcium ions, active zones and synaptic transmitter release. *Trends in Neurosciences* **11**, 458–464 (1988).

240. Swandulla, D., Hans, M., Zipser, K. & Augustine, G. J. Role of residual calcium in synaptic depression and posttetanic potentiation: Fast and slow calcium signaling in nerve terminals. *Neuron* **7**, 915–926 (1991).

241. Lasser-Ross, N., Miyakawa, H., Lev-Ram, V., Young, S. R. & Ross, W. N. High time resolution fluorescence imaging with a CCD camera. *J. Neurosci. Methods* **36**, 253–261 (1991).

242. Wang, S. S.-H. & Augustine, G. J. Confocal imaging and local photolysis of caged compounds: Dual probes of synaptic function. *Neuron* **15**, 755–760 (1995).

243. Yuste, R. & Denk, W. Dendritic spines as basic functional units of neuronal integration. *Nature* **375**, 682–684 (1995).

244. Hill, R. A., Damisah, E. C., Chen, F., Kwan, A. C. & Grutzendler, J. Targeted two-photon chemical apoptotic ablation of defined cell types in vivo. *Nat. Commun.* **8**, 1–15 (2017).

245. Grace, A. A. & Bunney, B. S. Intracellular and extracellular electrophysiology of nigral dopaminergic neurons-2. Action potential generating mechanisms and morphological correlates. *Neuroscience* **10**, 317–331 (1983).

246. Wilson, C. J. & Callaway, J. C. Coupled oscillator model of the dopaminergic neuron of the substantia nigra. *J. Neurophysiol.* **83**, 3084–100 (2000).

247. Tkatch, T. *et al.* 'Rejuvenation' protects neurons in mouse models of Parkinson's disease. *Nature* **447**, 1081–1086 (2007).

248. Hoda, J.-C. *et al.* Expression and 1,4-Dihydropyridine-Binding Properties of Brain L-Type Calcium Channel Isoforms. *Mol. Pharmacol.* **75**, 407–414 (2008).

249. Puopolo, M., Raviola, E. & Bean, B. P. Roles of Subthreshold Calcium Current and Sodium Current in Spontaneous Firing of Mouse Midbrain Dopamine Neurons. *J. Neurosci.* **27**, 645–656 (2007).

250. Chan, C. S., Gertler, T. S. & Surmeier, D. J. Calcium homeostasis, selective vulnerability and Parkinson's disease. *Trends in Neurosciences* **32**, 249–256 (2009).

251. Duda, J., Pötschke, C. & Liss, B. Converging roles of ion channels, calcium, metabolic stress, and activity pattern of Substantia nigra dopaminergic neurons in health and Parkinson's disease. *Journal of Neurochemistry* **139**, 156–178 (2016).

252. Matikainen-Ankney, B. A. *et al.* Altered Development of Synapse Structure and Function in Striatum Caused by Parkinson's Disease-Linked LRRK2-G2019S Mutation. *J. Neurosci.* **36**, 7128–7141 (2016).

253. Lechleiter, J. D. *et al.* Dopaminergic Neurons Exhibit an Age-Dependent Decline in Electrophysiological Parameters in the MitoPark Mouse Model of Parkinson's Disease. *J. Neurosci.* **36**, 4026–4037 (2016).

254. Bhat, S., Acharya, U. R., Hagiwara, Y., Dadmehr, N. & Adeli, H. Parkinson's disease: Cause factors, measurable indicators, and early diagnosis. *Computers in Biology and Medicine* **102**, 234–241 (2018).

255. Romero-Garcia, R., Atienza, M. & Cantero, J. L. Different Scales of Cortical Organization are Selectively Targeted in the Progression to Alzheimer's Disease. *Int. J. Neural Syst.* **26**, 1650003 (2015).

256. Martinez-Murcia, F. J., Górriz, J. M., Ramírez, J. & Ortiz, A. A Structural Parametrization of the Brain Using Hidden Markov Models-Based Paths in Alzheimer's Disease. *Int. J. Neural Syst.* **26**, 1650024 (2016).

257. Illán, I. A. *et al.* Independent Component Analysis-Support Vector Machine-Based Computer-Aided Diagnosis System for Alzheimer's with Visual Support. *Int. J. Neural Syst.* **27**, 1650050 (2016).

258. Sedano, J. *et al.* Generalized Models for the Classification of Abnormal Movements in Daily Life and its Applicability to Epilepsy Convulsion Recognition. *Int. J. Neural Syst.* **26**, 1650037 (2016).

259. Acharya, U. R., Vidya, S., Bhat, S., Adeli, H. & Adeli, A. Computer-aided diagnosis of alcoholism-related EEG signals. *Epilepsy and Behavior* **41**, 257–263 (2014).

260. Ahmadlou, M. & Adeli, H. Fuzzy synchronization likelihood with application to attention-deficit/ hyperactivity disorder. *Clinical EEG and Neuroscience* **42**, 6–13 (2011).

261. Ahmadlou, M., Adeli, H. & Adeli, A. Spatiotemporal analysis of relative convergence of EEGs reveals differences between brain dynamics of depressive women and men. *Clin. EEG Neurosci.* **44**, 175–181 (2013).

262. Ferdowsi, S., Sanei, S. & Abolghasemi, V. A Predictive Modeling Approach to Analyze Data in EEG–fMRI Experiments. *Int. J. Neural Syst.* **25**, 1440008 (2014).

263. Saignavongs, M. *et al.* Neural Activity Elicited by a Cognitive Task can be Detected in Single-Trials with Simultaneous Intracerebral EEG-fMRI Recordings. *Int. J. Neural Syst.* **27**, 1750001 (2016).

264. Tao, A., Chen, G., Deng, Y. & Xu, R. Accuracy of Transcranial Sonography of the Substantia Nigra for Detection of Parkinson's Disease: A Systematic Review and Meta-analysis. *Ultrasound in Medicine and Biology* **45**, 628–641 (2019).

265. Maestú, F. *et al.* Exploratory Analysis of Power Spectrum and Functional Connectivity During Resting State in Young Binge Drinkers: A MEG Study. *Int. J. Neural Syst.* **25**, 1550008 (2015).

266. Gao, L. lin & Wu, T. The study of brain functional connectivity in Parkinson's disease. *Translational Neurodegeneration* **5**, 18 (2016).

267. Friston, K. J. Functional and effective connectivity in neuroimaging: A synthesis. *Hum. Brain Mapp.* **2**, 56–78 (1994).

268. Seibert, T. M., Murphy, E. A., Kaestner, E. J. & Brewer, J. B. Interregional Correlations in Parkinson Disease and Parkinson-related Dementia with Resting Functional MR Imaging. *Radiology* **263**, 226–234 (2012).

269. Hu, X. *et al.* Altered resting-state brain activity and connectivity in depressed Parkinson's disease. *PLoS One* **10**, e0131133 (2015).

270. Kim, J. *et al.* Abnormal intrinsic brain functional network dynamics in Parkinson's disease. *Brain* **140**, 2955–2967 (2017).

271. Sánchez-Danés, a. *et al.* Efficient Generation of A9 Midbrain Dopaminergic Neurons by Lentiviral Delivery of LMX1A in Human Embryonic Stem Cells and Induced Pluripotent Stem Cells. *Hum. Gene Ther.* **23**, 56–69 (2012).

272. Horii, T. Genome engineering using the CRISPR/Cas system. *World J. Med. Genet.* **4**, 69 (2014).

273. Orlandi, J. G., Stetter, O., Soriano, J., Geisel, T. & Battaglia, D. Transfer entropy reconstruction and labeling of neuronal connections from simulated calcium imaging. *PLoS One* **9**, e98842 (2014).

274. Takahashi, N., Takahara, Y., Ishikawa, D., Matsuki, N. & Ikegaya, Y. Functional multineuron calcium imaging for systems pharmacology. *Analytical and Bioanalytical Chemistry* **398**, 211–218 (2010).

275. Orlandi, J. G. *et al.* NETCAL: An interactive platform for large-scale, NETwork and population dynamics analysis of CALcium imaging recordings. in *Neuroscience 2017* (2017). doi:10.5281/zenodo.1119026

276. Barabási, A. L. & Albert, R. Emergence of scaling in random networks. *Science (80-.).* **286**, 509–512 (1999).

277. Wolberg, J. *Data Analysis Using the Method of Least Squares*. (2006).

278. Glantz, S., Slinker, B. & Neilands, T. *Primer of Applied Regression & Analysis of Variance*. (2016).

279. Wu, D. *et al.* limma powers differential expression analyses for RNA-sequencing and microarray studies. *Nucleic Acids Res.* **43**, e47–e47 (2015).

280. CRAN - Package phenopix. Available at: https://cran.r-project.org/web/packages/fpc/index.html. (Accessed: 15th March 2019)

281. Romero, R. *et al.* A systems biology approach for pathway level analysis. *Genome Res.* **17**, 1537–1545 (2007).

282. Donato, M. *et al.* Analysis and correction of crosstalk effects in pathway analysis. *Genome Res.* **23**, 1885–1893 (2013).

283. Singh, H. *et al.* Simple Combinations of Lineage-Determining Transcription Factors Prime cis-Regulatory Elements Required for Macrophage and B Cell Identities. *Mol. Cell* **38**, 576–589 (2010).

284. Potter, S. C. *et al.* InterPro in 2019: improving coverage, classification and access to protein sequence annotations. *Nucleic Acids Res.* **47**, D351–D360 (2018).

285. Kanehisa, M. & Goto, S. KEGG: kyoto encyclopedia of genes and genomes. *Nucleic Acids Res.* **28**, 27–30 (2000).

286. Tanabe, M., Sato, Y., Morishima, K., Furumichi, M. & Kanehisa, M. KEGG: new perspectives on genomes, pathways, diseases and drugs. *Nucleic Acids Res.* **45**, D353–D361 (2016).

287. Kanehisa, M., Sato, Y., Furumichi, M., Morishima, K. & Tanabe, M. New approach for understanding genome variations in KEGG. *Nucleic Acids Res.* **47**, D590–D595 (2019).

288. Liberzon, A. *et al.* Molecular signatures database (MSigDB) 3.0. *Bioinformatics* **27**, 1739–1740 (2011).

289. Jassal, B. *et al.* The Reactome Pathway Knowledgebase. *Nucleic Acids Res.* **46**, D649–D655 (2017).

290. Nunes, N. *et al.* WikiPathways: a multifaceted pathway database bridging metabolomics to other omics research. *Nucleic Acids Res.* **46**, D661–D667 (2017).

291. Eguíluz, V. M., Chialvo, D. R., Cecchi, G. A., Baliki, M. & Apkarian, A. V. Scale-free brain functional networks. *Phys. Rev. Lett.* **94**, (2005).

292. Barabási, A. L. Scale-free networks: A decade and beyond. *Science* **325**, 412–413 (2009).

293. Mueller, K. *et al.* Brain connectivity changes when comparing effects of subthalamic deep brain stimulation with levodopa treatment in Parkinson's disease. *NeuroImage Clin.* **19**, 1025–1035 (2018).

294. Calatayud, C. *et al.* CRISPR/Cas9-mediated generation of a tyrosine hydroxylase reporter iPSC line for live imaging and isolation of dopaminergic neurons. *Sci. Rep.* **9**, 6811 (2019).

295. Shaner, N. C. *et al.* Improved monomeric red, orange and yellow fluorescent proteins derived from Discosoma sp. red fluorescent protein. *Nat. Biotechnol.* **22**, 1567–1572 (2004).

296. OnRamp. Rosalind. Available at: https://rosalind.onramp.bio/project-index/summary. (Accessed: 16th May 2019)

297. Marbacher, S. *et al.* Systematic Review of In Vivo Animal Models of Subarachnoid Hemorrhage: Species, Standard Parameters, and Outcomes. *Translational Stroke Research* 1–9 (2018). doi:10.1007/s12975-018-0657-4

298. Brai, E., Cogoni, A. & Greenfield, S. A. An Alternative Approach to Study Primary Events in Neurodegeneration Using Ex Vivo Rat Brain Slices. *J. Vis. Exp.* e57507 (2018). doi:10.3791/57507

299. Hauser, M. D. Costs of deception: cheaters are punished in rhesus monkeys (Macaca mulatta). *Proc. Natl. Acad. Sci.* **89**, 12137–12139 (2006).

300. Humpel, C. Organotypic brain slice cultures: A review. *Neuroscience* **305**, 86–98 (2015).

301. Dauguet, J. *et al.* Three-dimensional reconstruction of stained histological slices and 3D non-linear registration with in-vivo MRI for whole baboon brain. *J. Neurosci. Methods* **164**, 191–204 (2007).

302. Frega, M., Tedesco, M., Massobrio, P., Pesce, M. & Martinoia, S. Network dynamics of 3D engineered neuronal cultures: A new experimental model for in-vitro electrophysiology. *Sci. Rep.* **4**, 5489 (2014).

303. Lancaster, M. A. & Knoblich, J. A. Organogenesisin a dish: Modeling development and disease using organoid technologies. *Science* **345**, 1247125–1247125 (2014).

304. Monzel, A. S. *et al.* Derivation of Human Midbrain-Specific Organoids from Neuroepithelial Stem Cells. *Stem Cell Reports* **8**, 1144–1154 (2017).

305. Quadrato, G. *et al.* Cell diversity and network dynamics in photosensitive human brain organoids. *Nature* **545**, 48–53 (2017).

306. Campion, D. *et al.* Early-Onset Autosomal Dominant Alzheimer Disease: Prevalence, Genetic Heterogeneity, and Mutation Spectrum. *Am. J. Hum. Genet.* **65**, 664–670 (2002).

307. Raja, W. K. *et al.* Self-organizing 3D human neural tissue derived from induced pluripotent stem cells

recapitulate Alzheimer's disease phenotypes. *PLoS One* **11**, e0161969 (2016).

308. Javaherian, A. & Kriegstein, A. A stem cell niche for intermediate progenitor cells of the embryonic cortex. *Cereb. Cortex* **19**, i70–i77 (2009).

309. Bhatia, S. N. & Ingber, D. E. Microfluidic organs-on-chips. *Nat. Biotechnol.* **32**, 760–72 (2014).

310. Giobbe, G. G. *et al.* Functional differentiation of human pluripotent stem cells on a chip. *Nat. Methods* **12**, 637–640 (2015).

311. Shin, Y. *et al.* Reconstituting vascular microenvironment of neural stem cell niche in three-dimensional extracellular matrix. *Adv. Healthc. Mater.* **3**, 1457–1464 (2014).

312. Kusuma, S. *et al.* Self-organized vascular networks from human pluripotent stem cells in a synthetic matrix. *Proc. Natl. Acad. Sci.* **110**, 12601–12606 (2013).

313. Zanotelli, M. R. *et al.* Stable engineered vascular networks from human induced pluripotent stem cell-derived endothelial cells cultured in synthetic hydrogels. *Acta Biomater.* **35**, 32–41 (2016).

314. Signaevsky, M. *et al.* Artificial intelligence in neuropathology: deep learning-based assessment of tauopathy. *Lab. Investig.* (2019). doi:10.1038/s41374-019-0202-4

ANNEX

1. Techniques applied in other projects

1.1. HEK 293T

HEK 293T line were used to produce lentivirus. 1 million cells were thawed in a 10 cm dish using 10% FBS DMEM with 1% Pen/Strep and passed the next day 1:4. After reaching confluence (approx. 48h later), each 10 cm dish was passed in a 15 cm dish. Each virus production request 7 of the 150mm dish.

1.2. Kit Invitrogen

Next, we differentiate our iPSC in ventral midbrain dopaminergic neurons with a commercial kit from Thermo Fisher (CITE) that allows the expansion and storage of dopaminergic precursors.

This characteristic was tested in the previous 2 protocols but we notice that the precursors during the period of expansion and storage loose part of the dopaminergic differentiation potential while in this protocol the differentiation potential was descripted to be stable for 10 passages. We follow every step of the protocol with minor modification to adapt it to our iPSCs.

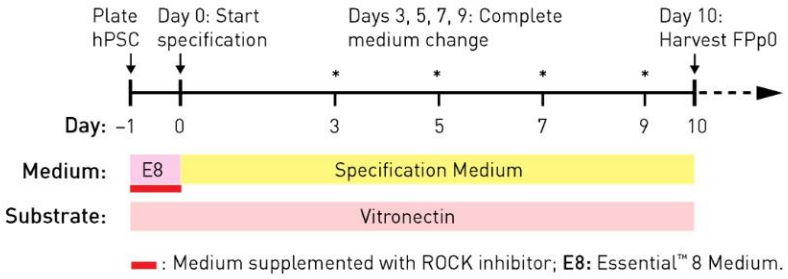

Fig 9. Schematic representation of the commercial protocol that we used to differentiate ventral midbrain specific DA NPCs

During the first step we maintain the cells in matrigel with conditioned HES medium and Specification medium. We tested again at different time (7, 9, 10, 11, 15) points the co-expression of FoxA2 and Lmx1A. The commercial protocol suggest DIV10 as the best timing to obtain ventral midbrain precursors but for our iPSC was necessary to wait until DIV15 (Fig.1.3)

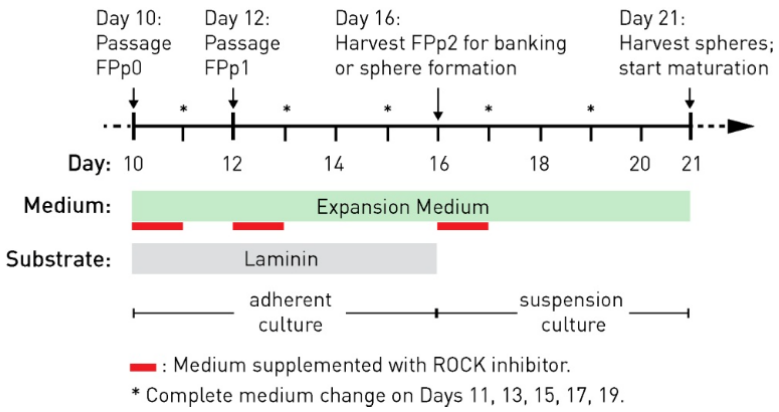

Fig 10. Schematic representation of the expansion step of the commercial protocol that allow us to store ventral midbrain DA progenitors.

When the cells reach confluence, we split them first on laminin and then maintain them in suspension to expand them and freeze them for banking.

At this stage our precursor was stored at passage 2 and they were able to be thawed and differentiate in ventral midbrain dopaminergic neurons.

1.3. SNCA flag editing

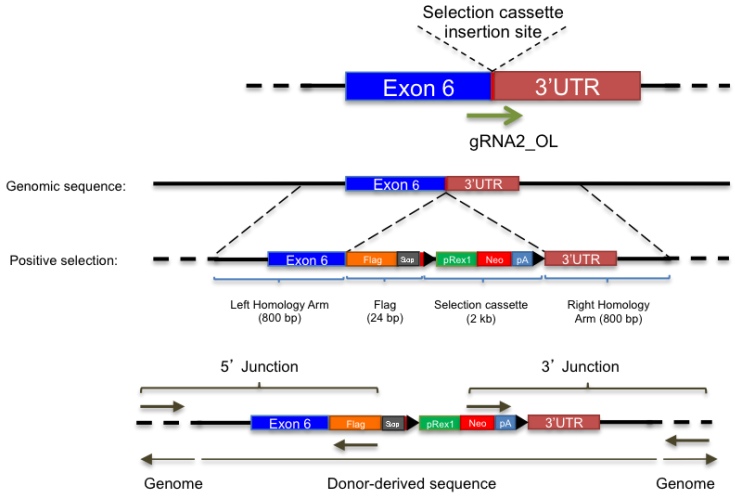

Fig 12. Scheme describing the recombination steps during the edition process. Green arrows represent the primers used for the PCR screening procedure. Black triangles represent LoxP sites surrounding the selection cassette.

We edited the synuclein locus with FLAG-TAG in CTR (SP11#1) and PD1 (SP12#3) lines using the CRISPR/Cas9 gene editing method. Complementary oligos encoding for the desired spacer sequences were annealed into the BbsI site of the gRNA scaffold of the Cas9-T2A-EGFP/gRNA co-expression plasmid px458 (Addgene, #48138). A full-length version of the CAGGS promoter was used to improve the expression in iPSC. The cleavage efficiency of two gRNAs was tested by T7EI assay. Both gRNAs displayed a similar cutting efficiency but gRNA2-OL was selected for the editing process. Donor plasmid for knocking-in a FLAG tag fused C-terminal to the α-synuclein open reading frame (ORF) was engineered using two homology arms (HAs) spanning approximately 800 bp from both sides of the STOP codon. The sequence encoding for the FLAG tag was placed immediately after the last codon of the SNCA ORF and before the STOP codon. A selection cassette (pRex1-NeoR) surrounded by loxP sites was cloned between the STOP codon and the 3'HA.

The clone, characterized by sequence, immunofluorescence and WB, was successfully edited and karyotypically normal.

Next we plate 800.000 iPSC in a 10cm dish with matrigel, the next day they were cotransfected with a mix of 6 µg of Cas9-T2A-EGFP/gRNA, 9 µg of the donor plasmid, 45 µL of FuGENE HD (Promega) transfection reagent, and KO-DMEM up to 750 µL. The mix was incubated for 15min at room temperature and added drop by drop in the culture dish. 72h later G-418 (50 µg/mL) selection was applied and the emerging colonies were selected and each one was transferred in a single well. The colonies that, by PCR, display the correct insertion were screened and then transfected with CRE-recombinase expressing plasmid. After that the cells were disaggregated to single cell and re-plated on top of human irradiated fibroblast feeder layer in presence of Rock inhibitor (Miltenyi). After the second screening for the selection cassette- excision the positive clones were expanded, characterized and stored.

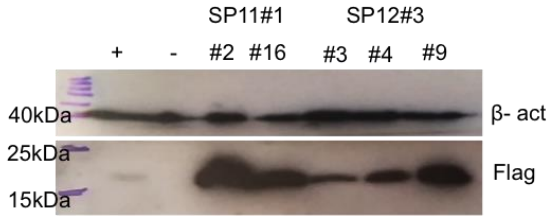

Fig 13. WB on SP11#1 SNCAflag and SP12#3 SNCAflag positive clones after 3 weeks of neuronal differentiation on PA6. Positive control is done using protein extraction from 293T transfected with plasmid expressing flag. Negative control is iPSC not transfected.

For the next experiments SP11#1_#2 and SP12#3_#3 were used and further characterized.

SP11#1_#2 neuron differentiation

SP12#3_#3 astrocyte differentiation

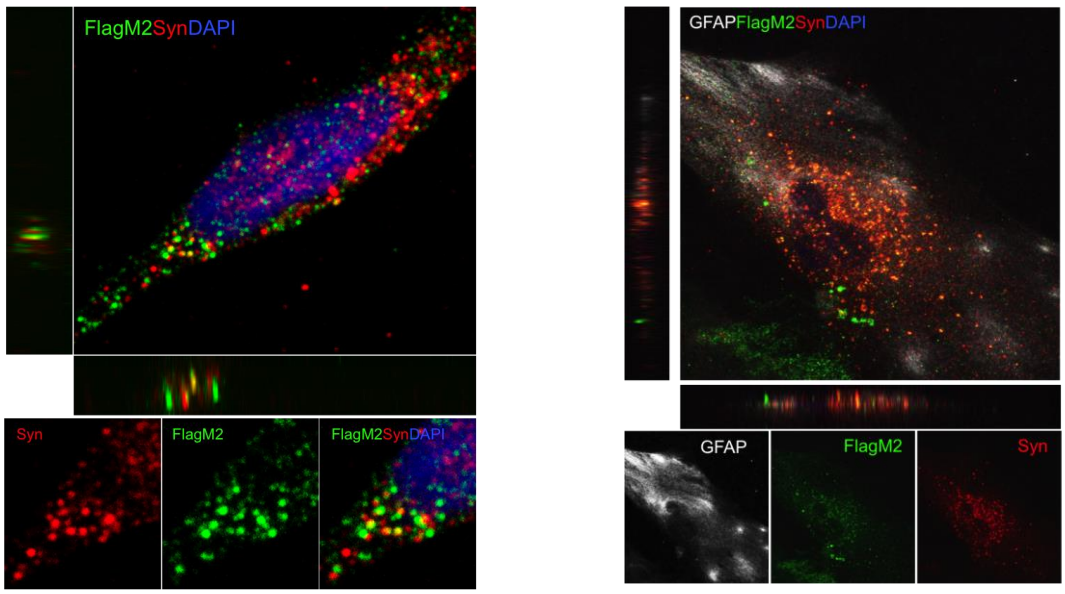

Fig 14. Immunofluorescent colocalization analysis of flag and alpha-synuclein in neurons from CTR (SP11#1 SNCAflag) after 3 weeks differentiation of EBs on PA6 and LRRK2-PD astrocytes (GFAP) after 14 days in culture.

1.4. Set up the co-culture system

DIV 35 immature/young neurons were used to set up and investigate the process of differentiation and maturation of neurons on top of iPSC derived astrocytes. 1 week before plating the neurons, 20.000 astrocytes were plated on the top of matrigel coated glass cover slides in 24-well plates to ensure their full development and to provide sufficient co-culturing time before the cells would be affected by prolonged placement in the culture. vmDAn from a LRRK2-PD line were generated and 5x104 cells/well were plated on the top of one-week-old astrocytes and left it for two and four weeks. The medium used contained Neurobasal, 2%B27, 1% NEAA, 1%PenStrep, and 1% Glutamax and half of it was changed twice a week. Cells were fixed with 4% PFA for 15 mins and washed three times with PBS for 15 minutes before performing ICC. After confocal images were acquired, TH positive cells and DAPI were counted for a series of 600 cells per condition using FIJI is Just ImageJ™ cell counter plugin.

1.5. Invitrogen kit

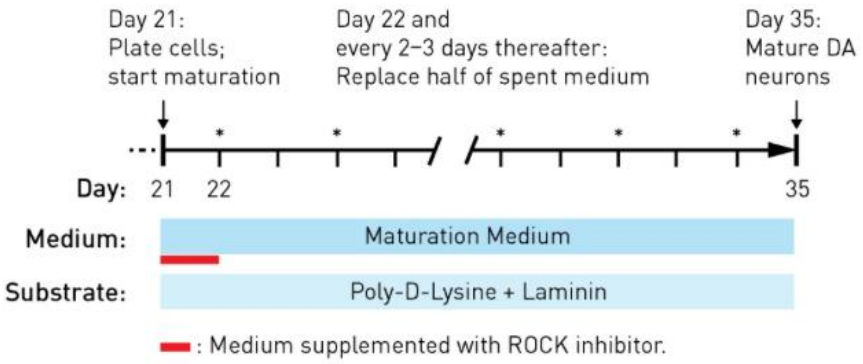

Fig 16. Schematic representation of the differentiation protocol from the commercial kit that were used to generate DA neurons

Following the kit instruction vmDA neurons were generated from the frozen precursors obtained with the kit. These sphere were thawed in commercial expansion medium supplemented with Rock inhibitor and after 3 days disaggregated and plated on top of 24 well plated cover glasses coated with Poly-D-Lysine) 100 µg/mL and Laminin (1 µg/mL). The disaggregation process start washing the spheres twice with PBS, then move them in a 15ml falcon and add 0,5ml of Accutase (eBiosciences), incubate the sphere for 10 min at 37°C. Next with the 200µl tip homogenize the spheres in smaller pieces and centrifuge them 800rpm for 5min. Re-suspend the cells in 1ml of expansion medium with Rock inhibitor and count them. Plate $1x10^5$ cells in each well. Fix the culture after 15 and 30 days (DIV30 and 50) with PFA4% and check the neural differentiation with TH, MAP2, FoxA2, DAT and Girk2.

1.6. Protein extraction

Live cells were washed twice with PBS, lifted with a scraper and collected DPBS. The samples were centrifuged at 800rpm for five minutes. After centrifugation, cells were re-suspended in cold PBS and placed in 1.5mL eppendorfs and centrifuged for five minutes at 4ºC at 600xg. Discart the supernatant and store the pellet at -80ºC. For extracting the proteins pellets were homogenized in 50 mM Tris-HCl, pH 7.4/150 mM NaCl/0.5% Triton X-100/0.5% Nonidet P-40 and a mixture of proteinase inhibitors (Sigma, Roche tablet). Samples were then centrifuged at 15,000xg for 20 minutes at 4ºC. The resulting supernatant was normalized for protein using BCA kit (Pierce).

Protein extraction for oligomeric α-synuclein:

Mila lysis buffer (0.5M Tris at pH 7.4 contains 0.5 methylenediaminetetra acetic acid at pH 8.0, 5M NaCl, 0.5% Na doxicholic, 0.5% Nonidet P-40, 1mM phenylmethylsulfonyl fluoride,

distilled water, protease and phosphatase inhibitor cocktails) (Roche Molecular Systems, Pleasanton, CA, USA), and then homogenized pellet with Mila buffer are centrifuged for 15 min at 13,000rpm at 4°C (Ultracentrifuge Beckman with 70Ti rotor, CA, USA).

These extracted proteins were used for WB analysis.

1.7. WB

Cell extracts were then boiled at 100ºC for 5 minutes, followed by 7-15% electrophoresis in Running buffer, then electro transferred in Transfer buffer at 100v to PVDF membranes for 1.5 hours at 4ºC. After treating the membranes with Ponceau S solution (Sigma) in order to cut separately the protein of interest and the loading control protein for separated antibody incubations, the membranes were then blocked in blocking solution for 1 hour and incubated overnight in containing primary antibodies. After incubation with peroxidase-tagged secondary antibodies (dilution 1:10,000), membranes were revealed with ECL-plus chemiluminescence Western blot kit (Amershan-Pharmacia Biotech).

1.8. Virus production

NaCl 281mM (16,42g/liter), Hepes 100mM (23,83g/liter), Na_2HPO_4 1,5mM (10 ml of a 150mM stock solution of 21,29g/liter) were diluted in 1 liter of H_2O sigma (W3500) to obtain HBS2x, necessary for lenti-virus home-made production.

Crucial for the protocol is the pH of the HBS2x, so for regulating the pH NaOH 2M (4g in 50ml) was freshly prepared dissolving the pellets little by little in 35ml of sterile water and then reach the 50 ml.

When the HBS2x solution reach the correct pH (7.09/7.10/7.12) leave it to stabilize 1h checking the pH every 15 minute and adjust it if change.

Filter the solution and store it in aliquots at - 20°C.

The second solution necessary for lentivirus production is $CaCl_2$ 2,5M (367,55g/liter). Aliquot were stored at -20ºC (exothermic reaction, will not freeze at -20ºC)

293T are used to produce lentivirus. Seed and incubate cells in a 15 cm dish: 18 x 10^6 cells, approximately 8 hours before transfection in 22 ml final volume. 9 x 10^6 cells, approximately 24 hours before transfection in 20 ml final volume.

It’s very important to not let the cells overgrow.

Change medium 2 hours before transfection with IMDM, 10% (heat inactivated) FBS, Penicillin (100U/ml), Streptomycin (100U/ml) and Glutamine (22 ml final volume).

For each dish prepare the following DNA mix:

7 µg of ENV plasmid (VSV-G)

12.5µg of PACKAGING plasmid, pMDLg/pRRE (III Gen.Pack)

6.25µg of REV plasmid

25µg or 32µg of TRANSFER VECTOR plasmid depending on the length of the transgene and promoter (1500bp or 3000 bp)

N.B never use more than 40µg. The plasmid solution is made up to a final volume of 1125µl (2250 µl) with 0.1X TE/dH2O (2:1). Finally, 125µl (250 µl) of 2.5M CaCl2 is added. Leave the mix at RT for 5'. The precipitate is formed by dropwise addition of 1250µl (2500 µl) of 2X HBS solution to the 1250µl DNA-TE-CaCl2 mixture from step 3 while vortexing at full speed. The precipitate should be added to the 293T cells immediately following the addition of the 2x HBS. High magnification microscopy of the cells should reveal a very small granular precipitate of the CaPi-precipitated plasmid DNA, initially above the cell monolayer, and after incubation in the 37°C incubator overnight, on the bottom of the plate in the large spaces between the cells.

The CaPi-precipitated plasmid DNA should be allowed to stay on the cells for 12 -14 hours, after which the media should be replaced with 1uM Na butyrate containing fresh media (16-18 ml per dish) for virus collection to begin.

Collect the cell supernatants at 30 hours after changing the media.

Ultracentrifuge at 19600 rpm for 2 hours and 20' in the SW28 rotor.

Re-suspend the pellet in PBS and concentrate again in SW55 rotor-23000 rpm, 2 hours and 20'. Aliquot the virus and store it at -80°C.

2. Patient-Specific iPSC-Derived Astrocytes Contribute to Non-Cell-Autonomous Neurodegeneration in Parkinson's Disease

3. CRISPR/Cas9-mediated generation of a tyrosine hydroxylase reporter iPSC line for live imaging and isolation of dopaminergic neurons